REFLECTION OF SLOW ELECTRONS FROM SOLID SURFACES.

Thesis submitted

by

JOHN THIRLWELL B.Sc.

for the degree

of

Doctor of Philosophy

in the

University of London.

September, 1966.

ABSTRACT

A brief review of characteristic electron energy losses in solids is given and experimental methods of identifying those energy losses due to the excitation of plasma oscillations are discussed. A novel and simple method of identifying these energy losses is described, which depends upon the intensity variation of the energy losses with the incidence and reflection angles of a slow primary electron beam against the specimen surface.

Various electron guns and electron analysers investigated during the development of the low energy spectrometer are described.

Freshly evaporated specimens of Al, Ge, Au and Cu were investigated using 200ev primary electrons. The specimens were deposited on a Eureka substrate maintained at 400°C to prevent contamination of the specimen by the incident electron beam. The results obtained showed that energy losses found for Al at 10.1 and 15.0ev are due to surface and volume plasma oscillations respectively. Similar conclusions were drawn concerning the 11.2 and 16.4ev energy losses found for Ge. For Au and Cu none of the energy losses observed could definitively be attributed to volume plasma oscillations, but the energy loss found at 3.6ev for Cu was identified as the surface plasma loss. No energy loss could be identified as the surface plasma loss for Au, but it is tentatively assumed to be the loss found at 3.0ev because of the time-dependence

of its intensity. Further losses found for Ge, Au and Cu are attributed to interband transitions.

The time-dependence of the spectra obtained was investigated and it was found that in all cases the specimens became contaminated as they aged. The nature of this contamination remains unidentified.

CONTENTS

ACKNOWLEDGEMENTS

The author wishes to express his gratitude to Dr. O. Klemperer for his constant encouragement throughout the course of this work and for suggesting the field of study. Thanks are due to Dr. P.C. Hedgecock for suggesting the automatic circuit for driving the electron deflection analyser, to the members of Mr. W. Shand's workshop for their skill in constructing the electron guns and analysers used, and for their helpful suggestions, and to Mr. O.R. Milbank, who carried out the glassblowing work, which included the manufacture of the high speed diffusion pump.

The author received a D.S.I.R. maintenance grant and a Research Assistantship at different times during the course of the work.

CHAPTER 1.

INTRODUCTION

When a monoenergetic electron beam is reflected from the surface of a solid, or transmitted through a thin film, the energy spectrum of the reflected or transmitted electrons is found to contain some groups of electrons which have suffered reasonably well defined energy losses in the range of about 0-50ev. These energy losses are called characteristic energy losses because they are characteristic for the solid involved and their magnitude (but not intensity) is independent of the energy of the incident electron beam and of the thickness of the material traversed (the thickness independence has an exception which is discussed later in this chapter).

The first quantitative investigation of characteristic energy losses was made by Rudberg (1930a) who observed them in the spectra of 40-900ev primary electrons reflected from various metals and metallic oxides. Rudberg's findings were confirmed by other workers also using the reflection technique with primary electrons of less than 100ev (see e.g. Haworth, 1931, and Turnbull and Farnsworth 1938). Proof that the characteristic energy losses were not just a surface effect, came when Ruthemann (1941, 1942) observed them in 2-8 kev electron beams transmitted through thin films of various materials. Since these early measurements much research has been carried out on the energy losses and various theories have been proposed to account for them. It is not proposed to

survey all the literature concerned, since this has been done adequately in a number of reviews (Marton, Leder and Mendlowitz 1955 a; Marton 1956; Pines 1955, 1956; Klemperer and Shepherd 1963; Pradal, Gout and Fabre 1965; Raether 1965) which deal with all aspects of the problems involved, both experimental and theoretical.

The earliest theory put forward to explain characteristic energy losses was the interband theory of Rudberg and Slater (1936). In this theory the energy losses are assumed to arise from single electron-electron interactions. The primary electron is considered to excite a valence or conduction electron from an occupied energy level in the material to a higher unoccupied energy level, which may lie in the same energy band or a higher energy band; these two processes leading to intraband and interband transitions respectively. Using this theory Rudberg and Slater calculated an energy loss curve for copper which was in fair agreement with Rudberg's experimental curve for energy losses <10 ev. Viatskin (1958) has developed the interband theory for weakly coupled lattice electrons and arrived at the conclusion that the incident electron can lose energy in quanta defined by

$$E_n \simeq \frac{\hbar^2}{2m} \, n^2 \quad \ldots\ldots\ldots\ldots \quad (1.1)$$

where $\frac{n}{2\pi}$ is a reciprocal lattice vector, $\hbar$ is Planck's constant divided by 2π and m is the electronic mass. Viatskin found some measure of agreement between the predicted energy losses and the measured energy losses of other authors for a number of metals. Gornyi (1957, 1961 for examples), using the reflection method with 30-260 ev primary electrons, has interpreted almost all the energy losses which he found for various

metallic oxides and germanium by using Viatskin's theory. A phenomenon closely associated with the interband theory is the fine-structure found on the short-wavelength side of the x-ray absorption edges of solids. This structure is also due to excitation of electrons (in this case bound electrons) from one energy level to higher allowed energy levels lying above the Fermi energy (see e.g. Mott and Jones 1958). Several investigators have attempted to correlate the characteristic energy losses of a material with the distances, in ev, between an absorption edge and the following absorption maxima in the fine structure (see e.g. Leder et al. 1956) with some degree of success. Gauthé (1958), however, has pointed out that the zero from which the absorption maxima should be measured is not the absorption edge but the peak of the corresponding x-ray emission band. Gauthé has identified a number of energy losses in metals using this procedure.

Sternglass (1956) put forward a theory that the characteristic energy losses were due to individual atomic ionisation and excitation processes. Leder (1957), following a suggestion by Sternglass, carried out electron energy loss experiments in metal vapours but found only energy losses corresponding to the known spectroscopic energy levels of the atoms and not to the characteristic energy losses found in the solid state, and thus did not confirm Sternglass' theory. Boersch et al. (1962) carried out similar experiments on Hg in the vapour, liquid and solid state and on Ag in the vapour and solid state. They found for both materials that there is, in particular, an energy loss in each state corresponding to the resonance line of the single atoms (Hg, 6.7 ev; Ag, 3.7e

and that the spectra in the different states are very similar, but Leder's (1957) results show that this is not generally true. However, some energy losses in metals and compounds have approximately the same values as ionisation energies of atomic energy levels (see e.g. Robins and Swan 1960 and Best 1962).

The experimental investigation of characteristic energy losses received a great stimulus in the 1950's due to the theoretical work of Bohm and Pines (1951, 1952, 1953), who considered a metal to be a solid state plasma consisting of the Fermi electron gas and the smeared out, fixed, positive ion charge. They showed that due to the long-range Coulomb interaction between electrons in the gas, the gas can execute collective longitudinal oscillations if the charge equilibrium of the plasma is disturbed. Therefore an incident electron beam can excite such oscillations, the electrons in the beam losing energy to the Fermi gas as a whole. The energy transfer in such an excitation can only take place in multiples of an elementary quantum of energy, $\bar{h}\omega_p$, which is called a plasmon, where ω_p is the angular frequency of the oscillations. Using Gaussian units,

$$\omega_p = \left(\frac{4\pi ne^2}{m}\right)^{\frac{1}{2}} \qquad \ldots\ldots\ldots\ldots\ldots\ldots\ldots\ldots (1.2)$$

Here n is the free electron density in the metal, e is the electronic charge and m is the electronic mass. Pines (1955) accounted for many characteristic energy losses in metals on this basis by assuming that all the valence electrons could be used to evaluate n in equn.(1.2). In general the agreement between the theoretical and experimental results is good for metals exhibiting sharp energy loss lines (Al, Mg, Be, Ge, etc)

but is bad for those having broad energy loss lines (Cu, Au, Ag, etc.). Here a sharp energy loss line may be defined as one having an experimental half-width of up to about three times the half-width of the energy distribution of the elastically scattered electron beam, which usually has a finite energy distribution of 1-2 ev. In the cases of aluminium and germanium, assuming 3 and 4 valence electrons respectively, $\bar{h}\omega_p = 15.8$ ev. The present author has measured these energy losses as 15.0 ± 0.2 ev and 16.4 ± 0.2 ev. The broadening and shift of the energy losses in the noble metals and transition metals has been attributed by Wolff (1953) to coupling of the s-electron plasma oscillations with the electrons in the d-band. Both s and d electrons can undergo interband transitions. Whether the plasmon energy is shifted to higher or lower energies depends on whether the interband transitions have a lower or higher energy than the plasmon respectively (Pines 1956).

The Bohm-Pines theory also predicts an angular dispersion for the plasma energy losses of the form

$$\Delta E = \bar{h}\omega_p + \frac{3}{5} \cdot \frac{E_f P^2}{m\bar{h}\omega_p} \theta^2 \qquad \ldots\ldots(1.3)$$

where ΔE is the energy loss, E_f is the energy of an electron at the top of the Fermi distribution, P is the momentum of the incident electron and θ is the angle through which the incident electron is scattered in exciting the plasmon. There is also a threshold for a maximum possible scattering angle, θ_c, given by

$$\theta_c = \frac{\bar{h} k_c}{P} \qquad \ldots\ldots(1.4)$$

where k_c is the maximum wave vector of the plasmon (cut-off wave vector)

beyond which a plasmon cannot be excited. k_c is given by Pines (1956) as

$$k_c \backsim 0.353 \; r_s^{\frac{1}{2}} k_o \qquad \ldots\ldots(1.5)$$

where r_s is the average interelectronic spacing measured in Bohr radii and k_o is the wave vector of an electron at the top of the Fermi distribution. Watanabe (1956), by means of a high energy transmission experiment, showed that the main energy losses in Be, Mg and Al, of 19, 10.3 and 14.8ev respectively, obey a dispersion relationship of the form given in equn.(1.3) and that the maximum scattering angle, θ_c, exists. He found that the corresponding loss in Ge (16.4 ev) showed an angular dependence but was not in such good agreement with theory as for the other materials mentioned. He also found that the broad energy losses of 25 ev in Au and Ag were not a function of θ and attributed them to single electron excitations. The dispersion of the energy losses in a number of materials has now been confirmed (see e.g. Schmüser 1964 and the review by Klemperer and Shepherd 1963).

Unfortunately the dispersion relation, equn.(1.3), does not offer a decisive test for determining which losses in a spectrum are caused by plasma oscillations. Viatskin (1958) derived a dispersion relationship of the form of equn.(1.3) for interband transitions and Creuzburg and Raether (1964a) have found that single electron transitions in the alkali halides do in fact exhibit such a dispersion.

Ferrell (1956, 1957) predicted that the differential scattering cross section, $d\sigma/d\Omega$, per valence electron, for scattering of an incident electron into a solid angle $d\Omega$ due to excitation of a plasmon, is given

by:-

$$\frac{d\sigma}{d\Omega} = \frac{1}{2\pi a_o n} \frac{\theta_E}{\theta^2+\theta_E^2} G(\theta,\theta_c)^{-1} \quad \ldots\ldots\ldots\ldots\ldots\ldots\ldots\ldots (1.6)$$

where $\theta_E = \Delta E/2E_o$, where $\Delta E = \hbar\omega_p$ and E_o is the incident electron energy, a_o is the Bohr radius and n is the free electron density. The factor $G(\theta,\theta_c)^{-1}$ decreases with θ and becomes zero at θ_c. Ferrell points out that the differential cross section for interband transitions will not differ greatly from that given in equn.(1.6). However, no cut-off angle, θ_c, has been predicted for interband transitions, therefore the factor $G(\theta,\theta_c)^{-1}$ would not be expected in this case. Early transmission experiments by Marton et al.(1955b) and Watanabe (1961) showed that the intensity of the 15 ev loss in Al and the 24 ev loss in Au decreased rapidly with scattering angle, θ. Kunz (1962) and Schmüser (1964) later verified equn.(1.6) for the main energy losses in Al, Mg and Si. Creuzburg and Raether (1964b) showed that for single electron excitations in the alkali halides the angular dependence of the intensity of the energy losses could also be expressed as a function of $1/(\theta_E^2+\theta^2)$, thus confirming Ferrell's (loc.cit.) prediction. Therefore the intensity distribution of the energy losses in a spectrum cannot be depended on to differentiate between plasma and interband energy losses.

Ritchie (1957) showed theoretically that in the region of the surface of a metal the frequency of the plasma oscillations should be modified. In the case of the metal specimen being a thin plane foil, the angular frequency of the plasma oscillations should be reduced from ω_p to $\omega_p/2^{\frac{1}{2}}$ at the surface of the foil and if the specimen is an agglomeration of spheres it should be reduced to $\omega_p/3^{\frac{1}{2}}$. Powell and Swan (1959a,b),

using the electron reflection technique to determine the characteristic losses of freshly evaporated plane films of Al and Mg, verified the existance of the energy loss at approximately $\hbar\omega_p/2^{\frac{1}{2}}$; this loss will be called a surface loss, or surface plasmon, in distinction to $\hbar\omega_p$ which will now be called a volume loss or volume plasmon. Powell and Swan (loc.cit.) also observed that the surface loss in Al fell below $\hbar\omega_p/3^{\frac{1}{2}}$ for very thin films (< 20 Å) where agglomeration of the film was expected, but the substrate may have influenced these results. In addition they verified another of Ritchie's predictions, namely that the ratio of the intensity of the surface plasma loss to that of the volume plasma loss increases as the thickness of the film decreases.

The surface plasma energy loss was investigated further theoretically by Stern and Ferrell (1960), who showed that the presence of contamination on the surface of a metal film would modify Ritchie's surface loss to $\hbar\omega_p/(1+\varepsilon)^{\frac{1}{2}}$, where ε is the dielectric constant of the contaminating layer; if $\varepsilon = 1$ (the bounding layer being a vacuum) then this expression is identical to Ritchie's. This was verified experimentally by Powell and Swan (1960) when they observed that surface oxidation of Al and Mg specimens results in the rapid disappearance of Ritchie's surface loss (10.3ev in Al and 7.1ev in Mg) and the appearance of Stern and Ferrell's modified surface loss (7.1ev in Al and 4.9ev in Mg). This experiment of Powell and Swan solved the problem of the identity of the 7ev energy loss which is usually observed, in addition to the 15ev loss and its multiples, in electron transmission experiments on Al (see Mendlowitz 1959). In most

transmission experiments the thin film specimens are prepared in a separate vacuum system and then transferred to the spectrometer for the energy loss measurements. The specimens thus oxidise when exposed to air during the transfer process and may also be contaminated by the substrate onto which they have been evaporated and which has subsequently been solved off. Wagner et al.(1960) performed a transmission experiment on oxide-free Al films and observed the 10ev surface loss which was superceded by the modified loss of 7ev on oxidation of the film. No gradual transition is observed between the two surface loss values; as the Ritchie loss disappears the Stern and Ferrell loss appears at its proper value.

Ritchie (1957) also showed that in a thin film of thickness d the surface plasma waves of the two opposite surfaces can interact with one another and cause a splitting of the surface wave frequency after the manner of coupled oscillators. The frequencies he obtained are

$$\omega_{\pm} = \frac{\omega_p}{2^{\frac{1}{2}}} (1 \pm e^{-Kd})^{\frac{1}{2}} \quad \ldots\ldots\ldots\ldots\ldots\ldots\ldots\ldots \quad (1.7)$$

where K is the wave number of the surface wave. For $Kd \ll 1$ there should be a measurable splitting. This is the exception, mentioned at the beginning of this chapter, to the independence of the energy loss values on the thickness of the material traversed. In transmission experiments K can be determined from the scattering angle, θ, of the primary electron after it has passed through the foil, by means of the relationship $K = K_{el}\theta$, where K_{el} is the wave vector of the incident electron. Schmüser (1964) has modified equn.(1.7) to take into account the effect of surface contamination and has confirmed that such splitting of the

modified surface loss of Al does in fact take place as Kd is decreased. Schmüser used 40kev electrons transmitted through films of 30 to about 150Å thick.

Stern and Ferrell (1960) give the differential probability for the excitation of surface waves on a single surface (this corresponds to Kd< 1) as

$$\mu = \frac{dP}{d\Omega} = \frac{e^2}{\pi \hbar v} \quad \frac{2}{1+\varepsilon} \quad \frac{\theta_E \theta}{(\theta_E^2+\theta^2)^2} \cdot \int \qquad \text{.....(1.8)}$$

where θ_E in this case is $\Delta E/2E_0 \backsim \hbar\omega_p/2E_0(1+\varepsilon)^{\frac{1}{2}}$, e is the electronic charge and v is the velocity of the incident electron. $\int$ is a correction factor for the case of non-normally incident electrons and is a function of θ, α and φ , where θ is the scattering angle (polar angle), α is the angle between the incident electron and the normal to the surface and φ is the azimuthal angle. There are several differences between equn.(1.8) and the corresponding equn.(1.6) for volume oscillations. Equn.(1.8) is dependent on α and φ whereas equn.(1.6) is not. If $\alpha=0$ (normal incidence) then $\int = 1$ and it is seen that $\mu = 0$ for $\theta = 0$, therefore an electron passing normally through the foil without deviation cannot excite surface waves. Also, for $\theta_c > \theta > \theta_E$ equn.(1.8) becomes a function of θ^{-3}, whereas equn.(1.6) becomes a function of θ^{-2} in the corresponding region. Therefore the intensity of the surface loss should decrease more rapidly with increasing θ than the volume loss. Geiger (1961) found that the intensity of the 3.6ev energy loss in Ag was a function of θ^{-3}; this has also been found for the modified surface loss in Al (Kunz 1962, 1964), for the low-lying losses (~5ev) in Ge and Si (Creuzburg 1963) and for the modified surface loss in Mg (Schmüser

1964). Such measurements can only be made using high energy transmission experiments. Due to the fact that $\int$ is a function of φ, when $a \neq 0$ the intensity distribution of transmitted electrons which have excited surface plasma waves is not symmetrical with respect to the incident electron beam. Hence for a beam scattered through a fixed angle Θ, the intensity of such electrons is not equal in the opposite azimuths, $\varphi = 0^{\circ}$ and $\varphi = 180^{\circ}$, where $\varphi = 0^{\circ}$ is defined by the plane containing the normal to the film and the direction of the incident electron. This has been confirmed for the low-lying losses of 6.3ev in Al and 3.6ev in Ag by Kunz and Raether (1963) and by Kunz (1964), also for the low-lying losses in Si and Ge by Creuzburg (1963) and for the 5.5ev modified surface loss in Mg by Schmüser (1964).

A further method of identifying the surface and volume plasma losses in solids is to perform high energy transmission experiments on specimens of varying thickness, due to its nature the intensity of the surface loss should remain constant for different film thickness but that of the volume loss should increase with thickness. This has been demonstrated by Kunz (1962)for the 6ev and 15ev energy losses in Al. He also showed that the 3.6ev loss in Ag was independent of film thickness. The study of the low-lying losses in solids, i.e. those energy losses less than about 12ev, has shown therefore that many of them behave in a manner characteristic of surface plasma losses.

It was found by Rudberg and Slater (1936) that when the excitation energy (energy loss) is small compared with the energy of the incident electrons, the transition probabilities approach those for excitation

by electromagnetic radiation which lead to optical absorption. Therefore maxima in the optical absorption curves for solids should correspond to energy losses suffered by incident electrons. Optical absorption frequently corresponds to single electron interband transitions. If the solid is treated as a dielectric with complex refractive index n-ik and with a complex dielectric constant $\varepsilon = \varepsilon_1 + i\varepsilon_2$, where all quantities are frequency dependent, the rate of loss of energy to the solid due to optical absorption is proportional to $\varepsilon_2 (= -2nk)$, (see e.g. Seitz 1940). However, due to the fact that incident electrons polarise the solid they are traversing, while photons do not, Hubbard (1955a,b) and Fröhlich and Pelzer (1955) showed that the rate of energy loss, dW/dt, to the solid from incident electrons is proportional to $\varepsilon_2/(\varepsilon_1^2+\varepsilon_2^2)$, or,

$$\frac{dW}{dt} \propto -\mathrm{Im}(1/\varepsilon) = \frac{2nk}{(n^2-k^2)^2+4n^2k^2} \qquad \ldots\ldots\ldots\ldots\ldots\ldots\ldots\ldots (1.9).$$

They also find that the condition for plasma oscillations to occur is

$$\varepsilon = 0 \qquad \ldots\ldots\ldots\ldots\ldots\ldots\ldots\ldots\ldots\ldots\ldots\ldots (1.10),$$

remembering that ε is frequency dependent. Now the denominator of equn.(1.9) is equal to $|\varepsilon|^2$, thus when plasma oscillations occur there is a maximum in the energy loss function, $-\mathrm{Im}(1/\varepsilon)$, also it can be seen that the numerator simply corresponds to the optical absorption (or interband) energy loss function. The dielectric formalism naturally accounts for both plasma and interband types of characteristic energy losses. The dielectric constant of the solid is assumed here to be the same for the electromagnetic radiation (transverse phenomenon) and for

the electron beam (longitudinal phenomenon). The condition for the existance of surface plasma oscillations to occur at the interface of a material with dielectric constant ε_A and one with dielectric constant ε_B, is given by Stern and Ferrell (1960) as

$$\varepsilon_A + \varepsilon_B = 0 \quad \ldots\ldots\ldots\ldots\ldots\ldots\ldots\ldots\ldots\ldots\ldots\ldots (1.11),$$

which reduces to $\varepsilon_A + 1 = 0$ for a surface bounded by a vacuum ($\varepsilon_B = 1$). Moreover, Hubbard (1955b) has derived an expression for the differential scattering cross section for either interband or plasma energy losses which is of the form $A.\mathrm{Im}(1/\varepsilon).\theta_E/(\theta^2+\theta_E^2)$, where A is a constant. This has the same dependence on the angle θ as equn.(1.6) and verifies that this is the same for both interband and plasma losses. Using the dielectric theory, Wilson (1960) has shown that the presence of an absorption band may shift the plasma frequency to either higher or lower frequencies or may completely screen out the plasma energy loss.

Measurements of the optical constants of Al in the ultra-violet region by Ehrenreich et al.(1963) fully confirm that the 15ev loss in Al is due to volume plasma oscillations. Similar measurements by Philipp and Ehrenreich (1963a) establish that the energy losses in Si and Ge at 16-17ev are due to volume plasma oscillations. Energy loss curves of 50kev electrons transmitted through 1000Å films of KCl and KBr obtained by Creuzburg and Raether (1964b) show remarkable similarity to the curves calculated from the optical data of Ehrenreich et al. (1963) and Philipp and Ehrenreich (1963b), showing the presence of exciton excitations and plasma oscillations. The correctness of the dielectric approach now seems to be established, but quantitative

comparisons between the theory and experiment have been made for only a few materials (see the reviews by Raether 1965 and Pradal et al. 1965) because there are, as yet, insufficient optical data available. Ferrell (1956) pointed out that solids should become transparent to electromagnetic radiation at the plasma frequency and he discussed this for the case of the alkali metals, while the experiments of Ehrenreich et al.(1963) verify this fact for Al.

There are now several methods of identifying plasma oscillations as the cause of energy losses in solids but it should be mentioned that the experimental verification of the existance of surface plasma losses provided one of the most convincing arguments for the validity of the plasma theory of the characteristic energy losses.

Some results on the mean free path for the production of a given energy loss, as obtained in high energy electron transmission experiments, could be interpreted in terms of either the plasma or interband theories (see the review by Klemperer and Shepherd 1963). However, Pines (1956) showed that for a sharp energy loss caused by interband transitions, the mean free path should be greater than that predicted by the plasma theory for a loss of the same magnitude. Creuzburg and Raether (1964a) have verified this for the 13.6ev loss in LiF, which they found to have a mean free path for excitation about one hundred times that predicted by the plasma theory at a primary beam energy of 50kev.

High energy transmission experiments have been used almost exclusively in recent years for the investigation of characteristic

energy losses. In these experiments electron beams of 10-100kev are transmitted through specimens of thickness from about 30 to 1000Å. As mentioned earlier, the specimens are usually contaminated on their surface because they cannot be prepared "in situ" in the vacuum of the spectrometer. The apparatus required for such experiments, where the dispersion and angular intensity distribution of the energy losses is measured, is highly refined. A specific energy resolution of the order of 1 part in 10^5 is required for the higher energy beams. Moreover, an angular resolution of better than θ_E of equn.(1.8) is required for the measurement of angular dispersion curves, since θ_E determines the shape of these curves (equns. 1.6 and 1.8). For instance, for the investigation of the 7ev modified surface loss in Al, using 20kev electrons, $\theta_E = 0.2$ milliradians, therefore the primary beam aperture must be less than 0.2 milliradians and as the primary energy is increased so the angular resolution must be improved upon. Brief surveys of such spectrometers are to be found in the papers by Klemperer and Shepherd (1963) and Klemperer (1965). The experimental and design problems are thus difficult and the experiments themselves, such as the measurement of the asymmetry of the surface loss intensity with scattering angle, or the splitting of the surface plasma frequency with decreasing speciment thickness (equn.1.7), are lengthy and difficult to perform.

The transmission experiments provide quantitative data which can be compared directly with theory. The results obtained by Powell and Swan (1959a,b), however, have shown that the low energy reflection

type of measurement offers a simple, direct, method of identifying the surface and volume plasma energy losses. In Powell and Swan's method low energy electrons (2020ev - 750ev) are reflected from specimens freshly evaporated onto a tantalum substrate. Electrons scattered through a fixed angle of 90° are analysed by an electrostatic deflection method. Powell and Swan showed that as the primary energy was decreased, the ratio of the surface plasma loss intensity to the volume plasma loss intensity increased. They attributed this to the fact that the penetration depth of the incident electrons decreases as the primary energy decreases, thus reducing the probability of excitation of volume plasma oscillations.

The experiments performed by the present author make use of the fact that the penetration depth of an electron beam incident on a specimen varies with the angle of incidence of the beam. This avoids the necessity of varying the primary energy of the beam, which affects the complete recorded energy spectrum and not just the losses in which the interest lies. The penetration depth of the incident beam decreases as its angle of incidence (measured with respect to the normal of the specimen surface) increases. One would expect the intensity of the surface plasma energy loss to increase with increasing angle of incidence and that of the volume plasma loss to decrease. The reflection angle at which the scattered electrons are collected is kept approximately equal to the incidence angle. The effect on interband transitions of varying the incidence and reflection angles of the primary beam is not known exactly. The interband transitions will

take place irrespective of the incidence angle and should be expected to appear with about equal intensity, with respect to the zero energy loss intensity, at all angles. Any variation in intensity will only be due to variation of the effective distance travelled in the specimen by the primary beam as the incidence angle is varied. But since the primary energy is kept constant in the present experiments one would not expect this distance to change appreciably. Also keeping the primary energy constant means that the mean free path for production of any type of energy loss remains constant throughout. It is thus anticipated that the intensity of interband transitions should not vary appreciably with variation of the incidence angle of the primary beam.

The experiments described here in later chapters were performed with 200ev primary electrons. The materials investigated were Al, Ge, Au and Cu. By using a low primary energy the surface plasma losses of the investigated materials were expected to appear strongly in their energy loss spectra since the incident electrons penetrate very small distances into the specimen surface. By extrapolation of the data of Young (1956) for Al, the range of 200ev electrons in this material is found to be only 52Å. Since in the present experiments the recorded electrons must be reflected in order to leave the specimen again, the penetration depth for the recorded electrons must be about 25Å, i.e. of the order of ten atomic layers on average. Therefore surface effects would be expected to be prominent.

Using the reflection method of measurement allows freshly evaporated specimens to be investigated, which is an advantage over the

transmission method. However, the dispersion and intensity relationships, equns.(1.3) and (1.6 and 1.8) cannot be verified by this method. At a primary energy of 200ev the maximum angle, θ_c (equn.1.4), through which an incident electron can be scattered after exciting a volume plasmon in Al is about 7°, therefore such an electron must suffer at least one additional scattering collision in the specimen before it can escape from the specimen surface again. The plasma energy losses thus measured are the average values of the loss given by equn.(1.3) integrated over all scattering angles up to θ_c. For such a low primary energy the energy analyser needs a specific energy resolution of the order of only 1 part in 100 to be able to resolve the characteristic energy losses.

Very little previous work has been done on the effect of the angles of incidence and reflection of the primary beam on the characteristic energy loss spectra. Rudberg (1930a), in his original low energy reflection measurements on characteristic losses, found that the energy loss values for Cu, Ag, Au and Pt were independent of the scattering angle and of the orientation of the target, but he made no measurements on the intensities of the energy losses. Turnbull and Farnsworth (1938) discovered that the intensity of the characteristic energy losses and of the inelastically scattered background, increased in the region of diffraction maxima observed for slow electrons reflected from an Ag single crystal. This occurs also in transmission as shown by the experiments of Marton et al.(1955b) on polycrystalline Au films. Creuzburg and Raether (1963) performed 50kev reflection

experiments on Si(111) cleavage surfaces and analysed the energies of the electrons scattered into the Bragg reflection spots. They found that the intensity of the surface plasma energy loss (~10ev) was dependent on the order (nnn) of the reflection spot investigated; decreasing as n increased. The surface plasma loss was thus more intense for smaller scattering angles, the incidence angle being about 1°. They also found, by etching the surface of the crystal, that the intensities of the volume and surface losses were dependent on the surface roughness of the crystal. The volume loss becoming predominant at all scattering angles as the surface roughness increased and the angular dependence of the surface loss becoming much less pronounced. Klemperer and Thirlwell (1966) have published some preliminary results of the present investigation. They showed that the intensities of the surface and volume plasma losses observed in a 200ev electron beam reflected from freshly evaporated Al specimens were strongly dependent on the angles of incidence and reflection of the electron beam. With incidence and reflection angles of ~80° (i.e.20° scattering) the energy loss spectrum was found to consist entirely of surface plasma losses, while at 45° incidence and reflection angles (i.e.90° scattering) both the surface and volume losses were present. Independently and almost simultaneously, Powell (1965a,b) reported similar reflection experiments with 8kev electrons. He investigated Al and Bi, reflecting the electrons from the molten metals and from the solid metals, as frozen from the molten state. He measured the reflected energy loss spectrum for a range of total scattering angles between 2° and 70°.

At large scattering angles he found that the volume plasma loss predominated the spectrum, while at small angles the excitation of the surface loss was predominant. He also found that if he evaporated a layer of the metal on top of the frozen solid then the volume loss was predominant at all scattering angles. The explanation for this being that the surface of the evaporated layer is not as smooth as the molten metal surface or that of the solid frozen from the molten state. This is in agreement with Creuzburg and Raether's (1963) findings mentioned above. The reason that Klemperer and Thirlwell (loc.cit.) observe a strong intensity effect using freshly evaporated Al layers while Powell (1965a) does not, is due to the much greater wavelength and smaller penetration depth of the 200ev electrons employed in the present experiments compared with the 8kev electrons used by Powell. Specimen surface roughness is thus much less important as a factor in the excitation probabilities of the plasma losses. Therefore, for the identification of plasma energy losses by the investigation of the reflected intensities of energy losses with scattering angle, the low energy method of Klemperer and Thirlwell offers the advantage, over the high energy methods, of ease of preparation of the specimen.

Finally, it should be mentioned that Ferrell (1958) predicted that plasma oscillations in metal films can decay by emission of a photon of energy equal to the plasmon energy. The intensity of the emitted radiation is an oscillatory function of the film thickness and a function of the angle of emission of the photon with respect to the foil normal. This was verified by Steinmann (1960) and Brown et al.

(1960) for Ag foils bombarded normally with 22 and 25kev electrons. Steinmann found a peak at 3300Å in the emitted radiation intensity (Brown et.al. found a value of 3400Å) which corresponds well with the energy of the volume plasmon in Ag, which is 3.75ev (3290Å) as obtained from the optical measurements of Ehrenreich and Philipp (1962). It was later shown theoretically by Stern (1962) and Ritchie and Eldridge (1962) that the peak in the radiation at the plasma frequency could be accounted for by transition radiation, but Stern (loc.cit.) pointed out that Ferrell's (1958) calculation is correct but the transition radiation treatment includes all radiation from the metal film and is thus more general. Ritchie and Eldridge (loc. cit.) show that the generalised transition radiation theory produces the same results as Ferrell's theory if the dielectric constant of the metal film is taken as the free electron gas value. The peak in the transition radiation and the plasma radiation peak are thus identical. Experiments by Arakawa et al.(1964) on a 660Å thick Ag film with 40kev electrons showed that the radiation spectrum in the region of photon wavelengths 2,500-5,600Å could be interpreted entirely on the basis of transition radiation, whereas for a 1980Å film the radiation was mainly due to bremsstrahlung. Boersch et al.(1965) carried out similar experiments with 6-40kev electrons on Ag films 20,000 to 50,000Å thick and concluded that for normal incidence of the electron beam the radiation spectrum could be separated into transition radiation and bremsstrahlung. However, they also found that for oblique incidence on the specimen (0.5° against the specimen surface) a new peak appears

in the radiation spectrum at 3,500Å which is 100x greater than the transition radiation peak for normal incidence. This corresponds to an energy of 3.55ev which agrees well with the surface plasma energy loss value of 3.60ev (see the review by Raether 1965, for an account of the energy loss spectrum of Ag). Jones et al.(1966) have confirmed these results using Ag foils several thousand angstroms thick. Hence it seems we now have another method of determining the volume and plasma energy losses of a solid by means of variation of the incidence angle of the primary electron beam on the specimen.

It seems that in the future, when the experimental difficulties of measuring the optical constants and radiation from electron bombarded specimens in the far ultra-violet are overcome, these two techniques, which were greatly stimulated by the original electron energy loss experiments, will provide effective complementary methods in the study of electronic transitions in solids.

CHAPTER 2.

BASIC APPARATUS AND PRECAUTIONS

2.1 Vacuum Apparatus

The vacuum system used in the following experiments was set up by the author and was of a standard demountable type. The work chamber was a 12" glass bell-jar, vacuum sealed to an alumium alloy base plate by means of an L-shaped neoprene rubber gasket. It was evacuated by means of a 2" glass-mercury diffusion pump, of the type described by Bull and Klemperer (1943), which was backed by a gas-ballast rotary pump. In the neck of the diffusion pump, between the pump and the work chamber, was situated a liquid nitrogen trap which is shown in Fig. 2.1. It can be seen there that it is impossible for any backstreaming mercury vapour to pass through the trap to the work chamber without striking a cooled surface, therefore, assuming 100% condensation, no mercury should reach the work chamber. The liquid nitrogen trap also increases the pumping speed of the system, since it condenses out water vapour and also hydrocarbons which may reach it from the rotary pump oil or from the rubber seals used in the system. The fore-vacuum pressure was measured by means of a nichrome-eureka thermocouple gauge, which was calibrated against a Pirani gauge. The high-vacuum in the work-chamber was measured with a magnetic ion gauge of the type described by Klemperer (1943). The

magnetic field for this gauge was produced by a solenoid so that it could be switched off while experiments were being performed in the work chamber. Rotary shafts and electrical connections required in the work chamber were led in through the base plate.

In order to accomodate the large number of electrical leads required in the work chamber a vacuum lead-in capable of carrying up to nine leads was designed and is shown in Fig.2.2.

The vacuum obtained in the work chamber under normal conditions was $2-3 \times 10^{-6}$ mm of mercury.

2.2 Evaporation Equipment

To produce the freshly evaporated specimens of material required for the electron reflection experiments to be described, an evaporation source was required inside the work chamber. Materials to be investigated were evaporated either from $\frac{1}{2}$ mm tungsten tri-stand, V-shaped, filaments or from $\frac{1}{2}$ mm tungsten conical basket filaments as described by Holland (1960). The specimen evaporation filament, F_1, is shown in Figs. 5.5(a) and (b), where a second evaporation filament, F_2, can also be seen which was used for firing a getter before evaporation of the specimen onto the target, T. F_2 was positioned so that the getter covered a large area of the work chamber when it was fired but did not reach the region in which the experiments were performed. F_1 was shielded by the eureka mask, M, containing an aperture which could be covered by the moveable shield, MS. In this way the target, T, was only exposed to the filament F, during the actual evaporation of a specimen.

2.3 Degaussing Coils

It was necessary to compensate for the magnetic field in the laboratory over the volume in which the experiments were performed. For this purpose a pair of concentric circular coils was designed according to data given by Craig (1947). Each coil was of 52 cm diameter and consisted of 100 turns of enamelled copper wire (S.W.G.24). The coils were separated by an axial distance of 25 cm, which is just smaller than the separation required for Helmholtz coils (see Fig.2.3). Using this separation the coils can produce an almost uniform magnetic field over an area of radius 7.6 cm in the mid-plane at the centre of symmetry of the coils. According to Craig's calculations, for two ideal current loops the deviation from field uniformity is 0.1% at the edge of the region and the field produced is uniform to about 1% for distances up to approximately 1.5 cm on either side of the mid-plane of the coils over this region.

The coils were mounted as shown in Fig. 2.3 so that the axis of the coils was lined up in the direction of the magnetic field present in the laboratory; this direction was measured with a dip-circle and the angle of dip was found to be $75^{\circ}59'$ at the centre of the work chamber. The calibration of the coils, with a search coil and sensitive galvanometer, showed that the magnetic field present in the work chamber could be compensated to less than 1% over the mid-plane of the coils up to a radius of 7.5 cm from the axis. The residual magnetic field was calculated to be 4×10^{-3} oersted.

In the following experiments the electron orbits never deviated

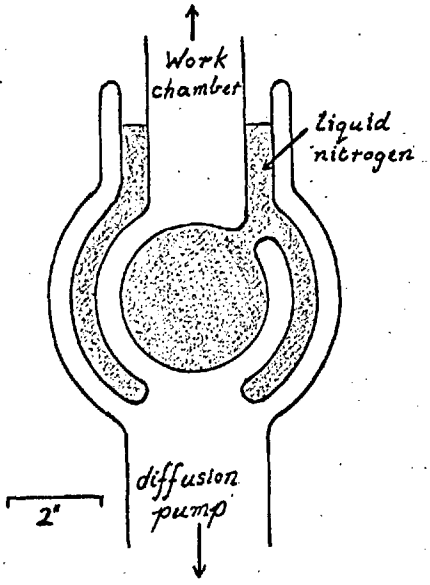

Fig 2.1

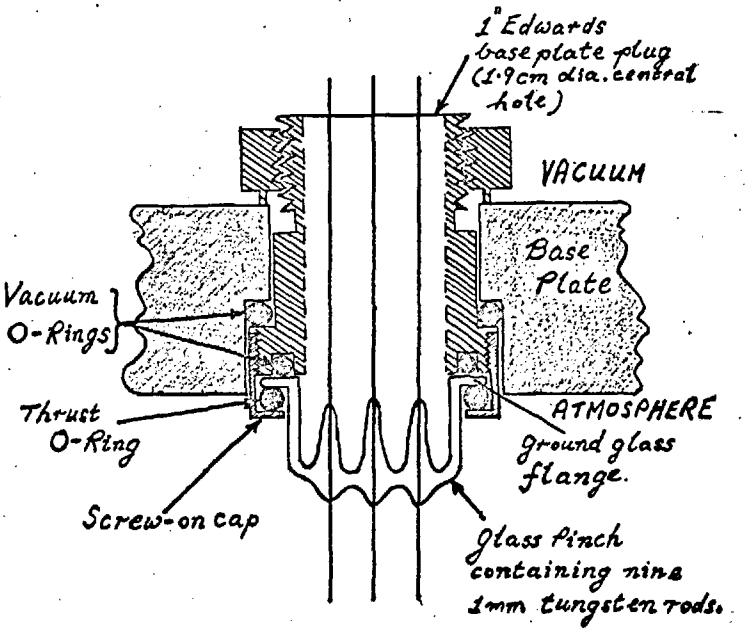

Fig 2.2

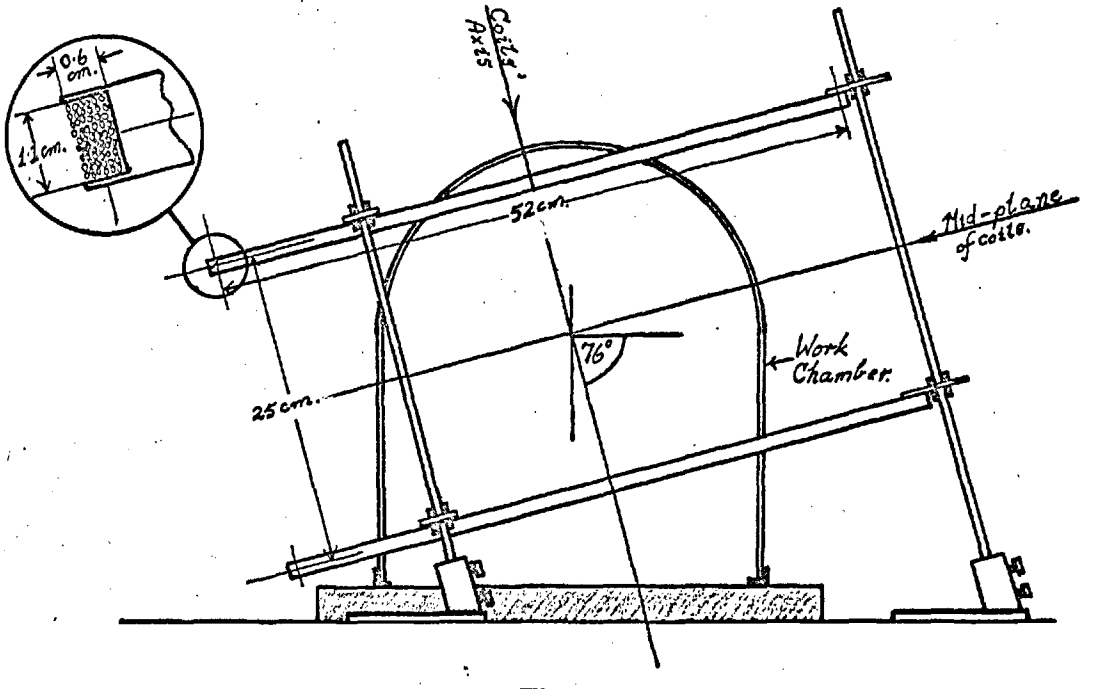

Fig 2.3

more than 0.5 cm from the mid-plane of the coils and never more than 7.0 cm from the axis.

In some of the preliminary experiments (Ch.5) the degaussing coils were mounted in a horizontal position and only the vertical component of the magnetic field present in the laboratory was compensated.

2.4 Elementary Precautions

In order to avoid disturbances of the slow electrons used in the experiments, all materials used in the vicinity of the work chamber were surrounded by earthed shields. The leads themselves were either P.T.F.E. covered or insulated with ceramic beads. All electrical lead-ins through the work chamber base plate were shielded by earthed caps. The inside of the glass bell-jar was electrostatically shielded by means of an earthed stainless steel gauze cage which fitted the bell-jar.

The usual cleanliness precautions required for vacuum work were observed. Articles for use in the work chamber were cleaned and degreased in acetone and thereafter only handled with rubber gloves on.

CHAPTER 3.

ELECTRON GUNS INVESTIGATED

3.1 Introductory Remarks concerning Spectrometer Components.

The essential equipment needed for the electron reflection experiments which were carried out consists of an electron gun, a specimen from which the electron beam projected from the gun is scattered, an electron energy analyser to measure the energy spectrum of the reflected electrons and an electron detector to measure the amount of current transmitted by the analyser. This complete arrangement is called a spectrometer. In this chapter the electron guns which were investigated will be discussed.

3.2 Requirements to be fulfilled by the Electron Gun

The electron current required in the beam projected by the gun depends on the geometry and type of spectrometer used and on the sensitivity of the electron detector. Order of magnitude calculations indicated that in this case a minimum current of 10μA, contained in a beam of total divergance of about 6° or less, was required. Also the beam energy was required to be variable between about 100 to 500 ev.

3.3 Evaluation of Low Energy Electron Beams. A Post-acceleration Target

To make observations on the size and shape of the low energy electron

beams used, a willemite phosphor screen was employed. Owing to the fact that the light output from the phosphor is dependent on the energy of the incident electrons striking it and is weak for electron energies of the order of 100 ev, a post-acceleration technique (see e.g. Butterworth 1964) was used to make the electron beam visible on the screen. The type of post-acceleration target constructed is shown in Fig.3.1. The willemite phosphor was deposited on the front surface of the circular glass plate, P, with a surface density of 1 mg./sq.cm. G_1 and G_2 are gauzes of non-magnetic stainless steel with pitch 0.5 mm and wire diameter 0.1 mm. G_2 is in contact with P but insulated from G_1 and the brass annulus supporting P by annular layers of mica, M , about 0.5 mm thick. Three clamps, C, of which one is shown, held the assembly together. G_1 was situated 1 mm in front of G_2. S is a eureka electrostatic shield connected to the copper gauze lining, D, of the vacuum chamber, W, by the contact spring, K. L is the electrical connection to G_2.

When observing an electron beam with the target, the gauze D, and hence G_1 and S, is connected to the final accelerating anode of the electron gun producing the beam, thus maintaining a field-free space between the gun and the target. An accelerating potential is applied between G_1 and G_2 such that electrons passing through G_1 are accelerated up to an energy of about 1 kev before they strike the phosphor. Thus low energy electron beams can be rendered visible on the screen. The distortion to the beam shape due to the field between G_1 and G_2 was neglected in measurements made using this target.

An estimate of the total current carried by an electron beam can be made by connecting the gauzes G_1 and G_2 together and isolating the target from D. The current to the target is then approximately that of the incident electron beam. In this case a small accelerating potential, dV, applied between the last anode of the gun and the target prevents escape of secondary electrons from the target. dV varies with the primary energy of the beam being investigated and was found to be +30V for a 450 ev beam and +10V for a 200 ev beam. By keeping the distance between the gun and target large, of the order of 10 cm, the field produced by dV had little effect on the current produced by the guns investigated, since these were of the diaphragm type with anode apertures of the order of 1 mm diameter.

3.4 A Tetrode Gun

Two tetrode guns were built based on a design by Bland (1961). The second of these is shown in Fig. 3.2. The gun contained three circular diaphragm electrodes which were the grid, U, and the two anodes, A_1 and A_2, each with a 1.0 mm diameter central aperture and made from non-magnetic stainless steel. These electrodes were supported in a tubular insulator, B, made from pyrophillite. The leads, L, to the electrodes were spot-welded to them and passed through holes in B. The source of electrons was a tungsten hairpin filament, F, of 0.1 mm diameter tungsten wire, which was spot welded to two 1 mm diameter eureka supports, W, held in the pyrophillite base, P. A shield, S, connected to the grid, U, attenuated any stray fields which could have reached the filament, F, and also prevented electrostatic charging up of the pyrophillite around

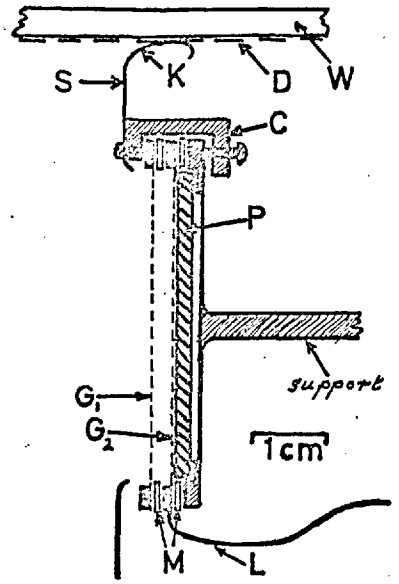

Fig 3.1

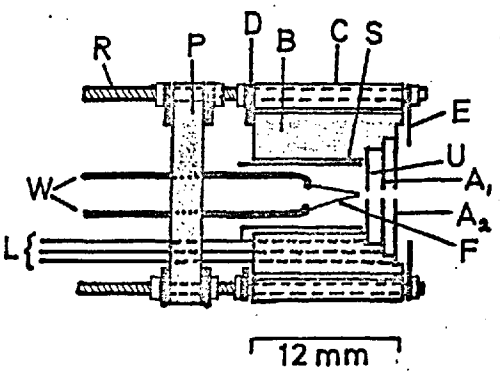

Fig 3.2

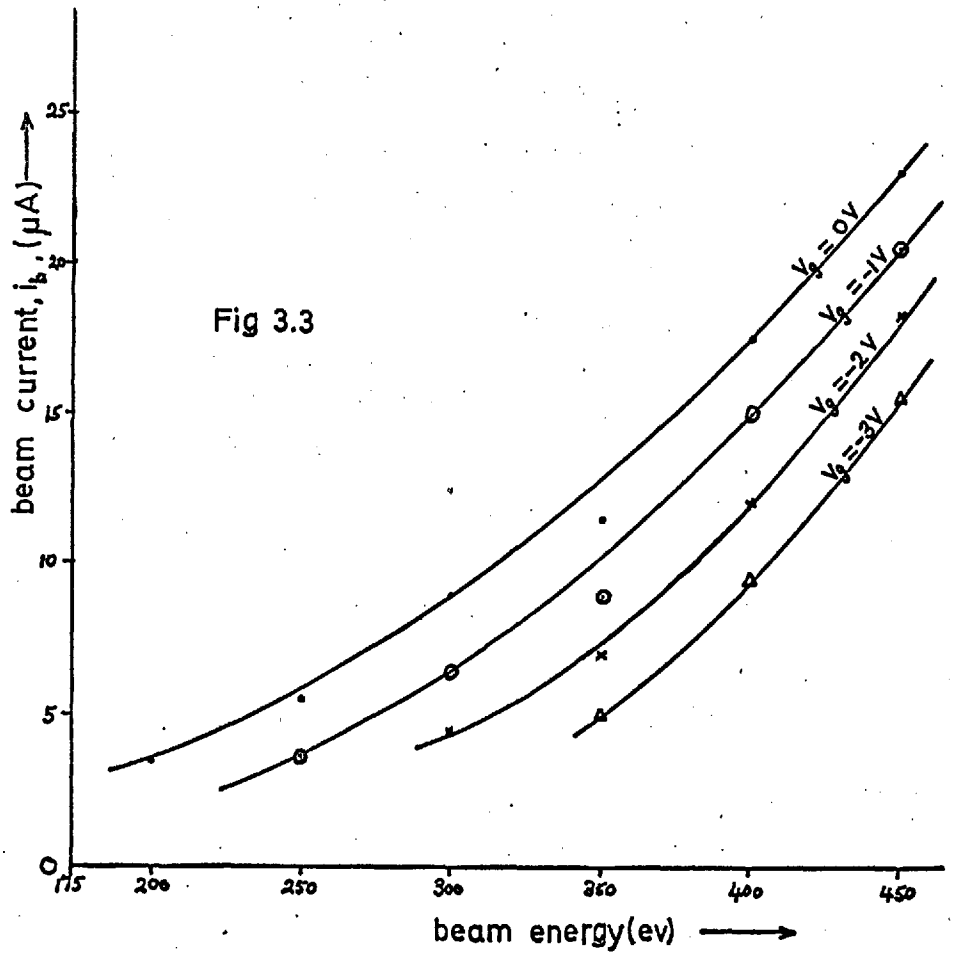

Fig 3.3

the filament. B slotted into a cylindrical copper collar, C, and was held in position by two copper end plates, D and E, which fitted onto three threaded rods, R, passing through C and were clamped by nuts. The base, P, was held in a similar fashion and could be moved to adjust the filament to grid separation and to align the filament with the holes in the electrodes. The diaphragms and the supports, W, were cemented to the pyrophillite by gun cement.

The separation of the elctrodes was as follows:-

Filament tip to U = 0.5 mm.

U to A_1 = 2.3 mm.

A_1 to A_2 = 1.4 mm.

where all the measurements were with respect to the sides of the electrodes furthest from the filament

3.5 The Performance of the Tetrode Gun

The gun was tested using the post-acceleration target described in Sect.3.3. The filament of the gun was a.c. heated. The voltages required on the electrodes to focus the thermionic emission from the cathode into an electron beam were provided by the necessary d.c. power supplies. The grid could be at filament potential or biased with a voltage, V_g, with respect to the filament.

There are two possible methods of producing a focussed beam of low voltage. The first method uses a saddle-field (see Simpson and Kuyatt 1963) whereby the electrons are accelerated between the filament and the first anode, A_1, and then decelerated to the final energy between A_1 and

the second anode, A_2. In the second method the electrons are accelerated between the filament and A_1 and then further accelerated between A_1 and A_2 to the final energy; both of these methods were investigated. The gun was always operated with the filament at a negative potential and A_2 at earth potential.

It was found in the case of saddle-field operation that the gun produced a very divergent beam unless the grid, U, was highly negative with respect to the filament. For beam energies between 100 ev and 300 ev, with U at zero volts with respect to the filament ($v_g = 0V$), at optimum focussing, the beam had a divergence of 12°. The emission current was 30 μA under these conditions and was temperature limited due to the strong field between A_1 and the filament. The focussing conditions were:-

Electrode	F	U	A_1	A_2
Voltage	V_f	V_f	$-3.9V_f$	0

where V_f is negative and $|V_f|$ is the final beam voltage. The divergence could be reduced by putting a negative bias on U, but at 300 ev the divergence was only reduced to 10° by a negative bias of -13.6V, whereas the emission current was reduced from 30μA to 20μA. At 100 ev the beam divergence was reduced from 12° to 5° by applying a grid bias of $v_g \doteq -12V$ but the emission current was reduced from 30μA to 5μA. This mode of operation was not considered satisfactory.

At a beam energy of 20 ev the beam current was found to be approximately 0.7μA and the beam divergence 7°.

The second method of operation was then investigated. There the beam could be focussed with the following conditions:-

Electrode	F	U	A_1	A_2
Voltage	V_f	V_f	$0.8V_f$	0

The beam divergence was 4.4° and these conditions held for the whole of the energy range investigated between 25 and 450 ev. In this case the emission current from the filament was space charge controlled. The current in the beam, i_b, was measured. This is shown in Fig.3.3 as a plot against beam energy and as a function of the grid bias voltage, V_g. The minimum useful working energy with $V_g = 0V$ was of the order of 200ev. These conditions were considered preferable to the saddle-field conditions and were normally used when beams of 200 to 500 ev were required.

Normally, if a well focussed beam is obtainable with the saddle-field conditions, it is preferable to the conditions used, since a higher electric field is present between the first anode and the filament and hence a larger beam current can be obtained.

The gun was used for some of the experiments described in Chapter 5, but was finally discarded because of instabilities which occurred in the beam current after it had been in use for some time. This may have been due to electrostatic charging up of the pyrophillite of the body of the gun, or to formation of contamination on the electrodes (Sect.5.10).

3.6 A Seven Electrode Gun

This gun was built to replace the tetrode gun. It was based on a design given by Hart and Weber (1961) and was a scaled-down version of

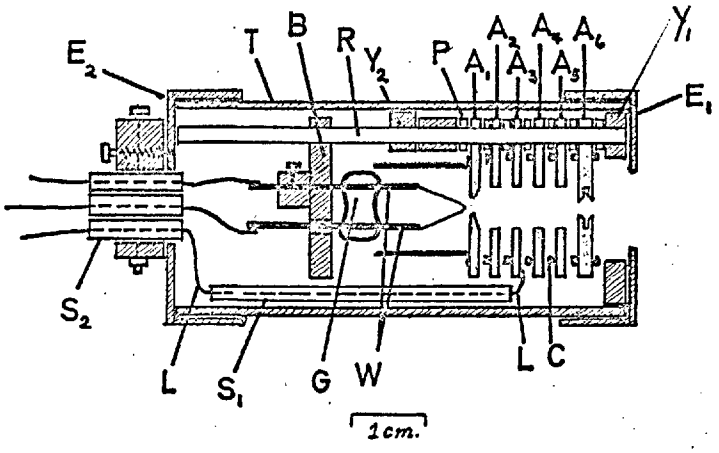

Fig 3.4(a)

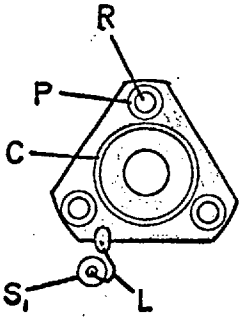

Fig 3.4(b)

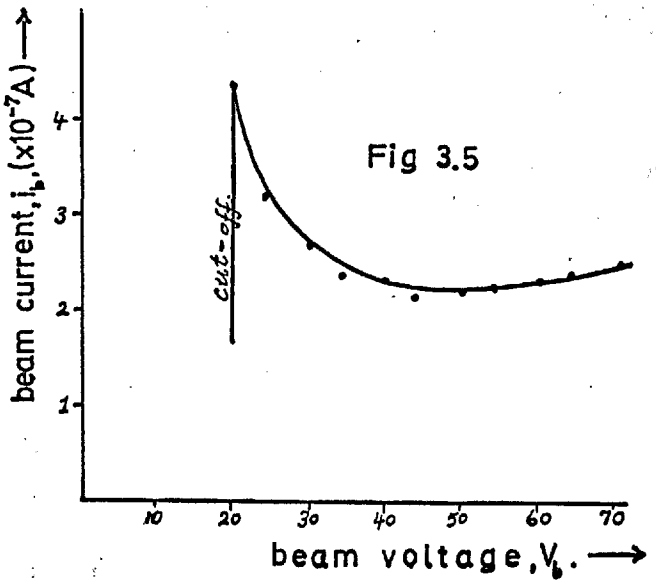

Fig 3.5

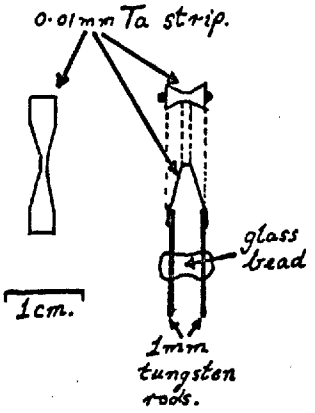

Fig 3.6

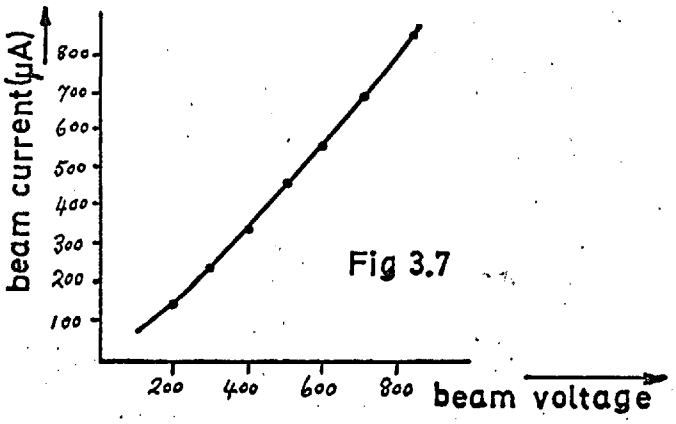

Fig 3.7

a gun used by Butterworth (1964). It is shown in Fig.3.4(a). There are six anodes, A_1.....A_6, supported on three steatite rods, R, and separated by 1 mm thick pyrophillite washers, P. A_3 is shown in detail in Fig.3.4(b) (letters denoting parts apply to both of Figs.3.4). The anodes were made of eureka, as were the flanges, C, which prevented, to some extent, charging up of the pyrophillite washers by stray electrons and penetration of stray fields to the electron beam. The anodes A_2.....A_5 were 1 mm thick with central apertures of 6 mm diameter. A_1 was 1 mm thick with a central aperture of 1.2 mm and A_6 was 2 mm thick with a central aperture of 2 mm. The filament, F, was supported on two 1 mm tungsten wires, W, sealed into the glass bead, G, one of which was clamped to the copper base, B. The gun was supported by the annular rings Y_1 and Y_2 inside the copper tube, T, which was closed by copper end-caps E_1 and E_2. The leads, L, to the electrodes were spot-welded on and passed through steatite rods, S_1, inside the gun and left the gun through similar rods, S_2, clamped into E_2. The filament to A_1 separation was 1 mm measured from the side of A_1 nearest to the filament.

3.7 The Performance of the Seven Electrode Gun in the Range 0-100 ev.

In the hope of being able to perform some very low energy experiments the gun was first tested in the range of 0-100 ev using a 0.1 mm tungsten hairpin cathode. The voltages for all the electrodes were provided by a single power supply via a resistance chain. The filament was d.c. heated. The following focussing conditions were obtained:-

Electrode	F	A_1	A_2	A_3	A_4	A_5	A_6
Voltage	V_f	$0.92V_f$	$-9.65V_f$	$-9.65V_f$	$-1.69V_f$	$-4.5V_f$	0

where V_f is negative.

The filament emission current had to be kept below a critical value to obtain a focussed beam. Using the conditions above, if an emission current of greater value than 40μA was used with $V_f = -76V$ the beam went completely out of focus, but providing this value was not exceeded the beam could be focussed in the energy range 30 - 80 ev. The beam divergence in this range was of the order of 0.5°. Below 30 ev the beam expanded until at 8 ev the divergence was about 8° and the beam was not well-defined. The current in the beam, i_b, was smaller than expected and is shown in Fig.3.5 as a function of beam voltage, V_b. The rapid cut-off of i_b was almost certainly due to electrostatic charging up inside the gun, since gold plating the electrodes removed the effect. However, the gun would only operate for about an hour after gold plating before the effect reappeared. Therefore the cut-off was a result of a time-dependent factor within the gun (see Sect.5.10).

3.8 Performance of the Seven Electrode Gun in the Range 200-800 ev.

The focussing conditions given in Sect. 3.7 were not suitable for use at higher energies than 100 ev because the voltages on anodes A_2 and A_3 became too large. Also, in order to achieve a higher beam current, the 0.1 mm tungsten filament was replaced by a tantalum strip filament, shown in Fig.3.6, from which a much larger emission current was obtainable. The following focussing conditions were found:-

Electrode	F	A_1	A_2	A_3	A_4	A_5	A_6
Voltage	V_f	$0.97V_f$	$-0.13V_f$	$0.31V_f$	0	$0.31V_f$	0

With these conditions the beam divergence was 8° at 800 ev and gradually increased to about 14° at 200 ev. A beam current of several hundred microamps was obtained in this energy range as shown in Fig. 3.7.

After the initial tests on the 127° deflection electron velocity analyser (Sect. 4.9), the tantalum strip cathode was replaced by a 0.2 mm diameter tungsten hairpin cathode. This was necessary because of overheating in the gun due to the large power dissipation of the strip cathode. The final characteristic energy loss experiments were carried out using the gun with the 0.2 mm tungsten hairpin cathode. The gun was operated under similar conditions as for the tantalum strip cathode and, although no accurate measurements were made on the beam characteristics, an experiment described in Sect. 5.13 indicated that the beam divergence was only 6° at a primary energy of 200 ev. Also there was sufficient current carried by the beam for the characteristic energy loss experiments to be carried out.

CHAPTER 4.

THE ELECTRON ENERGY ANALYSERS INVESTIGATED

4.1 Choice of Electron Energy Analyser and the Electron Detector

For the present research only electrostatic analysers were considered. These were preferred to magnetic analysers since the electric field required can be completely confined within the analyser by surrounding it with an earthed shield, leaving only one small entrance aperture for the electron beam.

Electrostatic analysers can be divided into the retarding field type, Simpson (1961), and the deflection type, Hughes and Rojansky (1929). Both types were investigated. A restriction on the type of retarding field analyser used was that the electron beam current collecting electrode of the analyser had to be at earth potential; this was in order that a sensitive vibrating reed electrometer could be used to detect the current. This confined this type of analyser to the electron filter lens type described in Sect.4.4, and a special type which will be described in Section 4.6.

The vibrating reed electrometer was an Ekco N572 type and was capable of detecting electron currents between 10^{-8}A and 10^{-15}A by suitable choice of the input resistance, which could be 10^{8}, 10^{10} or 10^{12} ohms, corresponding to the three ranges, R_3(10^{-8} to 3.10^{-10}A), R_2(10^{-10} to 3.10^{-12}A), and R_1(10^{-12} to 3.10^{-14}A).

4.2 The Energy Resolution of a Spectrometer. Definitions and Requirements

The overall energy resolution of a spectrometer (see Sect.3.1), which can be experimentally determined, may be defined as $\Delta V_b/V_o$, where eV_o is the mean energy, in electron volts, of the electron beam incident on the target and $e\Delta V_b$ may be taken here as the half-width, in electron volts, of the energy distribution of those electrons which have suffered zero energy loss in reflection from the target, after having passed through the analyser. $e\Delta V_b$ includes the energy spread present in the beam from the gun due to finite thermionic emission velocities of the electrons from the gun cathode and also the energy spread due to the imperfect electron optics of the gun and analyser. The finite entrance and exit apertures required for the electron beam in the analyser also contribute to $e\Delta V_b$.

The specific energy resolution, $\Delta V_a/V_o$, of the analyser is the theoretically determined energy resolution of a beam entering the analyser with perfectly homogeneous energy eV_o, and $e\Delta V_a$ is the total energy spread of the beam after having passed through the analyser.

For a given analyser $\Delta V_a/V_o$ is usually a constant, thus decreasing V_o results in a decrease of ΔV_a and therefore the ability of the analyser to resolve electron energies improves as V_o decreases.

For the characteristic energy loss experiments which were carried out, it was necessary to be able to resolve energy distributions differing by several electron volts ($\gtrsim 3$ ev) in the region of the primary electron beam energy, eV_o, where eV_o was of the order of 100-500 ev. An overall energy resolution of about 1% was thus required.

4.3 The Energy Resolution of the Retarding Field Analyser

The theory of the retarding field analyser has been dealt with by Simpson (1961) and therefore only a brief account will be given here.

If a perfectly collimated and homogeneous beam of electrons of energy eV_o, travelling in a field-free space (see Fig.4.1a), is incident at right-angles to the equipotentials of an opposing (retarding) electrostatic field, V_r/x_o, localised between the planes P_1 and P_2, the beam will only be able to surmount the potential difference, V_r, if $|V_o|>|V_r|$. Hence, if a current collecting plate is placed in the plane P_2, and the retarding potential, $-V_r$, is placed on this plate, then no current, I_c, is collected by the plate if $|V_r|>|V_o|$ and the total beam current, I_o, is collected if $|V_r|<|V_o|$, as shown in Fig.4.1(b).

The limit on the specific energy resolution of this type of analyser is fixed by the divergence of the incoming electron beam. It can be shown (see e.g. Simpson loc.cit.) that if the beam has a divergence of 2θ, then the specific energy resolution is given by

$$(\Delta V_a/V_o) = \mathrm{Sin}^2\theta \quad (\simeq\theta^2, \text{ for small } \theta) \qquad \ldots\ldots\ldots\ldots\ldots\ldots (4.1)$$

This is a result of the fact that it is the momentum of the electrons perpendicular to the equipotentials which is analysed and not the energy of the electrons. The effect of θ is shown in Fig.4.1(b), where first of all only those electrons travelling along the axis of the analyser, $\theta=0$, can surmount the retarding potential and then, as the retarding potential is gradually decreased, the electrons with $\theta>0$ are collected, until finally the retarding potential is small enough to allow those electrons travelling at the maximum value of θ to overcome it and be

collected.

In the practical case, where the plane P_1(see Fig.4.2) is kept at zero potential by placing an earthed metallic diaphragm there, the introduction of an aperture in this diaphragm, through which the beam has to pass, causes an increase in the specific energy resolution. This is due to the electron-optical lens effect at the aperture. In this case, Simpson (loc.cit.) has shown that for small θ the specific energy resolution is

$$\frac{\Delta V_a}{V_o} \simeq \frac{r_o^2 (p + 4x_o)^2}{16 x_o^2 \; p^2} \qquad \ldots\ldots\ldots\ldots\ldots\ldots\ldots\ldots\ldots\ldots (4.2)$$

where (see Fig.4.2) r_o is the radius of the aperture, x_o is the distance between the planes P_1 and P_2, between which the retarding potential is applied, and p is the distance between plane P_1 and the point from which the extreme rays of the electron beam entering the analyser appear to diverge.

For an electron beam containing electrons of all energies from zero to eV_o, only those electrons with sufficient longitudinal momentum will surmount the retarding potential barrier, $-V_r$, and hence by varying V_r the energy distribution of the electrons in the beam can be obtained in the form of an integral collected current versus energy curve.

4.4 The Electron Filter Lens

The electron filter lens (Simpson 1961) is a retarding field analyser in which the electrons which have surmounted the retarding potential are reaccelerated to their original energy before being

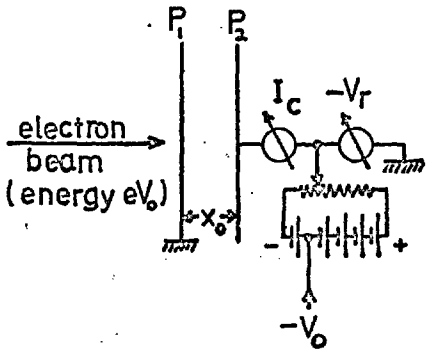

Fig 4.1(a)

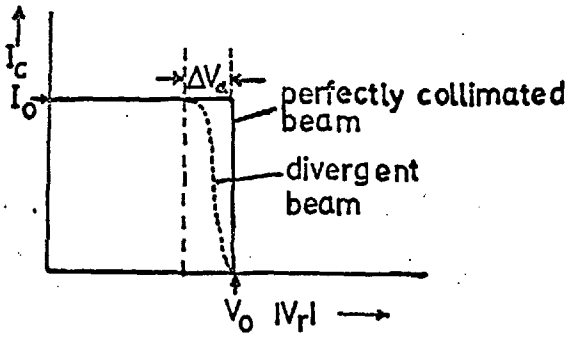

Fig 4.1(b)

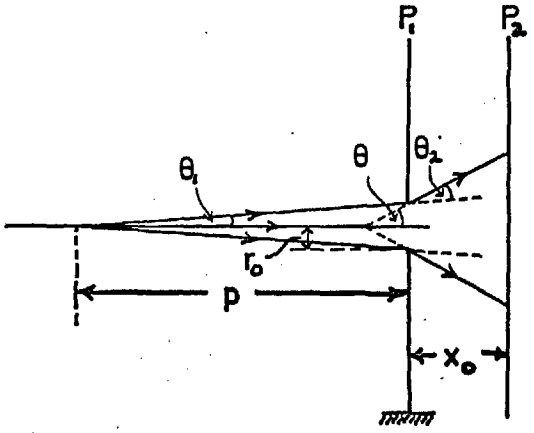

$$\theta = \theta_1 + \theta_2$$

$$\frac{\Delta V_a}{V_0} = \sin^2\theta \approx \theta^2$$

Fig 4.2

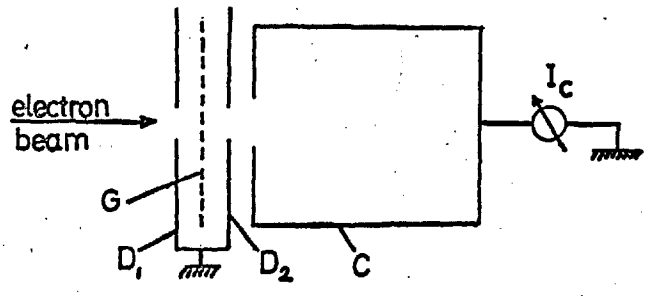

Fig 4.3

collected. A simple filter lens analyser is shown in Fig.4.3. There the retarding potential, $-V_r$, is applied between the gauze, G, and the earthed diaphragm D. Those electrons in the incoming beam which surmount the retarding potential are reaccelerated between G and the earthed diaphragm D_2 before being collected in the earthed collector cage, C. The main advantage of this type of analyser over the normal retarding field analyser, is that the collector, C, is at earth potential, thus making the measurement of the collected current, I_c, simpler.

Filter lens analysers have the advantage that secondary electrons produced at the current collecting electrode are automatically returned to this electrode by the accelerating potential between the filter lens and the collector. However, when a gauze is used in the lens, as shown in Fig.4.3, this same effect gives rise to a disadvatage, in that secondary electrons produced at the gauze are accelerated into the collector.

4.5 A Filter Lens Analyser

A simple version of this type of analyser was built and is shown in Fig.4.4. Diaphragms D_1 and D_2 are collimating diaphragms, with D_2 also being the first element of the filter lens which consisted of the diaphragms D_2, D_3 and D_4. The size of the apertures and their separation is given in the diagram. With the exception of D_3, the diaphragms mentioned were 0.4 mm thick. D_3 consisted of two diaphragms, of 0.4 mm thickness, in between which a piece of copper gauze, G, with 24 meshes per mm and 55% transmissivity, was clamped to cover the central aperture. D_3 was isolated from D_2 and D_4 by P.T.F.E. washers, P . The current

collecting cage, C_1, was situated inside an earthed shielding cage, C_2, and insulated from it by P.T.F.E. The cap, K, completed the shielding of C_1. D_5 and D_6 are the front diaphragms of C_2 and C_1 respectively. The diaphragms and cages were mounted on three steatite rods, S, of which one is shown and the whole assembly, supported on the rings, R, fitted inside the tube, T. The steatite rods were shielded by the caps, B, and the tubes, U. The whole construction was of brass and was gold plated to prevent the possibility of electrostatic charging up.

The retarding potential was applied to D_3 with D_2 and D_4 being earthed. Electrons which entered the analyser through the apertures in D_1 and D_2 and surmounted the potential barrier were thus reaccelerated to their original energies before collection in C_1, which was earthed via the electrometer, V.R.E.

The specific energy resolution of the analyser was determined by considering the retarding potential plane, defined by the gauze, G, as an equipotential, thus ignoring lens effects at the apertures of the gauze. Application of equn.(4.2) then gave a specific energy resolution of 1.6%.

In testing the analyser the overall energy resolution of the analyser and the tetrode gun (Sect.3.4) was measured for an 800 ev electron beam projected directly into the analyser. The result is shown in Fig.4.5. The half-width of the differential curve, D, obtained from the integral curve by numerical differentiation, was 3.7 ev, giving an overall energy resolution of 0.5%. This was smaller than the specific energy resolution of 1.6% because, in this case, the divergence of the electron beam

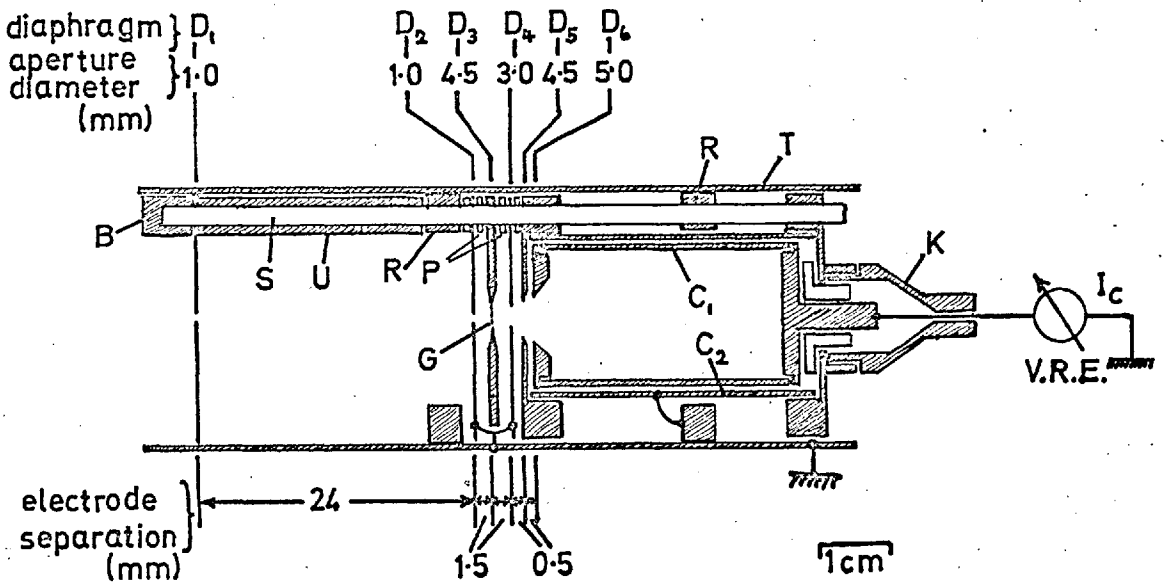
diaphragm aperture diameter (mm)
D1 1·0
D2 1·0
D3 4·5
D4 3·0
D5 4·5
D6 5·0
R
T
B
S
U
R
P
K
C1
C2
G
Ic
V.R.E.
electrode separation (mm)
24
1·5
0·5
1cm

Fig 4.4

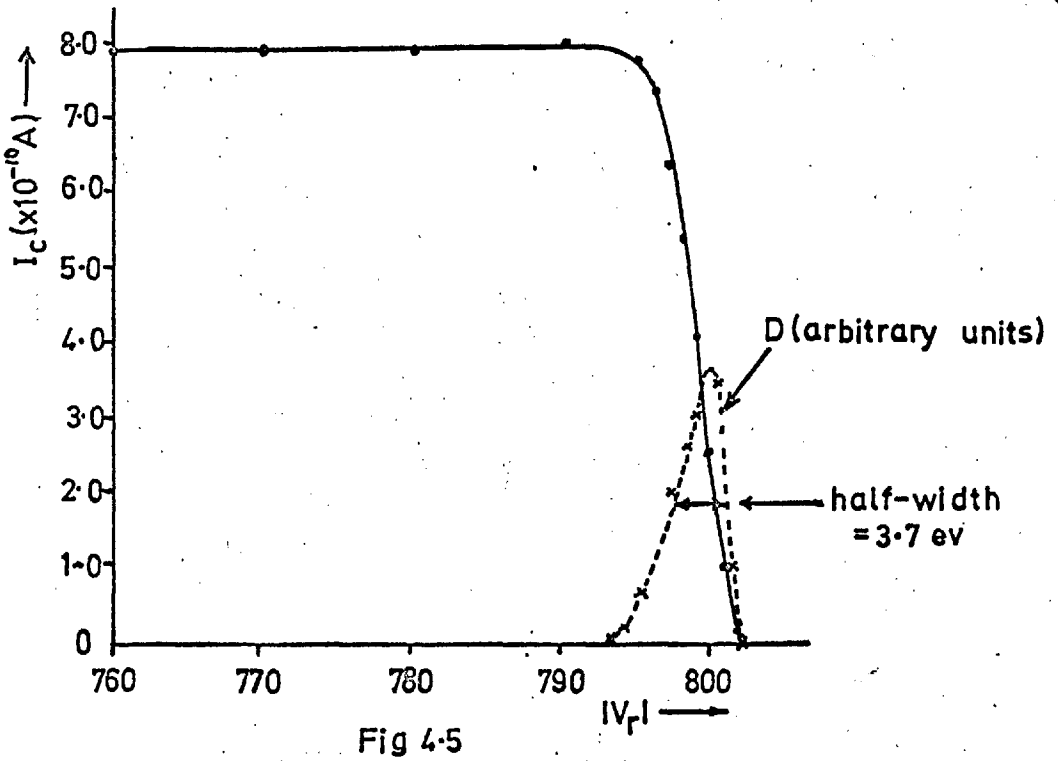
Ic (x10⁻¹⁰A)
8·0
7·0
6·0
5·0
4·0
3·0
2·0
1·0
0
760
770
780
790
800
|Vr| →
D (arbitrary units)
half-width
=3·7 ev

Fig 4·5

entering the analyser was fixed by the angle subtended by the aperture of radius r_o, in diaphragm D_2, at the last anode aperture of the gun. This divergence was only about an eighth of that set by the collimating apertures in D_1 and D_2. If, in equn.(4.2), we allow p to become very much greater than x_o, then $\Delta V_a/V_o$ becomes $r_o^2/16x_o^2$, which gives a specific energy resolution of 0.7%, which agrees quite well with the measured value of 0.5% mentioned above.

4.6 An Inverse Retarding Field Analyser

This analyser was based on a design by Boersch and Schweda (1962) and a schematic diagram explaining its operation is shown in Figs.4.6(a) and (b). An electron beam of energy eV_o enters the analyser through the collimating aperture in the diaphragm D. It passes through the earthed cage, R, and meets a retarding potential, $-V_r$, which is applied between R and the second cage, S. The retarding field acts an an electron mirror, returning those electrons which do not have sufficient energy to overcome the retarding potential to cage R, where they are collected and registered as the inverse current, I_r. Thus by varying the retarding potential, $-V_r$, and measuring the current, I_r, to R, the energy distribution of the electrons in the beam is obtained, as shown in Fig.4.6(b). The current I_r is complementary to the current, I_s, collected by the cage S. I_s is the current which would be collected in a normal retarding field analyser. By measuring the inverse current, I_r, instead of I_s, one takes advantage of the fact that R is at earth potential throughout, whereas S is at a negative potential which is varied in the region of the cathode voltage of the gun producing the electron beam.

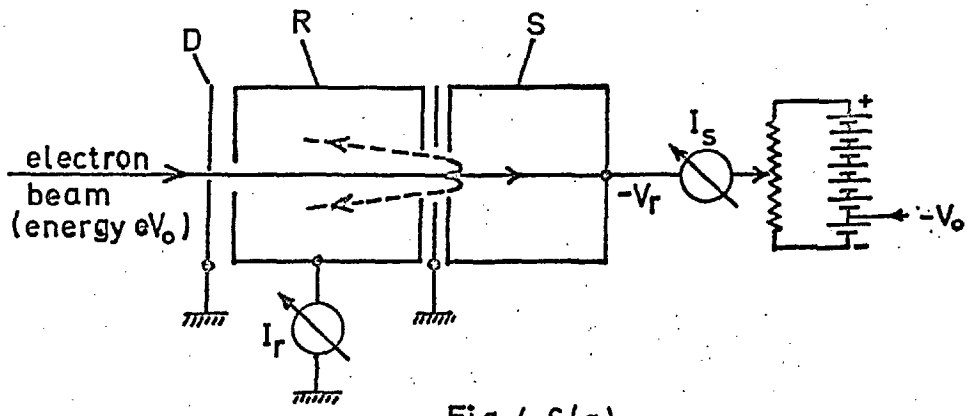

Fig 4.6(a)

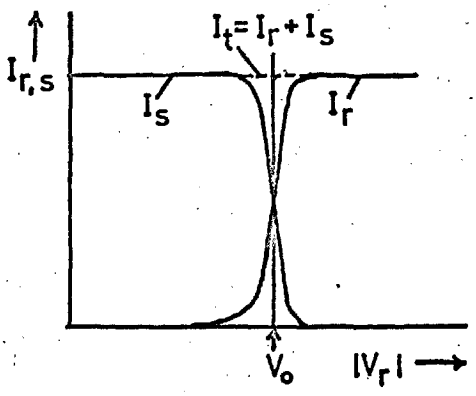

Fig 4.6(b)

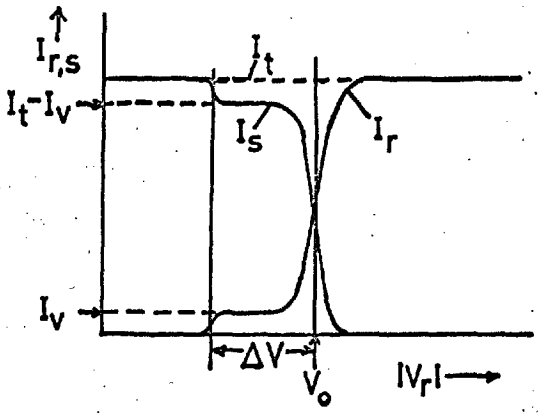

Fig 4.7

The sum of the currents I_r and I_s, which is denoted by I_t, is always the total current carried by the beam (see Fig.4.6 b). As shown in Fig.4.7, a group of electrons in the beam being analysed which has suffered a characteristic energy loss, $e\Delta V$, appears as a current step, I_v, in both the curves for I_r and I_s. Boersch and Schweda (loc.cit.) point out that the signal to noise ratio (where the noise is due to short term fluctuations in I_t over the time required to sweep through the energy spectrum of the beam) of the current which has suffered the energy loss, is increased in the inverse current curve, $I_r(V_r)$, by a factor of $(I_t-I_v)/I_v$ compared with the normal current curve $I_s(V_r)$.

The analyser which was built eventually is shown in Fig.4.8. It was developed from a first version with which preliminary tests were carried out. The electron beam was collimated by diaphragms D_1 and D_3. Diaphragms D_2, separated by brass spacers, B, suppressed secondary electrons produced at the aperture in D_1 by the electron beam entering the analyser. All of these diaphragms were earthed. Diaphragms D_4 and D_6 were held at a potential of -50V with respect to earth, when analysing beams of several hundred ev, in order to prevent secondary electrons entering the cage R and also to prevent escape of secondary electrons which were produced inside R. D_4 and D_6 were isolated from their neighbouring diaphragms by P.T.F.E. insulator, P. D_5 and D_7 are the end diaphragms of cage R, which was completely isolated from cage S by the earthed diaphragm D_8, which occupied the whole of the internal diameter of the cylinder, T, in which the cages were supported on the rings, O. The shielding of S was completed by the cap, C. Cage R and

the diaphragms which preceded it were mounted on three steatite rods, E_1, of which one is shown. These were shielded by the brass caps, K, at the front. Cage S was also mounted on three steatite rods, E_2. The washer, A, shielded the insulator P from stray electron current. The whole construction was of brass and all the diaphragms were 0.4 mm thick.

The specific energy resolution of the analyser was estimated by application of equn. (4.1). The angle of entry of the electron beam into the analyser was limited by diaphragms D_1 and D_3, which limited θ to 0.04 rad., and therefore gave a specific energy resolution of 0.16%, neglecting the curvature of the retarding field equipotentials.

The analyser was tested by projecting electron beams of 400 ev from the tetrode gun (Sect.3.4) into the analyser along its axis. An energy analysis curve of such a beam is shown in Fig.4.9, together with the differential curve obtained from it by numerical differentiation. The half-width of the beam was only 0.75 ev, which yielded an overall energy resolution under these conditions of 0.2%.

The deep minimum, M, to the right of the beam current step in Fig.4.9, was due to the fact that when the retarding field between the two cages, R and S, was varied, the focal length of the electron mirror formed between them also varied, and for a particular field the electrons reflected from the mirror were focussed back through the aperture in D_5 (Fig.4.8) and thus escaped detection in cage R. This was verified experimentally. The minimum, M, does not affect energy distribution measurements made with the analyser since its abscissa corresponds to an

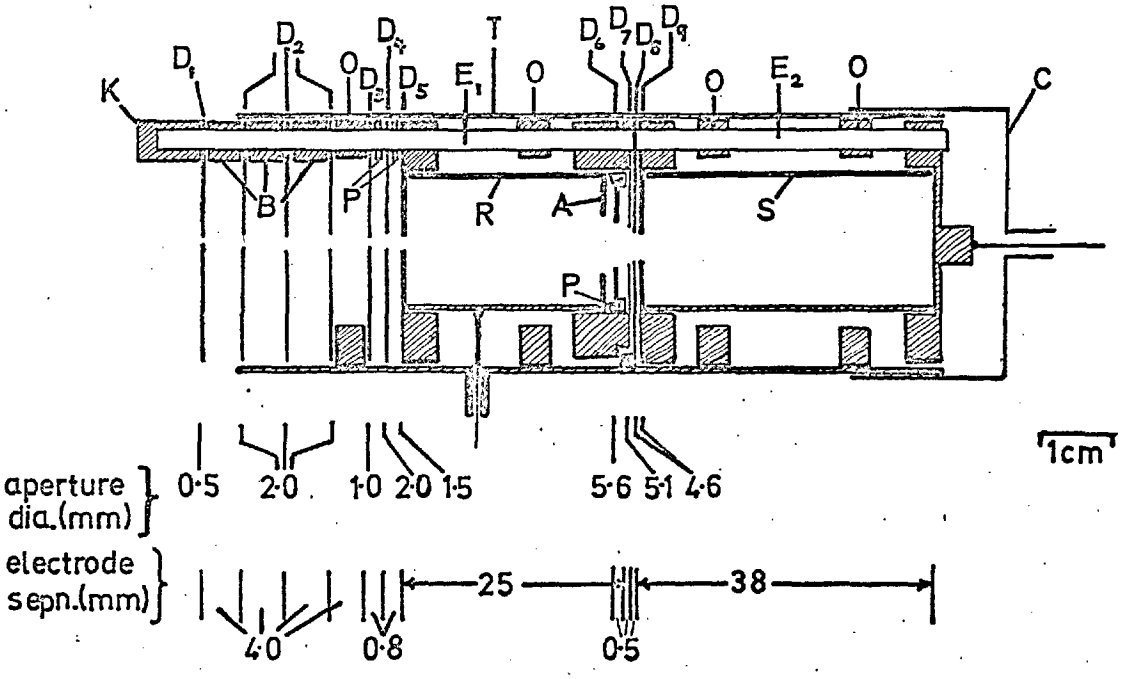
K
D1
D2
O
D3
D4
D5
E1
T
O
D6
D7
D8
D9
O
E2
O
C
B
P
R
A
S
P
1cm
aperture dia.(mm)
0·5
2·0
1·0
2·0
1·5
5·6
5·1
4·6
electrode sepn.(mm)
4·0
0·8
25
0·5
38

Fig 4.8

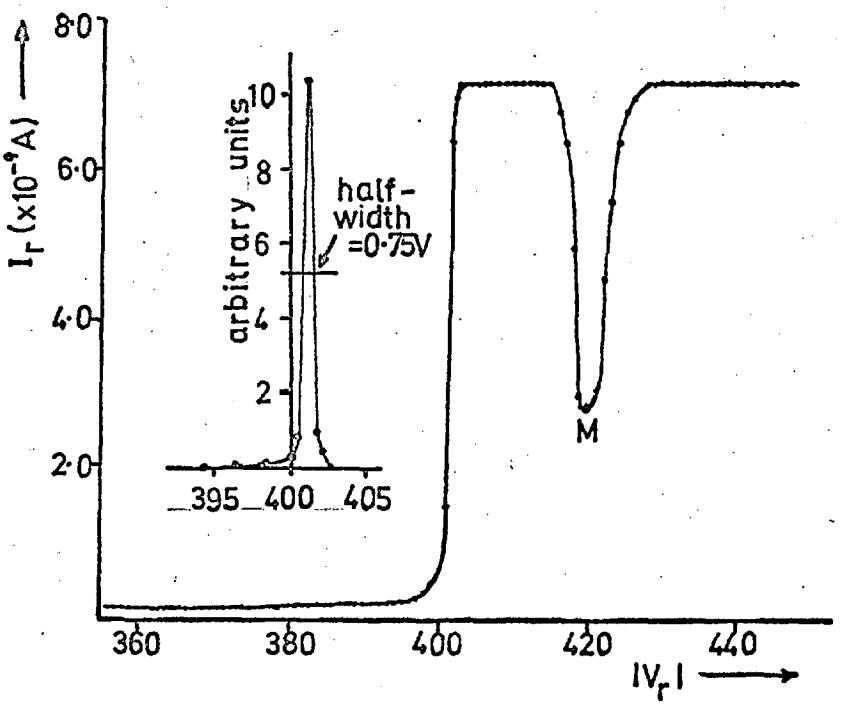
8·0
6·0
4·0
2·0
I_r (x10^{-9}A)
arbitrary units
10
8
6
4
2
half-width =0·75V
395
400
405
M
360
380
400
420
440
$|V_r|$

Fig 4.9

energy greater than that of the beam being investigated. This is true irrespective of the beam energy.

The curve shown in Fig.4.9 was the best of several obtained. It was found that the shape of the curve on the high energy side of the beam current step depended on the angle of entry of the beam into the analyser, indicating that stricter collimation of the beam was necessary. However, the important part of the curve, which is that on the low energy side of the beam current step, was not affected by this and therefore, in the present analyser, the collimation was not improved, since it would have reduced the collected current intensity to an unacceptable figure.

4.7 The Principle and Resolution of the 127° Electrostatic Deflection Analyser

Hughes and Rojansky (1929) showed theoretically that a divergent beam of monoenergetic electrons entering a radial electrostatic field at right angles, is refocussed after it has traversed a distance defined by the angle $\pi/2^{\frac{1}{2}}$ rad.($127°17^{\prime}$). This was verified experimentally by Hughes and McMillen (1929). The principle of the analyser is shown in Figs.4.10 (a) and (b). There A and B represent the cylindrical condenser plates, of radii r_a and r_b, between which the radial electrostatic field is produced by the application of symmetrical voltages, +V and -V, to A and B respectively. The entrance and exit slits of the analyser, in plates C and D, lie mid-way between A and B. They are on a radius r_o and are perpendicular to the plane of the diagram. 0, 1 and 2 represent the principal and marginal rays of a homogeneous electron beam, of energy eV_o,

entering the analyser with convergance 2α rad. The principal ray, 0, satisfies the condition,

$$V_d = 2V_o \log_e(r_b/r_a) \quad \ldots\ldots(4.3)$$

where $V_d = 2V$ and is the voltage difference between A and B. This ray travels on a circular orbit of radius r_o. The rays, 1 and 2, are refocussed at the exit slit in D as shown in Fig.4.10(a). Therefore a line image of the entrance slit is formed at the exit slit. Equation (4.3) shows there is a linear relationship between the energy of the focussed electrons and V_d. An inhomogeneous beam of electrons entering the analyser is thus dispersed by the electric field; electrons of higher energy striking the end plate, D, at larger radii than those of lower energy. Therefore, by varying V and measuring the current transmitted by the exit slit, the energy spectrum of the beam of electrons is obtained.

Fig.4.10(b) illustrates the fact that rays 0, 1 and 2, corresponding to electrons with the same velocity, v_o, are not perfectly refocussed in the plane of D. The departure from perfect refocussing is the distance s, given by Hughes and Rojansky (loc.cit.) as

$$s = \frac{4}{3}\alpha^2 r_o \quad \ldots\ldots(4.4),$$

where higher powers of α are neglected.

The electrons entering the analyser with velocity $v < v_o$ and at $\alpha = 0$, shown by the dotted line in Fig.4.10(b), strike plate D at a distance d from ray 0, where d is given by Hughes and Rojansky as

$$d = (2\beta - 4\beta^2)r_o \quad \ldots\ldots(4.5),$$

where $\beta = (v_o - v)/v_o$ and higher powers of β have been neglected. Now by

converting equn.(4.5) into its equivalent energy form, it can be shown that $d/r_o = \Delta V/V_o$ or, by putting $d = \Delta r$,

$$\frac{\Delta r}{r_o} = \frac{\Delta V}{V_o} \quad \ldots\ldots\ldots\ldots\ldots\ldots\ldots\ldots\ldots\ldots\ldots\ldots\ldots\ldots\ldots\ldots\ldots\ldots\ldots\ldots\ldots\ldots(4.6)$$

where eV_o and eV are the energies, in electron volts, of the electrons with velocities v_o and v respectively, $\Delta V = V_o - V$ and higher orders of $\Delta V/V_o$ have been neglected. Therefore, using equn.(4.4), we see that the departure from perfect refocussing of a homogeneous beam entering the analyser leads to an effective energy spread of ΔV_1 in the beam, given by

$$\frac{\Delta V_1}{V_o} = \frac{s}{r_o} = \frac{4}{3}\alpha^2 \quad \ldots\ldots\ldots\ldots\ldots\ldots\ldots\ldots\ldots\ldots\ldots\ldots\ldots\ldots\ldots\ldots\ldots\ldots\ldots\ldots\ldots\ldots(4.7),$$

which is just the specific energy resolution of the perfect analyser with infinitely small entrance and exit slits. If the analyser has finite entrance and exit slits of equal width, w, then according to equn.(4.6) an energy spread of ΔV_2 is introduced, where

$$\frac{\Delta V_2}{V_o} = \frac{w}{r_o} \quad \ldots\ldots\ldots\ldots\ldots\ldots\ldots\ldots\ldots\ldots\ldots\ldots\ldots\ldots\ldots\ldots\ldots\ldots\ldots\ldots\ldots\ldots(4.8).$$

Lastly, due to the divergence, θ, in the plane defined by the length of the entrance slit and the direction $\alpha = 0$, of the beam entering the analyser, an energy spread of ΔV_3 is introduced, where

$$\frac{\Delta V_3}{V_o} = \mathrm{Tan}^2\,\theta \simeq \theta^2 (\text{for small } \theta) \ldots\ldots\ldots\ldots\ldots\ldots\ldots\ldots\ldots\ldots(4.9),$$

as given by Rudberg (1930b). θ is limited by the geometry of the analyser and the spectrometer as a whole when it is being used in electron reflection experiments. The specific energy resolution of a

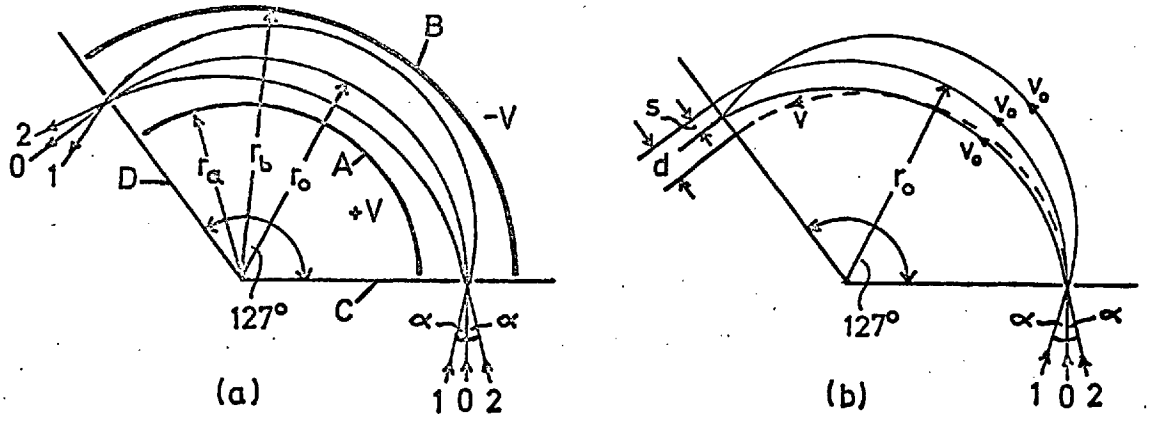

Fig 4.10

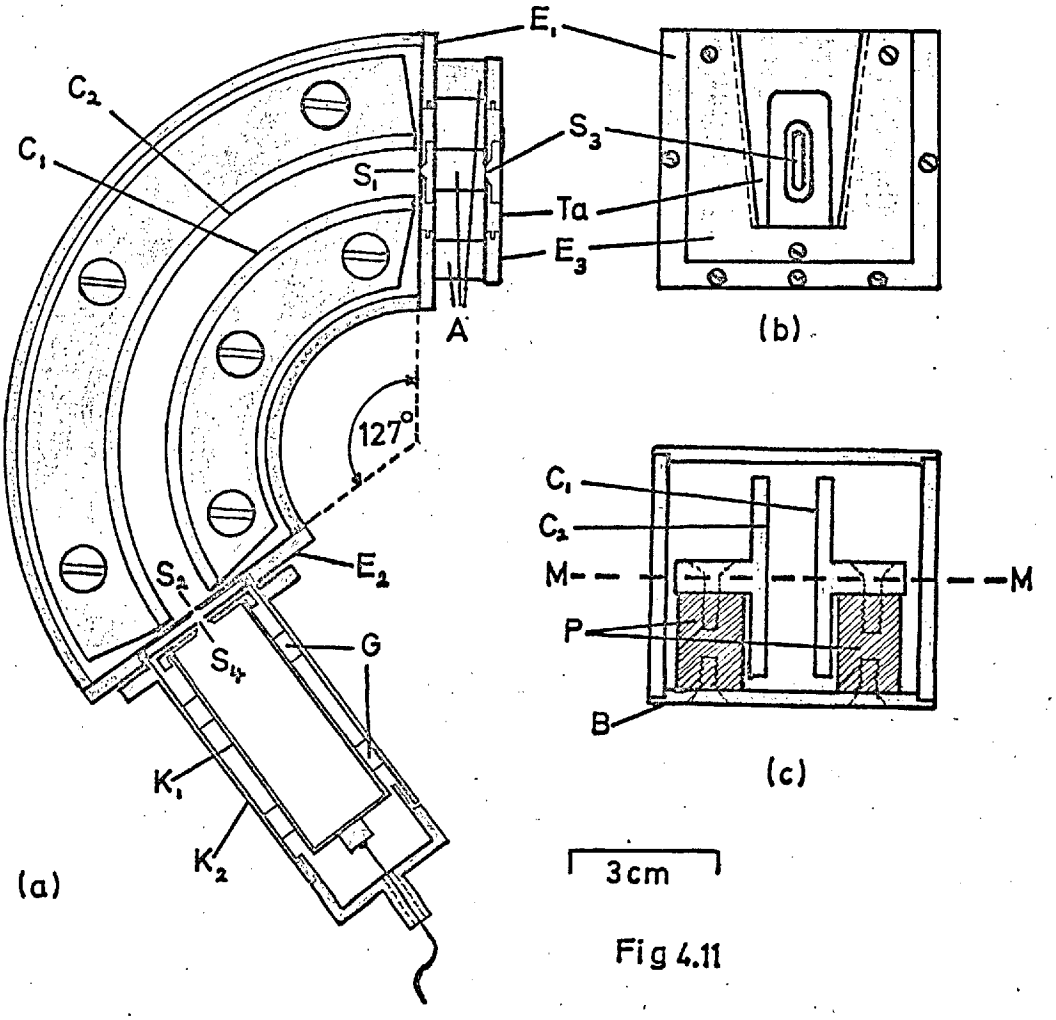

Fig 4.11

spectrometer incorporating such an analyser is therefore

$$\frac{\Delta V_a}{V_o} = \frac{\Delta V_1 + \Delta V_2 + \Delta V_3}{V_o} = \frac{4}{3}\alpha^2 + \frac{w}{r_o} + \mathrm{Tan}^2\theta \quad \ldots\ldots\ldots\ldots\ldots\ldots (4.10).$$

The fact that the $\mathrm{Tan}^2\theta$ term overlaps, to some extent, with the sum of the other two terms has been neglected. Note that, as in the case of retarding field analysers, $\Delta V_a/V_o$ is a constant and is therefore independent of V_o (see Sect.4.2).

The 127° deflection analyser yields the differential curve of the energy distribution of the beam passing through it, as opposed to the integral curve obtained with retarding field analysers.

4.8 Details of the 127° Electrostatic Deflection Analyser

The analyser used in the present research is shown in Figs.4.11(a), (b) and (c). It was made of brass. The condenser plates, C_1 and C_2, were each supported on the base, B, by three pyrophillite pillars, P, in the manner shown in Fig.4.11(c). C_1 and C_2 were surrounded by an earthed case, the important parts of which are B and the end plates, E_1 and E_2. The entrance and collimator slits, S_1 and S_3, were both mounted in the same fashion, which is shown in Figs. 4.11(a) and (b) for S_3. The slit, S_3, was machined on the tapered plate, Ta, which fitted into the corresponding tapered slot in the plate E_3. E_3 was supported on the three spacers, A, located on E_1. The exit slit S_2 was machined in the end plate E_2. Slit S_4 was introduced to prevent secondary electrons produced at the edges of S_2 from entering the collector cage, K_1, which was surrounded by the earthed cage, K_2. K_1 and K_2 were insulated from each other by the P.T.F.E. rings, G.

C_1 and C_2 were of 5.0 cm and 6.0 cm radius of curvature respectively and they reached to within 0.05 cm of the end plates E_1 and E_2. The vertical height of C_1 and C_2 was 4.0 cm and the slits S_1 and S_2 were only of 1.0 cm length and symmetrically situated about the mid-plane, M, shown in Fig.4.11(c). The slit widths and lengths were as follows.

S_1 = 0.23 mm ; length 1.0 cm

S_2 = 0.30 mm ; length 1.0 cm

S_3 = 0.97 mm ; length 0.4 cm

S_4 = 1.00 mm ; length 1.1 cm

The separation of S_1 and S_3 was 1.3 cm, which limited the angle of entry of electrons into the analyser to $\alpha = \pm 2^{\circ}\ 40'$ (see Fig.4.10). S_4 was 1.5 mm behind S_2 and 1.0 mm in front of the entrance aperture of K_1 which was 2.0 mm wide and 1.2 cm long.

Since there were no adjustments provided for the slits and deflection condenser plates, the important parts of the analyser (the base, B, condenser plates C_1 and C_2, the end plates, E_1, E_2 and E_3 and the slits) were all made to an accuracy of ± 0.003 cm and were held together by accurately countersunk screws. On assembly the separation of C_1 and C_2 was measured to be 1.014 ± 0.003 cm and the slits S_1 and S_2 were accurately central between C_1 and C_2 to ± 0.005 cm, where the measurements were made with a travelling microscope.

The whole of the inside of the analyser was covered with a thin layer of soot from a benzene flame before assembly to reduce secondary emission effects.

4.9 The Performance of the Deflection Analyser

The specific energy resolution of the analyser was best calculated by considering the analyser incorporated in the spectrometer in which it was eventually used, described in Sect. 5.8, because the term involving θ in equn.(4.10) was governed by the size of the electron beam at the target, and not by the length of the collimating slit. The size of the beam at the target was about 3 mm diameter (Sect.5.13) and the slit length was 4.0 mm. The specific energy resolution of the spectrometer was then calculated to be 0.9%. The finite slit-width term, ΔV_2, in equn. (4.10) accounted for half of this figure.

The analyser, with the collimating slit, S_3, removed, was tested by accelerating electrons into it from a 0.1 mm diameter tungsten hairpin filament cathode situated 0.5 cm in front of the entrance slit, S_1. Using a circuit similar to that shown in Fig.4.12(a), curves such as that shown in Fig.4.13 were obtained for electrons transmitted by the analyser and recorded as the collected current, I_c, by the vibrating reed electrometer, V.R.E. These curves showed that the overall energy resolution of the analyser and filament was just less than 1% under these conditions, which, in fact, were almost equivalent to those present in the spectrometer incorporating this analyser (Sect.5.8).

Substituting for r_a and r_b in equn.(4.3) gave the focussing condition

$$V_d = 0.365V_o \qquad \text{.....(4.11)}$$

for the analyser. With the analyser mounted in the spectrometer described in Sect.5.8, equn.(4.11) was tested experimentally. Electron beams of known energies were reflected from the target into the analyser and,

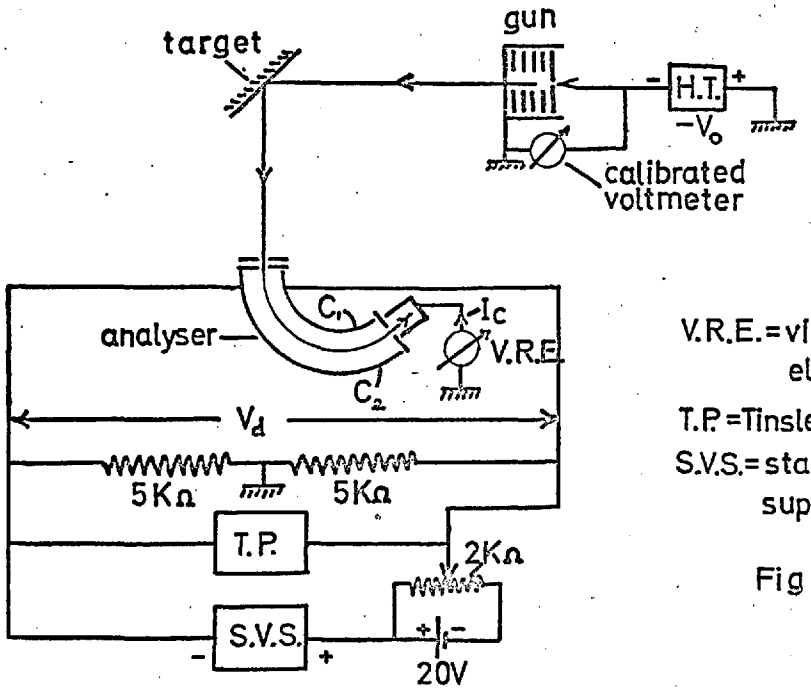

V.R.E. = vibrating reed electrometer.
T.P. = Tinsley potentiometer.
S.V.S. = stabilised voltage supply.

Fig 4.12(a)

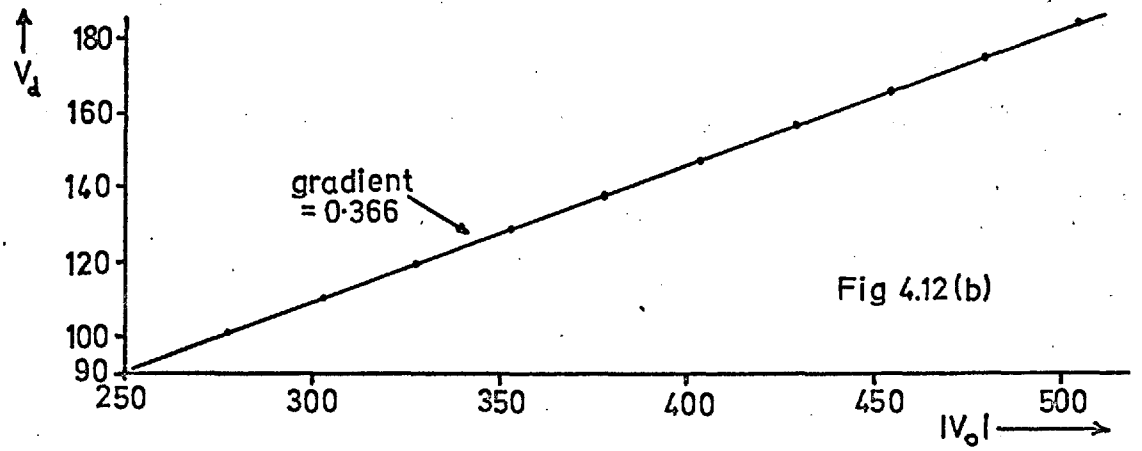

Fig 4.12(b)

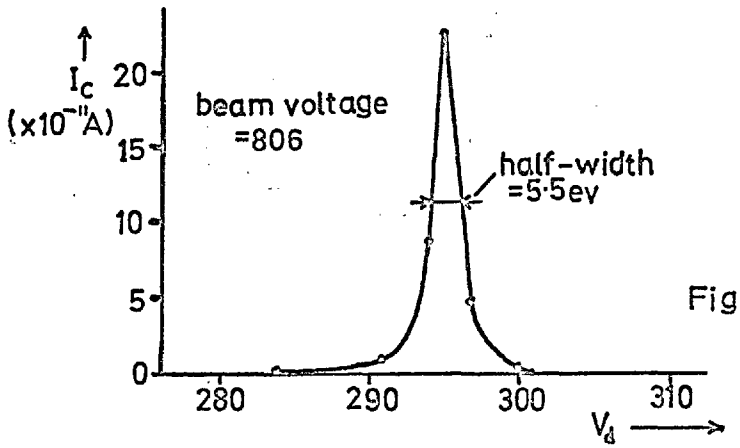

Fig 4.13

using the circuit shown in Fig.4.12(a), the deflection voltage, V_d, was adjusted so that those electrons which had lost zero energy on reflection at the target were transmitted by the spectrometer. The deflection voltage was then measured on the Tinsley potentiometer, which was connected into the circuit throughout the adjustments. These measurements (see Fig.4.12b) yielded the following focussing condition :-

$$V_d = (0.366 \pm 0.002)V_o \quad \ldots\ldots\ldots\ldots\ldots\ldots\ldots\ldots\ldots\ldots (4.12),$$

where the error is due to the accuracy with which the calibrated voltmeter, used for measuring the beam energies, could be read. Equation (4.12) is in excellent agreement with equn.(4.11). Measurements with two uncalibrated meters showed that a linear relationship between V_d and V_o existed over a range investigated from V_o = 50-800 ev.

CHAPTER 5.

THE DEVELOPMENT OF THE SPECTROMETER

5.1 The Arrangement of the Spectrometers

For the experiments described in this chapter involving the retarding field analysers (Ch.4) the degaussing coils (Sec.2.3) were set to compensate the vertical component of the magnetic field present in the laboratory. As shown in Figs.5.1(a) and 5.1(b), the gun, G, target, T, and analyser, A, were made to lie in the mid-plane of the coils. The gun and analyser were supported on extension arms attached to collars which fitted around the 9.5 mm diameter central shaft, S, on which the target was supported. The target was a 2 cm diameter disc of 0.25 mm eureka sheet. The gun and target could both be rotated about the axis, Ax, by means of pulleys operated via the rotary shafts, R_1 and R_2. The analyser was fixed. The target was situated 2.5 cm off the centre-line of the work chamber, so that the analysers used always lay within the region over which the vertical component of the magnetic field in the laboratory was compensated by the degaussing coils (see Sect.2.3). The last anode of the electron gun was always situated about 3.6 cm from the target and the entrance aperture of the analyser lay between 3.0 and 4.0 cm from the target. The analysers were lined-up in the direction of the horizontal component of the magnetic field present in the laboratory, thus electrons reflected from the target into the analyser suffered no

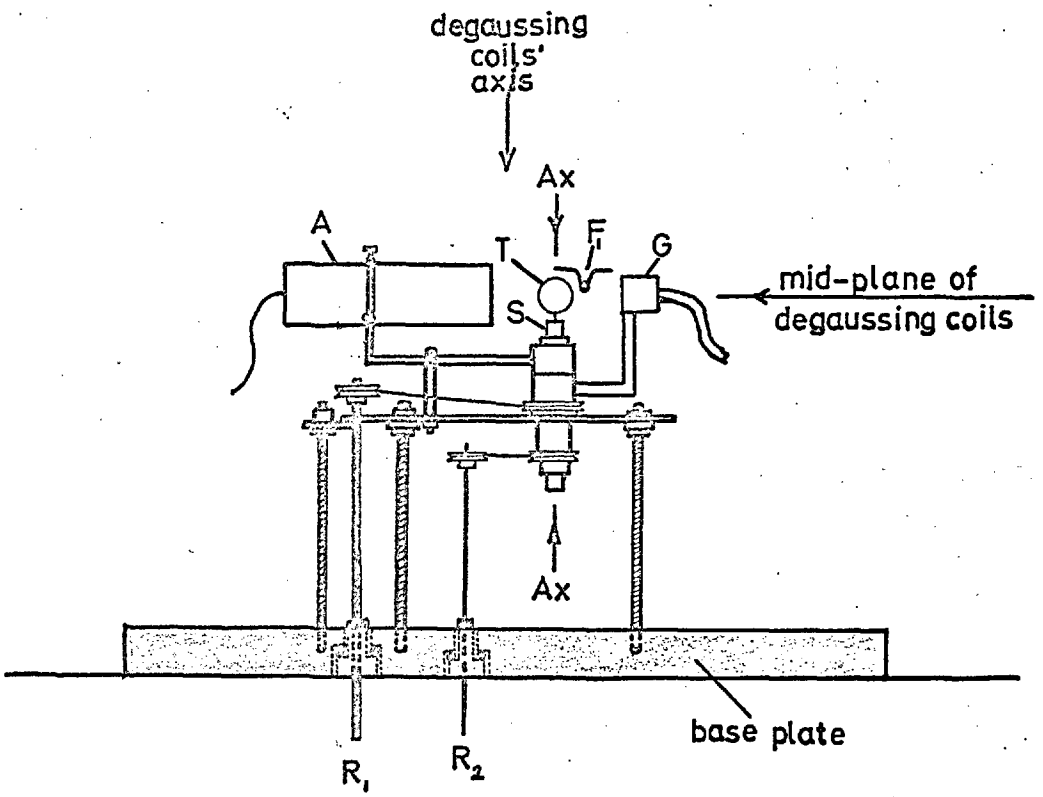

Fig 5.1(a)

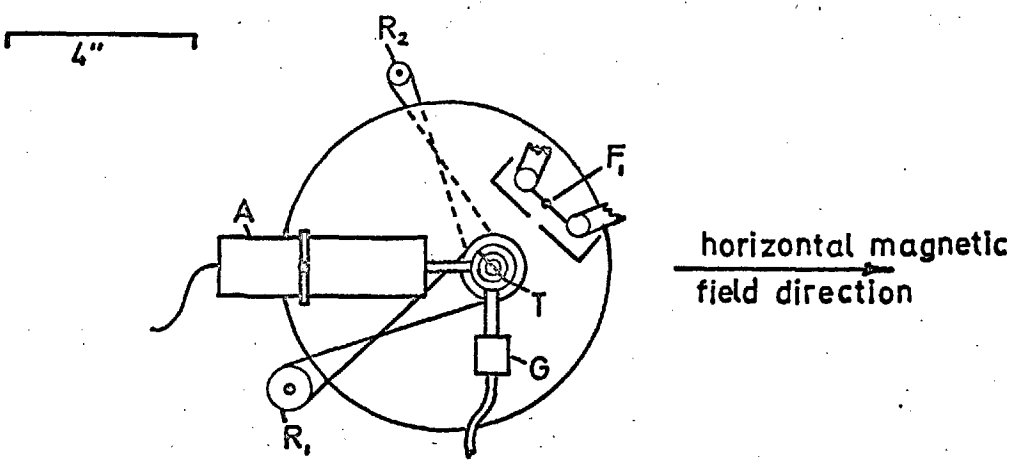

Fig 5.1(b)

magnetic deflection once they had left the target.

5.2 The Effect of the Uncompensated Horizontal Magnetic Field

The electron beam travelling between the gun and the target was acted upon by the uncompensated horizontal component of the magnetic field present in the laboratory. This effect being greatest when the beam travelled perpendicular to the field. The uncompensated field was approximately 0.09 oersted, as calculated from the known angle of dip (Sect.2.3) and the value of the vertical component of the magnetic field calculated from the known current in the degaussing coils when this component was compensated. Thus, as the electron beam travelled a distance of 3.6 cm from the gun to the target, the maximum possible deflection of the beam before it struck the target could be calculated. It was found that a beam of 100 ev energy suffered a vertical deflection of only 0.3 mm at the target. Such a deflection was not considered serious for the preliminary experiments which were to be performed.

5.3 The Testing of the Spectrometers

The spectrometers were tested by carrying out electron reflection experiments, usually on freshly evaporated aluminium specimens. Aluminium was chosen because its characteristic energy losses are very discrete and pronounced, for example see Powell and Swan (1959a), therefore aluminium provided a standard by which the performance of the spectrometers could be evaluated. The specimens were evaporated onto the target by rotating the target, T, (Fig.5.1b) to face the evaporation filament, F_1, and, after deposition of the specimen, the target was

immediately rotated back into the reflection position and the reflection measurements made. Details of the evaporation technique will be given later (Sect.6.1). The overall energy resolutions of the spectrometers were evaluated from the curves obtained.

5.4 Note on Contamination of Specimens

It was found later that, in spite of using freshly evaporated specimens, the specimen surfaces were almost certainly contaminated by residual gases and vapours in the vacuum system. The specimens which were used for evaluating the performances of the retarding field spectromters will thus be termed contaminated aluminium(see Sects.5.10 - 5.12 and Sect.7.7).

5.5 The Inverse Retarding Field Spectrometer

A spectrometer was constructed using the inverse retarding field analyser (Sect.4.6) and the tetrode gun (Sect.3.4). The arrangement was as shown in Figs.5.1(a) and (b). The electrical circuit employed is shown schematically in Fig.5.2. The retarding potential, $-V_r$, required on the cage S of the analyser, was derived from the beam accelerating voltage, $-V_o$, applied to the cathode of the gun, and the H.T. battery shown. V_r was varied by means of the potentiometer, P. $e\delta V = e(V_o - V_r)$ is the minimum energy, in ev, which an electron in the reflected beam must have lost in order to be collected in cage R. The current collected by R, I_r, was measured with the vibrating reed electrometer, V.R.E. The gun was operated under the second set of conditions given in Sect.3.5.

Fig.5.3 shows part of the energy spectrum of a 400 ev beam scattered

through approximately 30° from a contaminated aluminium evaporated layer (correspondent conditions were later found to be excellent for the excitation of the surface plasma oscillations in aluminium, see Sect.7.3). The differential curve, D, of the zero energy loss step was obtained from the integral curve, A, of Fig.5.3 by numerical differentiation. It is in arbitrary units and its half-width is 1.3 ev, giving an overall energy resolution for the spectrometer of 0.3%, which is in reasonable agreement with the calculated specific energy resolution of 0.16% (Sect.4.6).

No characteristic energy losses are apparent in Fig.5.3 but the great disadvantage of this type of analyser can be seen. This is the presence of the large background current and is due to the fact that the cage R of the analyser collected not only the high energy electrons which had been returned to it by the retarding field, but also the slow and secondary electrons in the selected beam and these were not of interest in the present experiments. The size of the signal compared with the background prohibited the detection of any energy losses. Therefore, in order to make the maximum use of a spectrometer utilising this type of analyser, it would be necessary to precede the analyser by an electron filter which would remove all electrons with energies up to the lowest energy of interest from the beam entering the analyser. This was not considered to be a practical proposition and the analyser was discarded for the measurement of characteristic energy losses.

A final discussion on the use of retarding field analysers for measuring energy losses is given in Sect.5.7.

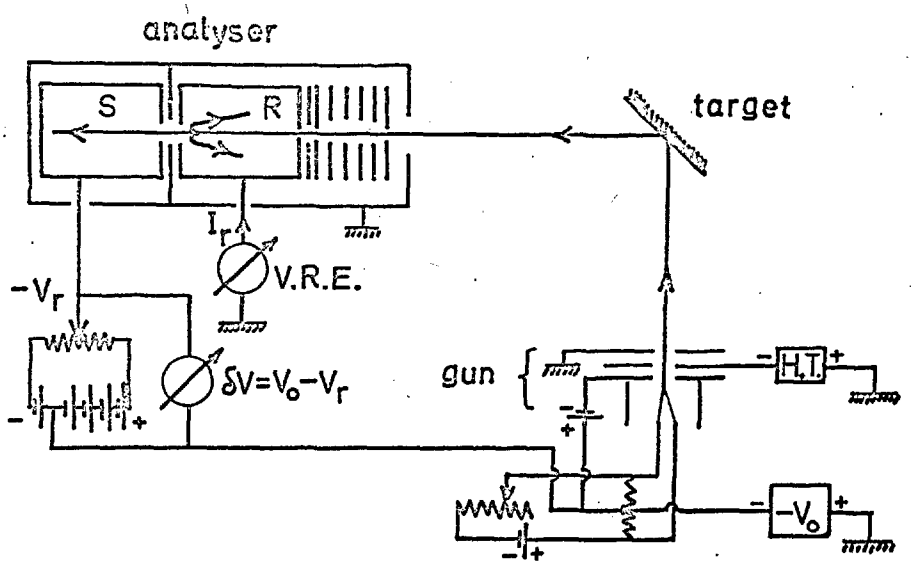

Fig 5.2

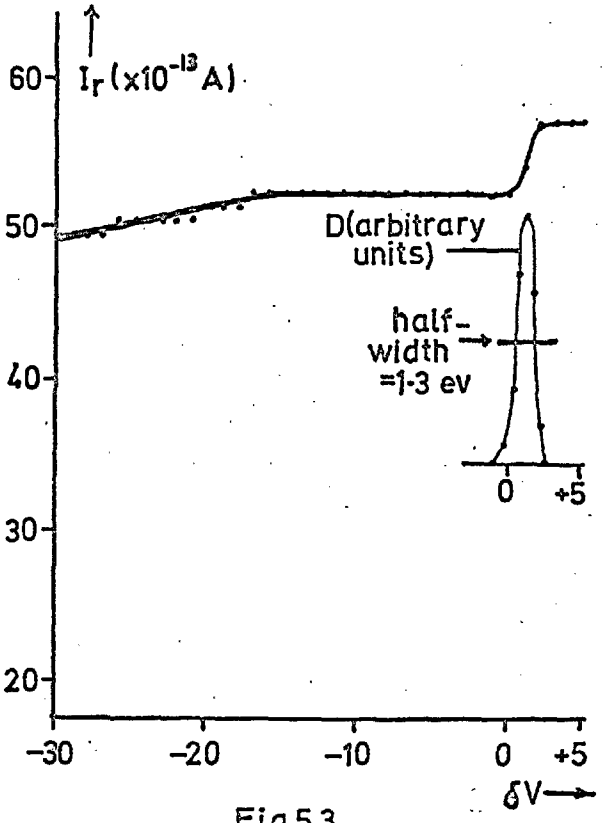

Fig 5.3

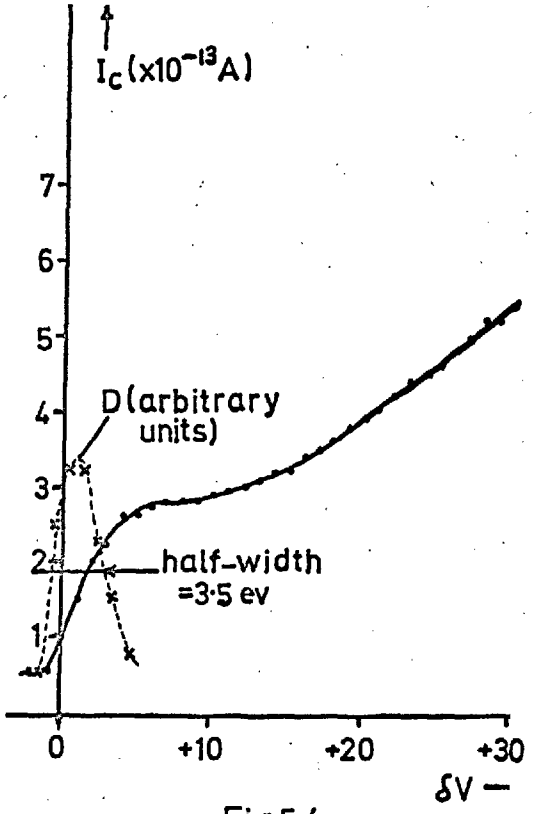

Fig 5.4

5.6 The Filter Lens Spectrometer

The ordinary retarding field analyser and the filter lens analyser do not suffer from the background problem described in Sect.5.5. A spectrometer was constructed using the filter lens analyser described in Sect.4.5 and the tetrode gun (Sect.3.4). The layout was as shown in Figs.5.1(a) and (b) and the electrical circuit similar to that in Fig.5.2, where the retarding potential, $-V_r$, in this case was applied to the gauze, G, of the analyser and the current, I_c, to the cage, C_1, was measured (see Fig.4.4).

Figure 5.4 shows part of the energy spectrum of 400 ev electrons reflected from a contaminated aluminium specimen using this spectrometer. The half-width of the zero energy loss step obtained from the differential curve, D, was 3.5 ev, giving an overall energy resolution for the spectrometer of about 1%, which was smaller than the calculated specific energy resolution of 1.6% given in Sect.4.5. Once again it was impossible to distinguish any characteristic losses in the energy spectrum. See Sect. 5.7.

5.7 The Usefulness of Retarding Field Spectrometers in measuring Characteristic Energy Losses

It was found that the retarding field spectrometers were unsuitable for the observation of characteristic energy losses in low energy electron beams reflected from evaporated specimens. The major fault being that the energy losses were of insufficient intensity to be detected, as compared with the zero energy loss step in the reflected

energy spectrum. It was obvious that if a spectrometer of this type were to be used, then automatic electrical differentiation of the integral collected current curves obtained with the spectrometer would be necessary, in a similar manner to that described by Leder and Simpson (1958). The advantage of obtaining the reflected electron energy spectrum in the differential form, rather than the integral form, is that any energy losses show up as peaks and not as steps in the spectrum, therefore the sensitivity of the recording equipment can be adjusted to accomodate each peak if necessary, whereas this is not possible in the case of the integral curve.

The actual energy resolutions of the spectrometers investigated were good and, in particular, that of the inverse retarding field spectrometer was outstanding, but the problem mentioned in Sect.5.5, together with that mentioned above, ruled it out as far as characteristic energy loss measurements were concerned.

Retarding field analysers have been used in spectrometers by Haberstroh (1956) and Meyer (1957) to observe characteristic energy losses in 30-40 kev electron beams transmitted through thin films of aluminium and germanium. In both of these cases the intensities of the plasma energy losses were approximately equal to the intensity of the group of electrons transmitted with zero energy loss, therefore the losses were easily observed. However, this was not true of gold and silver, where the energy losses appeared with only about ½% of the intensity of the zero energy loss, see Haberstroh (loc.cit.). Therefore it seems that, even under these conditions, in order to make full use of

the retarding field analyser, automatic electrical differentiation of the integral collected current curve is required.

In order to obtain the energy loss spectra in the differential form, the deflection spectrometer described in the following section was constructed. This was considered preferable to the development of the necessary electronic circuits to differentiate the integral curves obtained with the retarding field spectrometers.

Finally, it should be mentioned that, for a given specific energy resolution, a retarding field analyser can probably always be made dimensionally smaller than a deflection analyser, this is because its energy resolution is virtually independent of its size. This, and the relatively simple mechanical construction of such analysers, form the basic advantages of the retarding field analyser when compared with deflection analysers.

5.8 The Final Spectrometer

The spectrometer used in the final experiments consisted of the seven-electrode gun described in Sect.3.6 and the 127° deflection analyser described in Sect.4.8. The arrangement of the spectrometer is shown in Figs.5.5(a) and (b). The target, T, was situated 6.5 cm from the axis, Ox, of the degaussing coils and 2.0 cm from the collimating slit of the analyser, A. The gun, G, was 1.8 cm from the target. In this case the degaussing coils were arranged to cancel the total magnetic field present over the region in which the experiments were carried out (see Sect.2.3). Therefore the plate, P, on which the spectrometer was

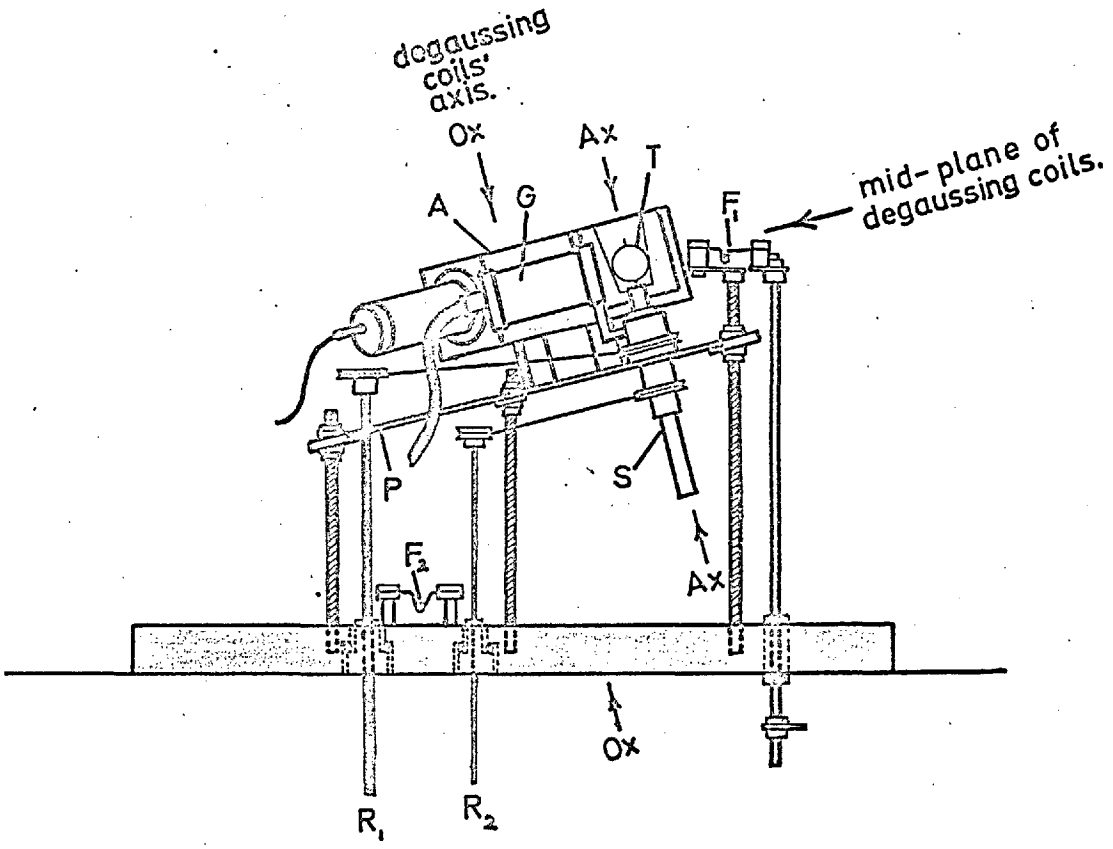

Fig 5.5(a)

4"

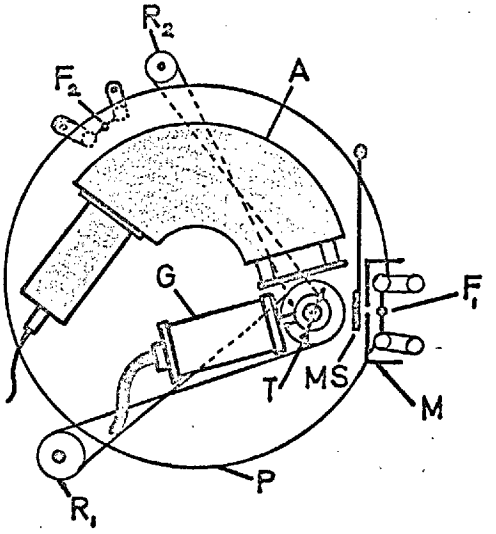

Fig 5.5(b)

supported was arranged as shown in Fig.5.5(b). The gun and target could both be rotated about the axis, Ax, of the shaft, S, supporting the target, by means of pulleys operated by the rotary shafts, R, and R_2 Also shown are the specimen evaporation filament, F_1, and the getter evaporation filament, F_2, as described in Sect.2.2. M and MS, shown in Fig.5.5(a), are the eureka mask and moveable shield described in Sect.2.2. The target initially was of eureka, as described in Sect.5.1, but see Sect. 5.11 for modifications to the target.

5.9 Preliminary Experiments with the Final Spectrometer

Using a circuit like that shown in Fig.4.12(a) and operating the gun under the conditions given in Sect.3.8, experiments were carried out to try to observe the characteristic energy losses in approximately 800 ev electron beams reflected through 90° from freshly evaporated aluminium films, deposited as described briefly in Sect.5.3. The current, I_c, transmitted by the analyser, was measured with the vibrating reed electrometer, V.R.E.(Fig.4.12 a) . Curves such as that shown in Fig.5.6 were obtained, showing only one broad energy loss of about 23 ev and none of the well-known characteristic energy losses of aluminium. It was also found that exactly the same energy loss spectrum was obtained if the electrons were reflected from the eureka target before the evaporation of aluminium onto it. It was thus decided that the spectrum obtained was neither that of aluminium nor eureka, but was in fact the spectrum of some form of contamination present on the target surface.

The overall energy resolution of the spectrometer estimated from the curve in Fig.5.6 was 0.8%, as shown, and was found to be constant

down to primary energies of less than 200 ev. This figure varied slightly with the operating conditions used in the gun for a fixed primary energy, but was in good agreement with the estimated specific energy resolution of the analyser, given in Sect.4.9 as 0.9%.

5.10 Specimen Contamination

Rudberg (1930a) had observed during his original experiments on characteristic energy losses that unless he heated his specimens to incandescence they all exhibited the same energy spectrum with one broad energy loss of 25 ev. Rudberg used solid specimens and not freshly evaporated specimens as in the experiments described in Sect.5.9. However, the present author was forced to the conclusion that the loss mentioned in Sect.5.9 was identical with that mentioned by Rudberg.

Observation of the target while it was under bombardment by a beam from the electron gun showed that a noticeable stain appeared on the target after a period of a few minutes at the point where it was struck by the beam. This effect has been studied in detail by Ennos (1953, 1954) and is due to carbonaceous contamination of the specimen as a result of interaction of the electron beam with hydrocarbons at its surface. These hydrocarbons are present in the residual atmosphere of the vacuum chamber and arise from the backing pump oil, rubber gaskets and other sources, as mentioned by Ennos (1954).

Ennos (1953) claimed that this contamination could be prevented by heating the specimen to about 250°C. However, Powell et al. (1958) found that the specimen needed to be heated to about 400°C. Both Ennos and Powell et al. carried out their experiments in vacua of the order of

10^{-5} mm of mercury, as compared with the normal vacuum of 3×10^{-6} mm of mercury used in the present experiments.

A second form of contamination, which is more difficult to remove but is less serious, is the adsorption of gas by the specimen. According to Harrower (1956a) the monolayer adsorption time for this form of contamination is of the order of one second at a pressure of 10^{-6} mm of mercury. Harrower (1956b) studied the effect of this contamination on the electron reflectivity of tungsten at pressures of the order of 10^{-8} mm of mercury and found that the reflectivity either increased or decreased during the formation of the monolayer, depending on the primary energy of the electrons in the range 3-1000 ev. Powell et al.(loc.cit.), working at about 10^{-5} mm of mercury, found that this form of contamination could be removed from a tungsten specimen by heating it to 1500°C.

Oxidation of some specimens can occur and this was discussed Chapter 1.

The first type of contamination mentioned is a possible explanation for the irregularities, mentioned in Ch.3, in the performances of the electron guns at low energies, since it forms on the electrodes of the guns, and thick layers of contamination can build up after prolonged operation. In fact after operation of the seven electrode gun, under the conditions described in Sect.3.8, for a number of weeks, the contamination formed on some of the electrodes was thick enough to be peeled off. Although the carbonaceous contamination is not insulating, siliceous contamination might also be expected to be formed from the vapour of silicone vacuum grease used on seals in the vacuum system and this is

insulating (Ennos 1954).

A target capable of being heated to over 400°C was constructed in order to verify the assumptions made concerning the contamination of the specimen in the present experiments.

It should be noted that these remarks on contamination do not invalidate the comments made in Sect.5.7 about the usefulness of the retarding field spectrometers since the contamination layer has a characteristic energy loss spectrum (Figs.7.10 and 7.13) which was not observed in the energy spectra obtained using these spectrometers.

5.11 The Heated Target

The target is shown in Fig. 5.7. The heating element was 21 cm of 0.2 x 1.6 mm nichrome strip, of 3.5 ohms/m resistance, non-inductively wound on the mica former shown in Fig. 5.7(a). This fitted inside the tantalum box shown in Fig.5.7(b) and was insulated from it by thin sheets of mica. The tantalum box was constructed from 0.1 mm sheet. The whole target assembly was then clamped between two stainless steel, L-shaped brackets, L, one of which can be seen in Fig.5.7(c), which were then clamped into a slot in the top of the supporting shaft, S, (see also Fig.5.5b). The actual surface onto which the specimens were evaporated was the eureka surface shown in Fig.5.7(d), which was clipped onto the front of the tantalum box by the flanges, F. This surface was thus replaceable.

The heating element was a.c. heated so that any magnetic disturbance to the electron beam incident on the target due to the heating current was averaged out. The temperature of the target was measured with a

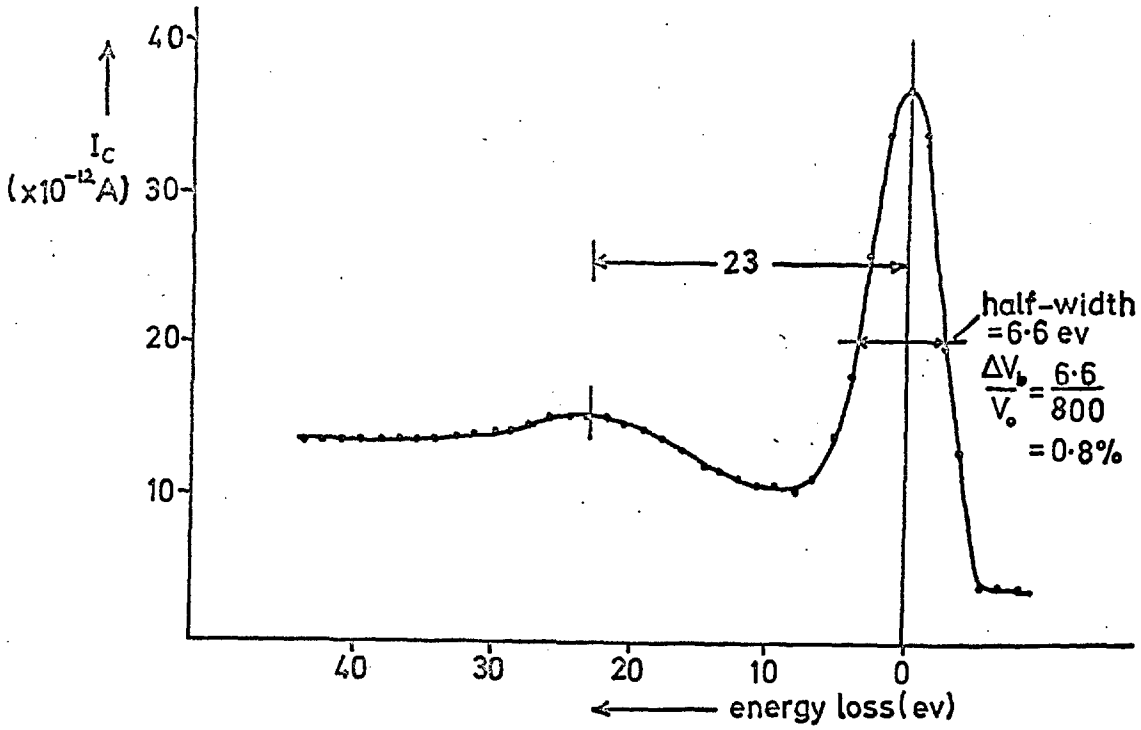
I_c
($\times 10^{-12}$A)
40
30
20
10
23
half-width
=6·6 ev
$\frac{\Delta V_b}{V_o} = \frac{6·6}{800}$
=0·8%
40
30
20
10
0
energy loss(ev)

Fig 5.6

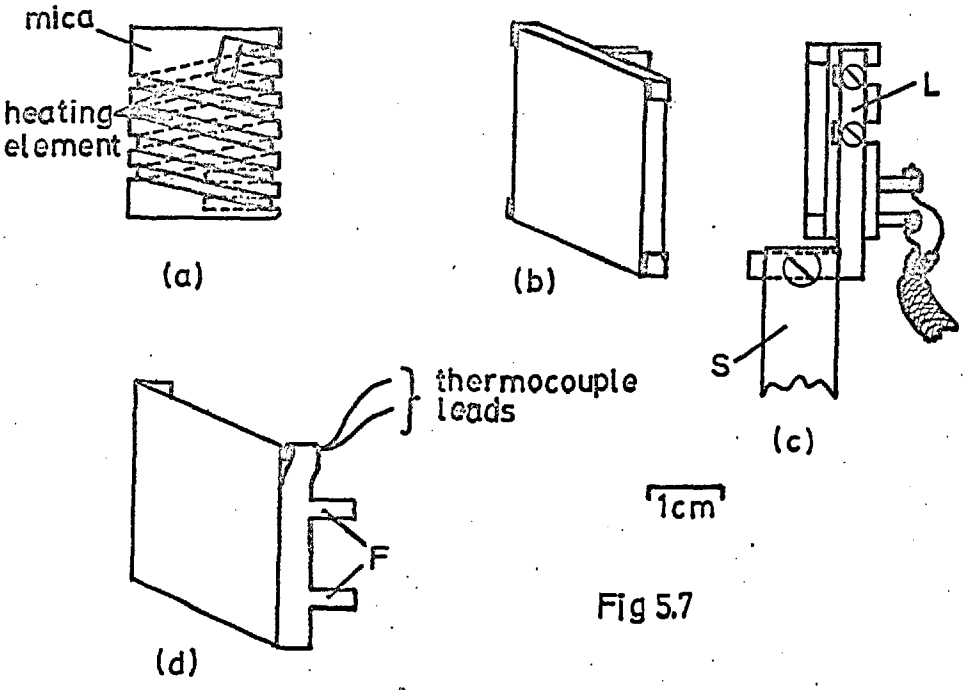
mica
heating
element
(a)
(b)
L
S
(c)
thermocouple
leads
F
(d)
1cm

Fig 5.7

nichrome-constantan thermocouple which was pinched into one of the top corners of the replaceable eureka surface, as shown in Fig.5.7(d). The output of the thermocouple ws measured with a microammeter, and it was calibrated up to 400°C against a nitrogen filled mercury thermometer. The temperature measurements obtained with the thermocouple were accurate to ±5%.

5.12 The Effect of the Specimen Temperature

The target was incorporated in the deflection spectrometer (Fig.5.5). Using the circuit shown in Fig.12(a), 800 and 267 ev electron beams were reflected through approximately 90° from freshly evaporated aluminium layers maintained at 400°C. The energy spectra of the reflected electrons obtained in the two cases are shown in Figs.5.8 and 5.9 respectively. The well-known characteristic energy losses of aluminium were present in both of these curves, as can be seen, although at the higher energy the resolution of the spectrometer was not sufficient to resolve the 10 ev and 15 ev loss peaks which are apparent in Fig.5.9 for the lower energy of the primary electron beam. This is a direct consequence of the specific energy resolution of the analyser being a constant (Sect.4.7).

The experiment proved, beyond doubt, that, unless the precaution of heating the target was taken, even freshly evaporated specimens were contaminated so rapidly by electron bombardment and by the surrounding residual gas, that their energy loss spectra were completely masked by that of the contaminating layer within a minute or so after their evaporation. Further experiments showed that if the target temperature was

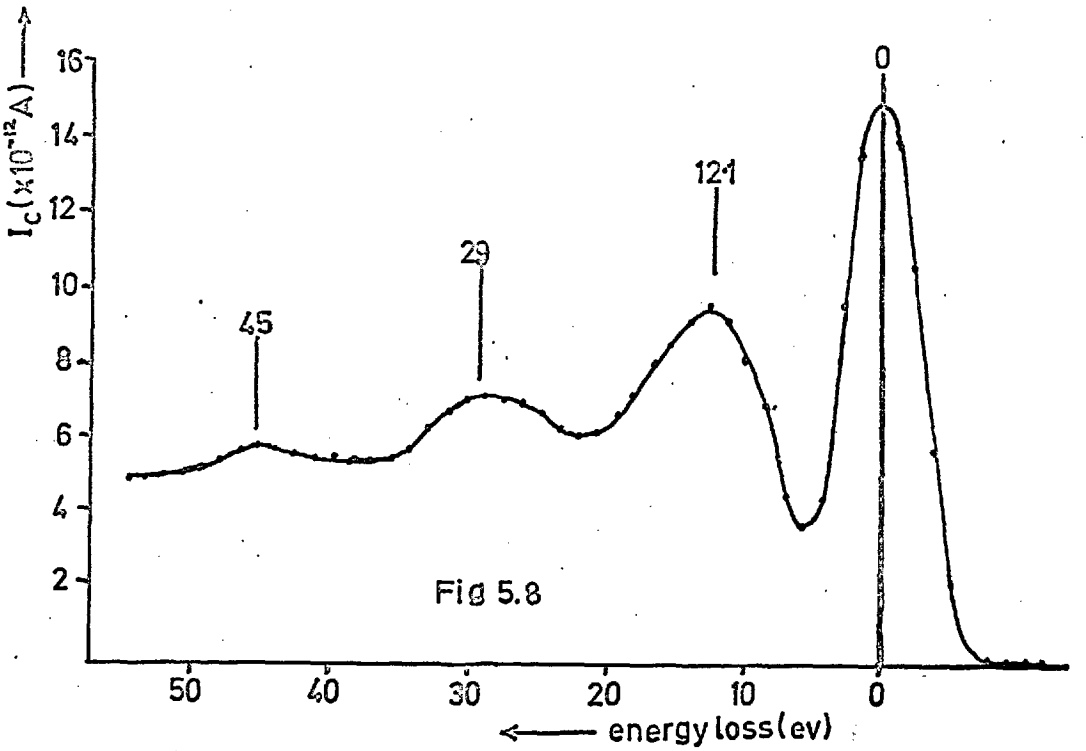
I_c (x10^{-12}A)
16
14
12
10
8
6
4
2
0
12·1
29
45
50
40
30
20
10
0
energy loss (ev)

Fig 5.8

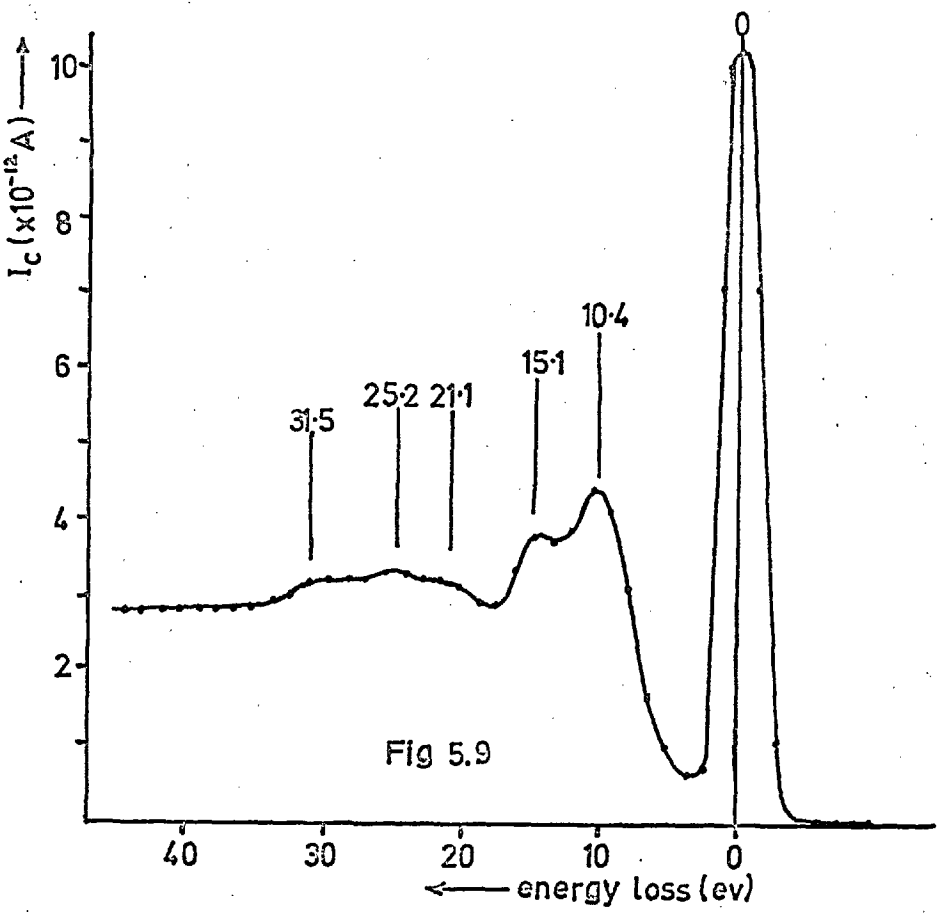
I_c (x10^{-12}A)
10
8
6
4
2
0
10·4
15·1
25·2
21·1
31·5
40
30
20
10
0
energy loss (ev)

Fig 5.9

lowered to 200°C good spectra could still be obtained but at 100°C the energy losses in the spectrum were only just visible on top of the spectrum of the contaminating layer. Hereafter, all of the energy loss spectra were taken with the target at 400°C and with primary electron beams of 200 ev, in order to make the best use of the analyser's resolution.

5.13 The Size of the Primary Electron Beam

By bombarding the target at room temperature with various energy primary beams from the gun for twenty to thirty minutes, the well-defined layer of contamination formed on the target was clearly visible. The extent of this contamination was taken as a measure of the size of the electron beam at the specimen. At 200 ev primary energy, the energy at which the final experiments were performed, the diameter of the beam at the specimen was about 3 mm. No measurements on the amount of current carried by the beam were undertaken, but an estimate of the divergence of the beam from the gun was made using the above method and this was found to be about 6° at 200 ev.

5.14 The Final Spectrometer Circuits

In order to reduce the time necessary to sweep through the energy spectrum of the electrons entering the analyser, the manually operated circuit with which the spectrometer was tested (Fig.4.12a) was discarded and was replaced by the circuit shown in Fig.5.10(a). There, a synchronous-motor-driven potentiometer, P, revolving at 20 revs/hour and with a dead-time of 30 seconds per revolution, produced a saw-tooth

voltage. This was applied to the grid of a triode valve, V (which was a double triode, type CV4024, of which only one half was used). The anode and cathode loads on the valve were equal, thus, by the change of the impedance of the valve, symmetrical positive and negative saw-tooth voltages were generated at the cathode and anode. These were superimposed over a constant voltage which was dependent on the load in series with the valve and the voltage of the stabilised power supply. The amplitude of the saw-tooth waveforms, ΔV_{c1} and ΔV_{c2}, was controlled by the magnitude of the resistances X and Y (increasing as X and Y were decreased) and by the adjustment of the potentiometer T. The constant deflection voltage, V_{do}, applied across the analyser deflector plates, C_1 and C_2, was tapped from the potentiometers R and S, the voltage on each plate being made equal and opposite. The voltage wavoforms thus produced on C_1 and C_2 are shown in Fig.5.10(b). The total, time-dependent, deflection voltage, $V_d(t)$, over one cycle of the sweep was,

$$V_d(t) = V_{do} + V_{so}\frac{(150-t)}{150} \qquad \ldots\ldots\ldots\ldots\ldots\ldots\ldots\ldots\ldots\ldots (5.1)$$

where t is the time in seconds, V_{so} is the sweep voltage amplitude $2\Delta V_c$ (ΔV_c being the amplitude of the saw-tooth voltage on either C_1 or C_2) and 150 was the active-time, in seconds, of the motor-driven potentiometer per three minute revolution. Referring again to Fig.5.10(a), $V_d(t)$ was the difference in the readings shown by the voltmeters M_1 and M_2, and $V_{so}(150-t)/150$, which is called the sweep voltage, $V_s(t)$, was indicated by the voltmeter M_3, from which V_{do} was backed-off by the H.T. battery shown. Voltmeter M_4 was a calibration meter (see Sect.6.3); it was

disconnected when the circuit was in operation. The 5M-ohm resistance, in parallel with M_4, served to prevent the grid of the valve from floating and causing the valve to be cut-off when the wiper of P left the resistance track at the end of a revolution. The two 1K-ohm resistances were included when it was found that the voltage ripple on the deflection voltage, $V_d(t)$, could be reduced by increasing the current drain on the power supply. A second precaution taken to remove spurious ripple on $V_d(t)$, was the heating of the valve filament with accumulators in place of the original a.c. supply used. With these precautions the ripple was reduced to 0.2V peak to peak on C_1 and C_2. The effect of this ripple is discussed in Sect.6.3.

An analysis of the circuit, assuming that the current drain through the R-S branch was small compared to the current, I_a, passing through the valve, showed that by means of R and S, the maximum value of $V_d(t=0)$ could be varied between 100V and 33V. The maximum values of the sweep voltage, V_{so}, corresponding to these values of V_d were 22V and 7.3V. In this case, the saw-tooth voltage across the valve was produced by a change in the grid bias, v_g, from -1.0V to -0.5V (0.5V volts change in the grid bias corresponds to a change in the absolute grid voltage of 10.3V, due to the cathode follower action of the cathode load). In practice, it was found that the maximum value of $V_d(t=0)$ could be varied between 96V and 32V, and that the maximum values of V_{so} at these voltages were 19.4V and 6.5V, giving good agreement with the calculated values allowing for tolerances in the values of components and the assumption made. Deflection voltages of 96V and 32V applied to the

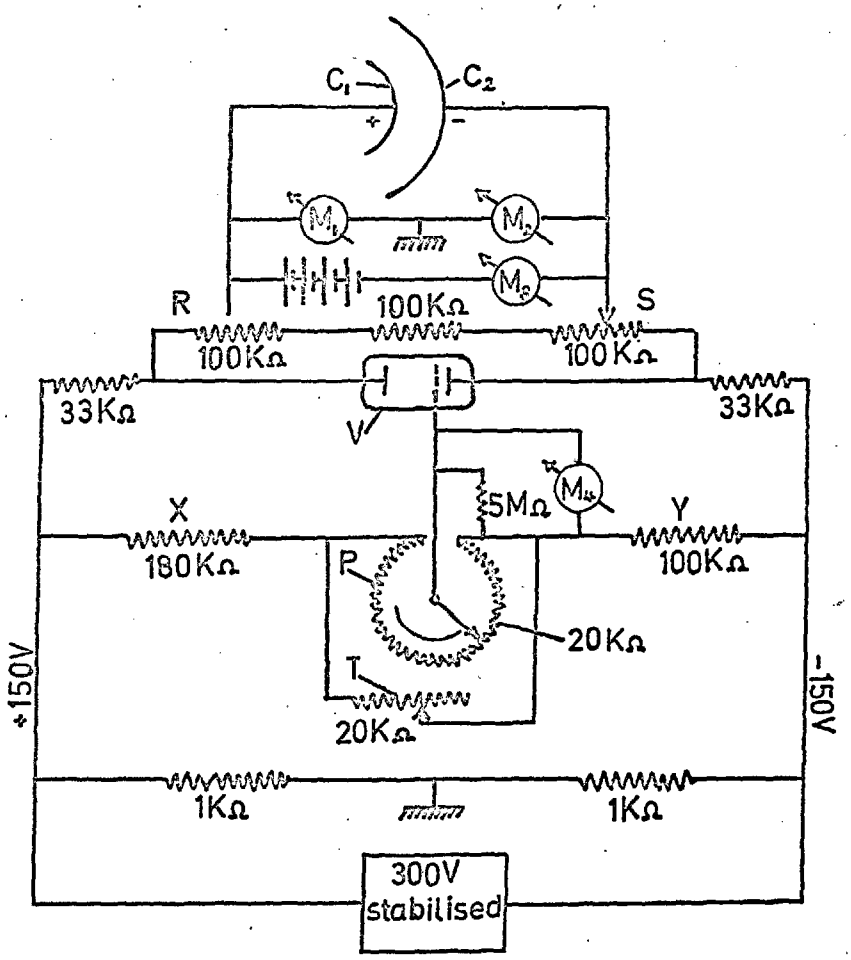

Fig 5.10(a)

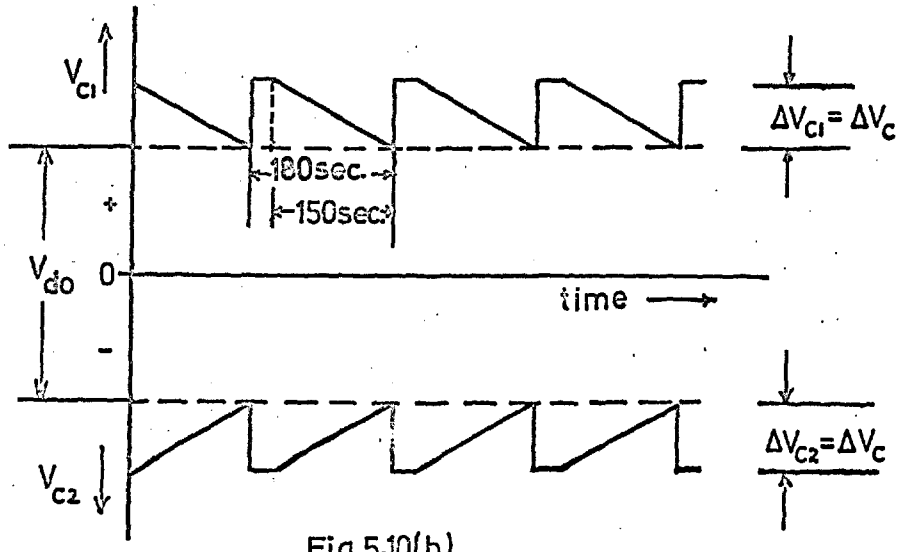

Fig 5.10(b)

analyser would focus 262 ev and 87.4 ev electron beams respectively (equn.4.12), thus these are the extreme primary beam energies which can be made use of with the present circuit for driving the analyser.

A disadvantage of the circuit, is that the sweep voltage amplitude V_{so}, is linearly dependent on the constant deflection voltage, V_{do}, as a result of the potential drop across the R-S branch (Fig.5.10a). Therefore it is advantageous to make V_{so} as large as possible at the maximum value of $V_d(t=0)$. This can be done by decreasing X and Y in Fig.5.10(a), but a limitation is set by the linearity of the characteristics of the valve which affect the linearity of the saw-tooth waveforms. In fact, if the differential anode resistance of the valve, $r_a = (\delta V_a/\delta I_a)_{vg}$, and the mutual conductance, $g_m = (\delta I_a/\delta v_g)_{Va}$, were constant, then the sweep voltage would be perfectly linear. It is because these two quantities are not constant that the amplitude of the sweep voltage, V_{so}, had to be limited if good linearity of the sweep was to be obtained (see also Sect.6.3). The final characteristic energy loss experiments were carried out with 200 ev primary electrons, and by setting X and Y to the values shown in Fig.5.10(a), a sweep voltage of amplitude $V_{so} = 13.7V$ was obtained, superimposed on the required constant deflection voltage, V_{do} of 60.3V. $V_{do} + V_{so} = 74V$ is the maximum value of the deflection voltage, $V_d(t)$, and is sufficient to focus 202 ev electrons through the analyser. The maximum deflection voltage was always arranged slightly greater than that required to focus the primary electrons; this was in order to obtain the complete distribution of the elastically reflected electrons on the measured spectra. In the region in which the valve was operating r_a

and g_m, as given by the manufacturers, were 16.7 K-ohm and 3.8 mA/V respectively.

The voltmeters, M_1, M_2, M_3 and M_4, were all converted microammeters and thus had high resistances (400-500 K-ohm) so that they did not seriously affect the circuit, and all had been calibrated against a Tinsley potentiometer.

Using the circuit described above to drive the analyser, the beam current, I_c, transmitted by the analyser, was now automatically plotted as a function of the deflection voltage by means of a pen-recorder, which was driven by the vibrating reed electrometer used to measure I_c. The pen-recorder had two possible chart speeds, of 1"/min. and 6"/min. Knowing the amplitude of the sweep voltage, V_{so}, it was a simple matter to express distances measured along the length (x-axis) of the chart in terms of an energy loss scale. The energy loss corresponding to one inch of the chart was given by,

$$\left(\frac{V_{so}}{0.366}\right) \Big/ \left(\frac{5}{2} \cdot S\right) \text{Volts} \qquad \ldots\ldots(5.2)$$

where S is the chart speed in inches per minute and equn.(4.12) has been used. The factor 5/2 accounts for the active-time per revolution of the motor-driven potentiometer in minutes. As mentioned earlier, for the final experiments V_{so} was 13.7V. The chart speed was 6"/min. The energy loss scale on the charts, calculated from equn.(5.2), was therefore 2.5 Volts/inch or 0.25 Volts/sec.

The circuit used for the gun is shown in Fig.5.11 and is straightforward.

In Fig.5.12 a schematic diagram of the complete spectrometer is given.

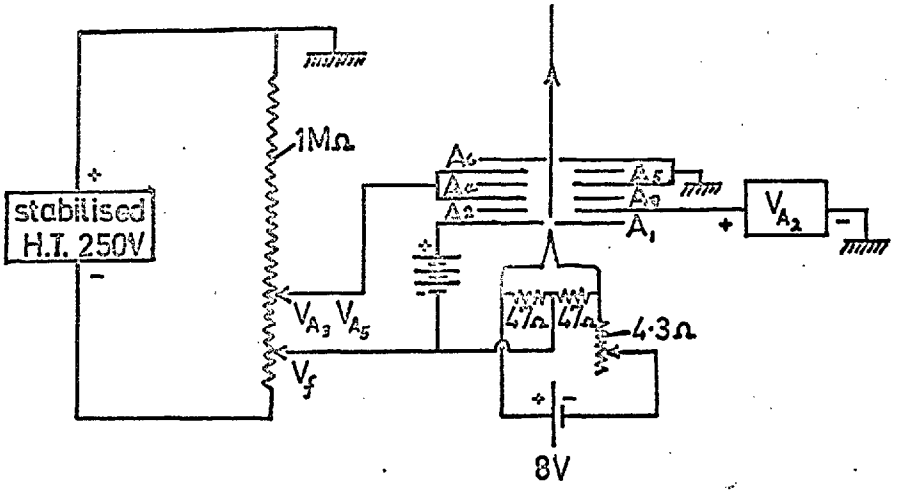

Fig 5.11

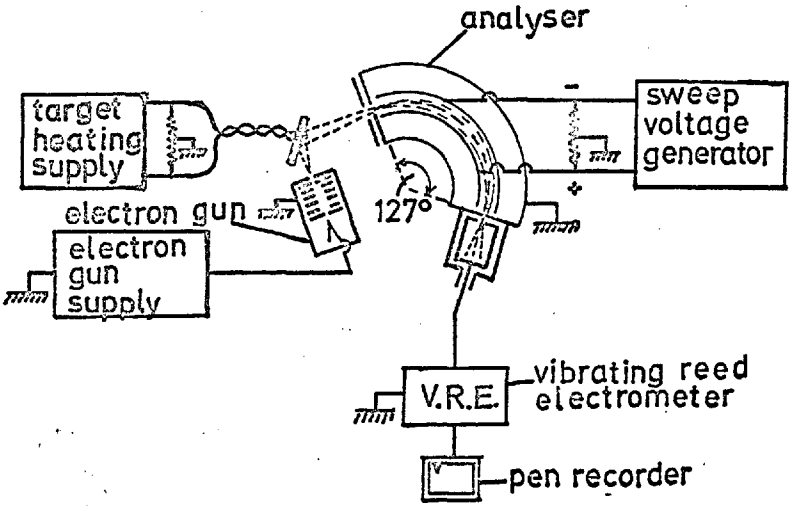

Fig 5.12

CHAPTER 6.

EXPERIMENTAL TECHNIQUES AND PRECAUTIONS

Some basic experimental precautions have already been mentioned in Section 2.4.

6.1 Specimen Preparation and Purity.

The specimen metals and the getters were evaporated from tungsten filaments (Sect.2.2). These filaments were first cleaned electrolytically in 20% w/w KOH solution in order to remove a layer of graphite present on the tungsten surface. After rinsing in distilled water they were degassed at progressively higher temperatures, in a vacuum of about 10^{-5}mm of mercury, until they could be flashed to white heat for several seconds without causing the pressure in the vacuum chamber to fall below 10^{-4}mm of mercury. These precautions were taken to avoid, as far as possible, contamination of the evaporant and hence the specimen by the evaporation filament.

The specimen material itself had also to be degassed prior to evaporation onto the target. For this purpose it was loaded onto the specimen evaporating filament, F_1, shown in Fig.5.5. It was degassed for several minutes just below its melting point and was then melted and degassed for a further period of a minute or so, depending on the material being evaporated. During this period it was shielded from the target, T, by the moveable shield, MS, as shown in Fig.5.5(a), which

covered the aperture in the mask, M. The target, T, which was kept at 400°C, was rotated to face F_1, which was then heated until the specimen metal was seen to be freely evaporating; this could be seen from the deposition of the metal vapour on the glass bell-jar which formed the vacuum chamber. The moveable shield, MS, was then drawn away from the aperture in M, allowing evaporation onto the target.

No estimate of the thickness of the specimens evaporated was made, nor was the evaporation rate checked for successive evaporation. However, experience showed that the best characteristic energy loss spectra were obtained from specimens which had been evaporated rapidly; that is the evaporant was heated to the stage where it was freely evaporating, as described above, and was then flashed to a much higher temperature for a few seconds. Up to ten or more evaporations could be achieved from one loading of the filament F_1, depending on the material being evaporated.

In the cases of evaporating aluminium and germanium, it was found advantageous to getter the chamber before the specimen evaporation, otherwise the first two or three evaporations were wasted due to what was thought to be oxidation of the specimen; this was achieved by firing an aluminium getter twice at a three minute interval from the filament F_2, shown in Fig.5.5 and then waiting a further three minutes before evaporating the specimen. By using this method the first specimen evaporation gave a specimen whose characteristic energy loss spectrum was typical of the fresh material. This precaution was not necessary when evaporating gold and copper.

When specimens had oxidised, or had otherwise been contaminated, a fresh specimen was evaporated on top of the old one, but different metals were never evaporated on top of each other. A fresh target surface (Sect.5.11) was always used when the type of specimen being investigated was altered.

Rapid evaporation of the evaporant onto the target has the advantages that the specimen produced is purer and suffers from less agglomeration than one formed by slow evaporation, see for example Holland, (1960).

6.2 Energy Loss Measurement Procedure

The specimen, having been evaporated onto the target, was immediately rotated into the reflection position to be bombarded by the primary electron beam from the gun. The specimens investigated were usually about 30 seconds old before their energy loss spectra began to be recorded. Due to the 3 minute period of the sweep voltage circuit, the specimen was about 3 minutes old at the completion of the first sweep through the energy loss spectrum.

For all the materials investigated the energy loss spectra were recorded for two scattering angles. These were approximately 90° and 20° respectively (Sect.7.1). In both cases, the angles of incidence of the primary beam on the target and of reflection of the selected ray scattered from the target were made approximately equal.

6.3 Stability of the Spectrometer Circuits and Accuracy of Results

A check on the stability of the primary electron beam voltage could

be kept throughout the experiments, since the zero energy loss peaks of consecutively recorded spectra, should always have been separated by 18 inches on the recording chart when it was running at 6 inches per minute. It was found that the beam voltage of 200V was constant to within ± 0.2V over the three minute cycle; giving a stability ratio of one part in 10^3. This variation accounts for the major part of the statistical fluctuation in the accuracy of the measured energy loss values. Voltage ripple on the gun filament amounted to 0.08V peak to peak with a frequency of 50 c/s and this contributed to the energy spread present in the primary electron beam.

The stabilised power supply which supplied the sweep voltage circuit (Fig.5.10a) was stable to within ±0.1V at 300V over a period of an hour and this corresponded to ±0.02V fluctuations in the deflection voltage, $V_d(t)$, appearing across the condenser plates C_1 and C_2 of the analyser; or a stability ratio of about one part in 3×10^3 at the deflection voltages used ($V_d \simeq 73V$ for the analyser to focus a 200 ev electron beam). The ripple on the deflector plates of the analyser amounted to 0.2V peak to peak and was 50 c/s. Although this figure seemed large, it was found that the resolution of the spectrometer (0.8%) was unaltered when the ripple was reduced to 0.015V peak to peak. The resolution of the spectrometer was not worse than 1.9% with 10V peak to peak ripple on both deflector plates; however, in this case the recorded energy loss peaks on each spectrum were visibly distorted.

The stability of the voltage supplies was measured by a compensation method, a voltmeter being connected to the output terminals and backed-off

by means of H.T. batteries, so that only the last few volts of the output showed up on the meter. In this manner variations of less than a tenth of a volt in the output voltage of the supplies were easily detected. The ripple on the output of the supplies was measured directly with an oscilloscope.

The linearity of the sweep voltage waveform produced by the circuit shown in Fig.5.10(a), depended on the linearity of the motor-driven potentiometer and on the properties of the valve used. The effect of the valve was measured by means of the voltmeters M_3 and M_4, shown in Fig.5.10(a). The variation of the sweep voltage, V_s, across the analyser deflection plates was plotted as a function of the variation of the absolute grid voltage, V_g, on the valve (not the grid bias), with the reference point being the negative end of the motor-driven potentiometer P. The V_s versus V_g graph thus obtained, though slightly curved, was found to be linear to within $\pm 0.1V$ in V_s. The motor-driven potentiometer was linear to 0.1%. However, due to the 5M-ohm shunt between its negative terminal and its wiper contact (Fig.5.10a) (and possibly due to grid current in the valve), the saw-tooth voltage, $V_g(t)$, which it generated on the grid of the valve, was found to be linear to only 0.5%. This non-linearity was thus also present in the actual sweep voltage, $V_s(t)$, applied to the analyser. By good fortune, the distortion in the sweep voltage curve, due to this non-linearity of the potentiometer output, was such that it slightly corrected for the non-linearity of the V_s versus V_g curve. This can be seen from Fig.6.1(a), which represents an exaggerated example of the $V_s(V_g)$ curve, and Fig.6.1(b), which is a

similar example of the absolute grid voltage, V_g, on the valve plotted as a function of the time of the sweep. Now we wish to know $V_s(t)$, rather than $V_s(V_g)$; this involves plotting time, t, as the ordinate in Fig.6.1(a) in place of V_g. Since $V_g(t)$ is not linear, the V_g scale in Fig.6.1(a) must be adjusted in order to accomodate a linear time scale. After this adjustment V_g at a given time, t_o, will be lower by δV_g than it was on the previously linear V_g scale; this is shown on Figs.6.1. Therefore, when the ordinate axis of Fig.6.1(a) is converted from a linear V_g scale to a linear time scale, the V_s curve is moved slightly to the right as shown by the dotted curve in Fig.6.1(a); e.g. at time t_o it is shifted from P_1 to P_2. The amount of the shift, $V_{s2} - V_{s1} = \delta V_s$, depends on δV_g, which is zero at the ends of the $V_g(t)$ curve and has a maximum of 0.03V in the central region; this corresponds to a maximum value of δV_s of 0.04V. The $V_g(t)$ distortion therefore opposes the $V_s(V_g)$ distortion. The $V_s(t)$ curve therefore remains linear to within $\pm$0.1V.

The nature of the non-linearity in $V_s(t)$ meant that energy losses recorded would be slightly larger than their true values. This effect being most pronounced for losses falling in the central region of the sweep ($\sim$12 - 23 ev) where it was estimated to be of the order of 0.1 ev. It was not really feasible to correct for this, since the point on the $V_s(t)$ curve corresponding to the zero energy loss peak on the recorder chart (from which all the other losses were measured) could not be determined exactly. The measured energy loss values were therefore considered to be correct to 1%.

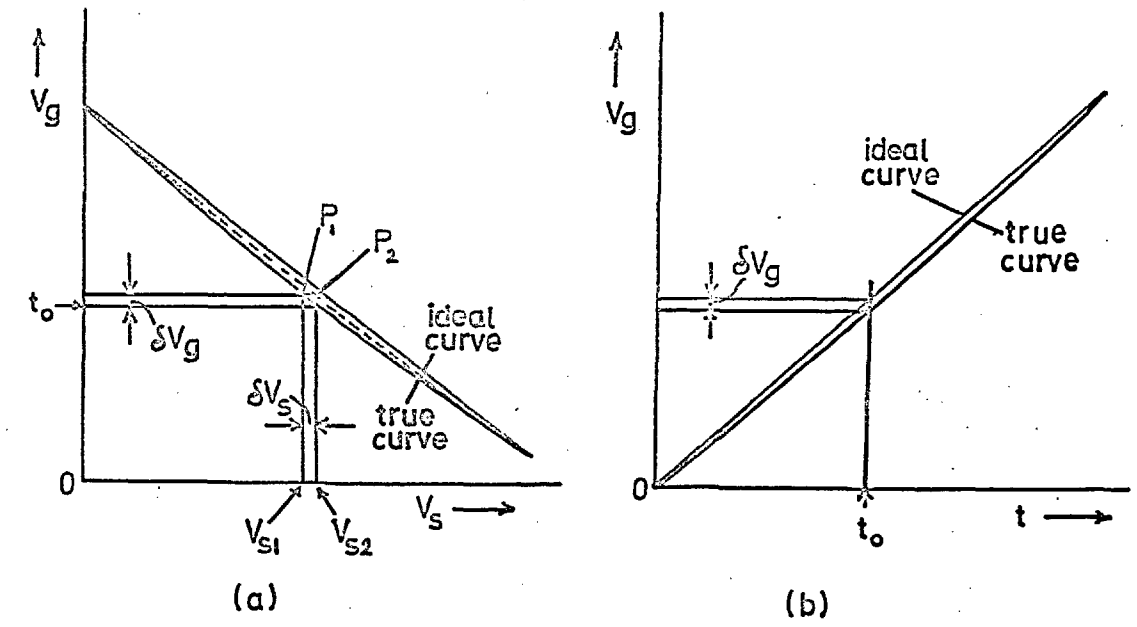
Vg
P1
P2
to
δVg
ideal curve
δVs
true curve
0
Vs1
Vs2
Vs
(a)
Vg
ideal curve
true curve
δVg
0
to
t
(b)

Fig 6.1

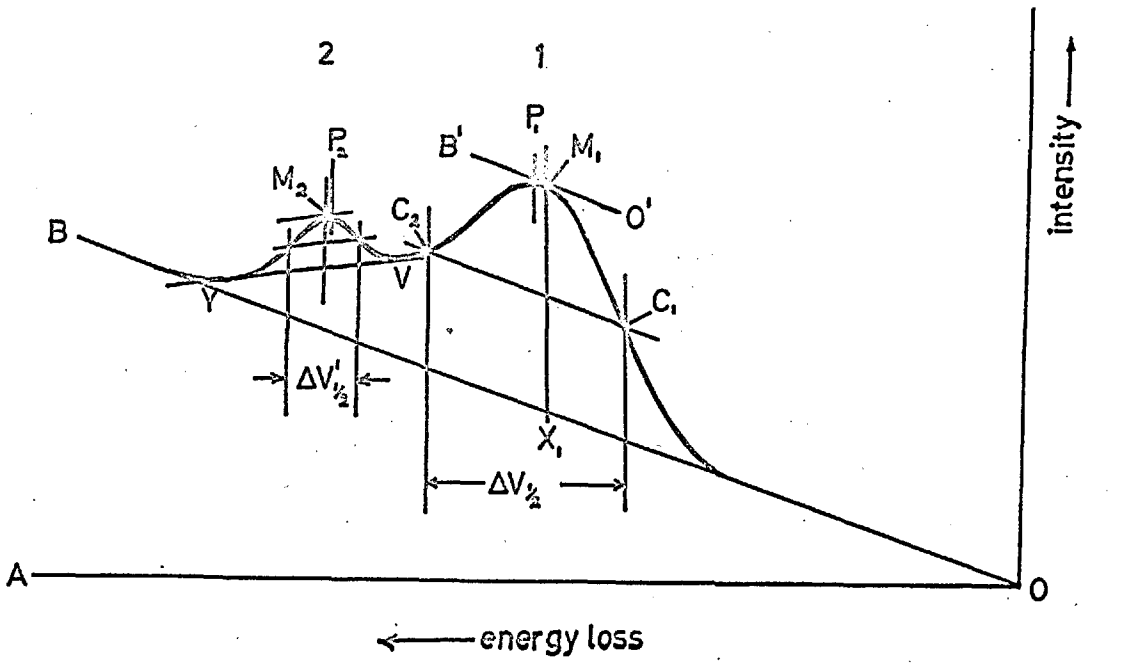
2
1
P2
P1
B'
M1
M2
C2
O'
B
V
Y
C1
ΔV'½
X1
ΔV½
intensity
A
O
energy loss

Fig 6.2

Another possible source of error in the deflection voltage across the analyser is due to the current which reaches the deflector plates from the beam entering the analyser. This current goes to earth via the external sweep voltage circuit (Fig.5.10a) and produces a change in the deflection voltage. The main effect is produced at the positive deflector plate, C_1, since slow electrons entering the analyser, and secondary electrons produced in the analyser, proceed to C_1 under the influence of the deflection voltage. Measurements showed that the currents to the deflector plate C_1 were of the order of 10^{-8} Amp. and therefore negligible, since they would only produce a change of about 1 mV in the voltage on C_1 when the analyser was used with the circuit of Fig.5.10(a).

6.4 Evaluation of the Recorded Spectra

A procedure for determining the values of the energy losses from the curves registered by the recorder has been worked out by Shepherd (1962). His procedure was adopted essentially in the present investigations.

The recorder used utilised a chart on which the y-axis (current-axis) was curved with a radius of 6 inches, therefore a template of radius 6 inches (accurate to 0.01") was used to draw lines along the y-axis through relevant points in the spectrum, in order to find their abscissae. The zero of the abscissa axis (energy-loss axis) was always taken to correspond to the maximum of the elastically-scattered electron distribution peak, which is called the zero energy loss. From the distances measured along the abscissa from the zero energy loss, the energy losses were evaluated with the aid of equn.(5.2). However the

following corrections have to be considered before the losses can be measured. The sloping background, on which the energy loss peaks are invariably situated, shifts the maximum of a loss distribution to either a higher or lower value, depending on the sign of its slope. This error becomes more serious as the half-width of the energy loss distribution involved becomes larger. The method used for finding the true maxima of the energy loss distributions is shown in Fig.6.2, where two such distributions, 1 and 2 are shown on the sloping background OB. The apparent maximum of the loss distribution 1 is P_1, but the true maximum, M_1, of the loss, lies at the point where the tangent, O'B' (drawn parallel to OB), touches the distribution. The correct half-width of the distribution is now found by drawing a line parallel to OB through the mid-point of M_1X_1, which is perpendicular to OA. The horizontal separation of the points C_1 and C_2, where this line intersects the loss distribution, is the half-width, $\Delta V_{\frac{1}{2}}$, of the curve. M_1X_1 is called the intensity of the loss distribution. The true background underneath the loss distribution 2 is uncertain, due to the close neighbourhood of the other intensity maximum, 1. In such a case the background has to be estimated from the general shape of the complete spectrum. If the peaks of the distribution are reasonably well separated, as in Fig.6.2, the background is drawn as a tangent to the two minima on either side of the peak. Applying this method to the energy loss distribution 2, the background YV is found. The true maximum, M_2, and the half-width, $\Delta V_{\frac{1}{2}}'$, are then found in the same way as for the distribution 1. The background drawn was always assumed to be linear. All energy losses were measured

on the recorder chart to an accuracy of ±0.01". This corresponds to an error of about ±0.03 ev in the value of the measured loss (see Sect.5.14). This error, however, is relatively small as compared with the fluctuation in the beam voltage supply mentioned in Sect.6.3, but both of these errors will be averaged out over a large number of measurements.

6.5 The Effect of the Time Constant of the Recording System

The finite time constant of the system used for recording the characteristic energy loss spectra introduces distortion on the recorded spectra. This time constant is defined as the time taken for the output of the recording system to fall by a factor of 1/e(=1/2.72) of an initial steady value when the input to the system is suddenly switched off. All the spectra obtained were recorded on one particular range (R_2) of a vibrating reed electrometer (Sect.4.1) and therefore the time constant of the combined electrometer and pen-recorder system was only determined for this range. It was measured directly from recorded spectra as follows. At the end of each sweep through an energy loss spectrum, taken in the direction of decreasing energy, the dispersed electron beam in the analyser was swept instantaneously back across the exit slit of the analyser. This happened as the wiper of the motor-driven potentiometer of the sweep voltage circuit (Fig.5.10a) left the end of its track and became stabilised at the voltage of the negative end of the track. When this occurred the current collected by the electrometer dropped immediately to zero. The reading indicated by the pen-recorder, however, fell exponentially to zero and a measurement of the time constant of this decay yielded directly the overall time constant of the electrometer and pen-

recorder. The time constant thus measured was 0.7 sec. and it was mainly due to the inertia of the pen-recorder for which the manufacturers state a time constant of 0.6 sec.

In order to calculate the effect of the time constant, τ, on the recorded spectra, Shepherd (1962) represented the recording system as a resistance, R, in parallel with a condenser, C, where R and C are constants of the recording system. One end of this circuit is earthed, and the input current pulse, i(t), representing an energy loss distribution, is applied to the opposite end, from which also the output voltage pulse, $V_o(t)$, is taken, where t represents time. The equation representing the circuit is

$$\frac{dV_o}{dt} + \frac{V_o}{\tau} = \frac{R}{\tau} i(t) \qquad \ldots\ldots(6.1)$$

where $\tau = RC$ = the time constant of the circuit.

In order to solve this equation Shepherd assumed an input current pulse, corresponding to an energy loss distribution, of the form

$$i(t) = c - d\left[t - (c/d)^{\frac{1}{2}}\right]^2 \qquad \ldots\ldots(6.2)$$

where c and d are constants. Equation (6.2) represents the parabola shown in Fig.6.3 whose maximum value is c, at time $(c/d)^{\frac{1}{2}}$, and whose half-width is $(2c/d)^{\frac{1}{2}}$ secs. A more accurate form for i(t) would be the Gaussian distribution shown in Fig.6.3 but Shepherd chose the distribution given in equn.(6.2) in order to simplify the solution of equn. (6.1).

Without quoting the solution to equn.(6.1), it will be stated that the relationship between the time, t', at which the maximum of the output pulse, $V_o(t)$, is registered and the time, $t = (c/d)^{\frac{1}{2}}$, at which the

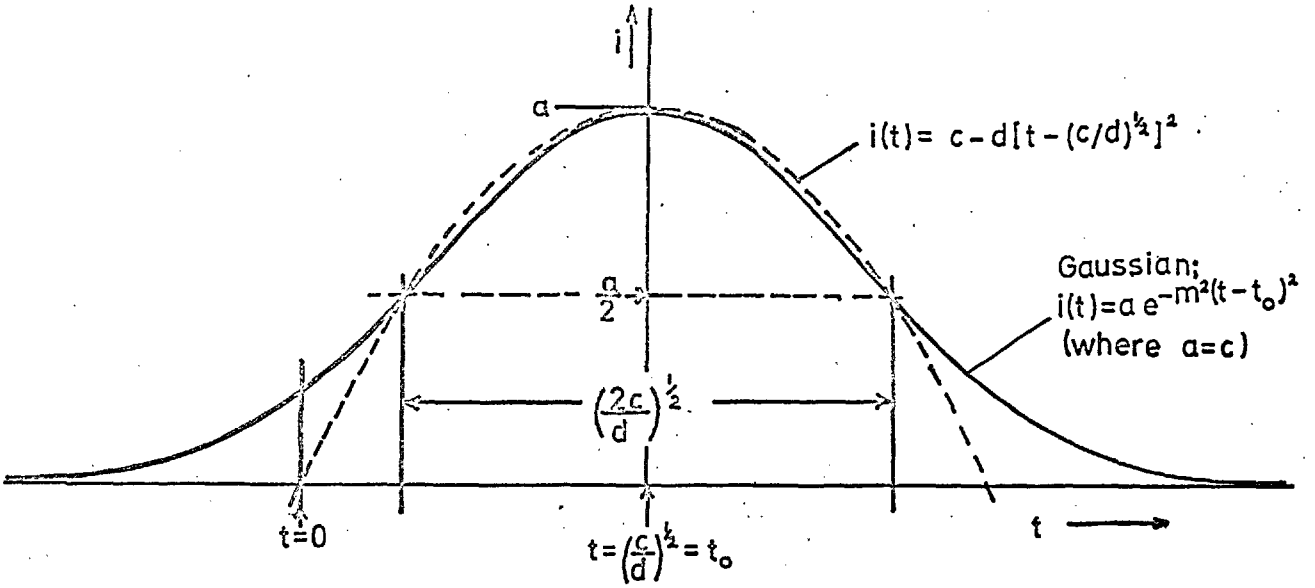
i
a
i(t)= c - d[t - (c/d)^½]²
Gaussian;
i(t)=a e^-m²(t-t_o)²
(where a=c)
a/2
(2c/d)^½
t=0
t=(c/d)^½ = t_o
t

Fig 6.3

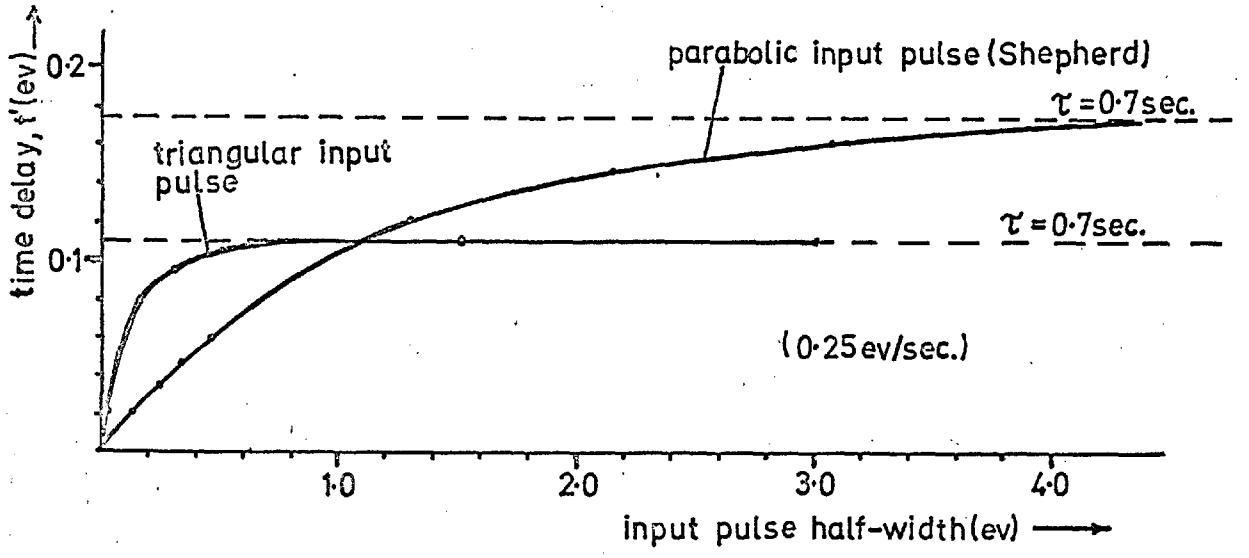
time delay, t'(ev)
0·2
0·1
parabolic input pulse (Shepherd)
τ = 0·7sec.
triangular input pulse
τ = 0·7sec.
(0·25ev/sec.)
1·0
2·0
3·0
4·0
input pulse half-width (ev)

Fig 6.4

maximum of the input pulse occurs is given by

$$\frac{t}{\tau} = \frac{(c/d)^{\frac{1}{2}}}{\tau} = \frac{t'/\tau}{(1-e^{-t'/\tau})} - 1 \qquad \ldots\ldots(6.3).$$

The output maximum is thus delayed by $t' - (c/d)^{\frac{1}{2}}$ secs. which is a function of $(c/d)^{\frac{1}{2}}$ and τ. In the present case it is the $(c/d)^{\frac{1}{2}}$ dependence which is important since $(c/d)^{\frac{1}{2}} = 2^{-\frac{1}{2}}$ x (the input pulse half-width), while τ is a constant. Using equn.(6.3) and remembering that 1 sec. is equivalent to 0.25 ev (Sect.5.14), the time delay, $t' - (c/d)^{\frac{1}{2}}$, expressed in ev, has been plotted in Fig.6.4 against the input pulse half-width, $(2c/d)^{\frac{1}{2}}$, expressed in ev, for τ=0.7 sec. It can be seen there that the delay reaches a limiting value of 0.18 ev for an input pulse half-width of 4.0 ev. The smallest half-width (output pulse) measured experimentally was of the order of 1.3 ev, therefore it can be anticipated that no correction greater than -0.05 ev is required for any of the measured energy losses. However, before one can be certain of this it is necessary to determine the effect of the time constant, τ, on the half-widths of the loss peaks in the recorded spectra. In order to do this and to calculate the recorded intensity as a function of τ, Shepherd (loc.cit.) assumed a rectangular input current pulse of amplitude A and width b secs. The present author considers that a triangular input current pulse should be a more realistic approximation upon which to base the calculation. This is shown in Fig.6.5, where the two pulses mentioned are shown in comparison with a Gaussian pulse. Therefore the problem is now to solve equation (6.1) with a current pulse of the form

$$i(t)=\begin{cases}0 & \text{for } t<0\\ kt & " \quad 0\leqslant t\leqslant t_o\\ k(t_o-t) & " \quad t_o<t\leqslant 2t_o\\ 0 & " \quad 2t_o<t\end{cases} \qquad \ldots\ldots\ldots\ldots\ldots\ldots\ldots\ldots\ldots\ldots(6.4)$$

where $\pm k$ = the slope of the two sides of the pulse. It will be useful in the following to introduce

$$\begin{aligned} kt_o &= a = \text{ the intensity of the pulse}\\ t_o &= b = \text{ the half-width of the pulse}\end{aligned} \qquad \ldots\ldots\ldots(6.5)$$

The solution of equation (6.1) can now be obtained by splitting the problem into three parts, as shown in Fig.6.6, corresponding to the regions 1, 2 and 3 shown on the time axis there. Banner (1966) has carried out the analagous problem to this for a triangular voltage pulse, $V(t)$, applied to a series resistance and capacitance, the output, $V_o(t)$, being measured across the capacitance. The solution to equation (6.1) is straightforward for each region and the results are:-

$$\begin{aligned} \text{Region 1} \quad V_1(t) &= (Ra/b)\left[t-\tau(1-e^{-t/\tau})\right]\\ \text{Region 2} \quad V_2(t) &= (Ra/b)\left[b+\tau-t-\tau(2-e^{-b/\tau})e^{-t/\tau}\right] \qquad \ldots\ldots(6.6)\\ \text{Region 3} \quad V_3(t) &= (Ra/b)\,\tau(1-e^{-b/\tau})2e^{-t/\tau}\end{aligned}$$

where t, in each region, is measured from the beginning of that region. These solutions have been plotted for $\tau = 0.7$ sec. and for various values of b in Fig.6.6.

In order to find the recorded intensity as a function of b it is first necessary to find the time at which the recorded maximum occurs. This is achieved by finding the condition for $dV_2(t)/dt = 0$, which gives

$$t_d = \tau \ln(2-e^{-b/\tau}) \qquad \ldots\ldots\ldots\ldots\ldots\ldots\ldots\ldots(6.7)$$

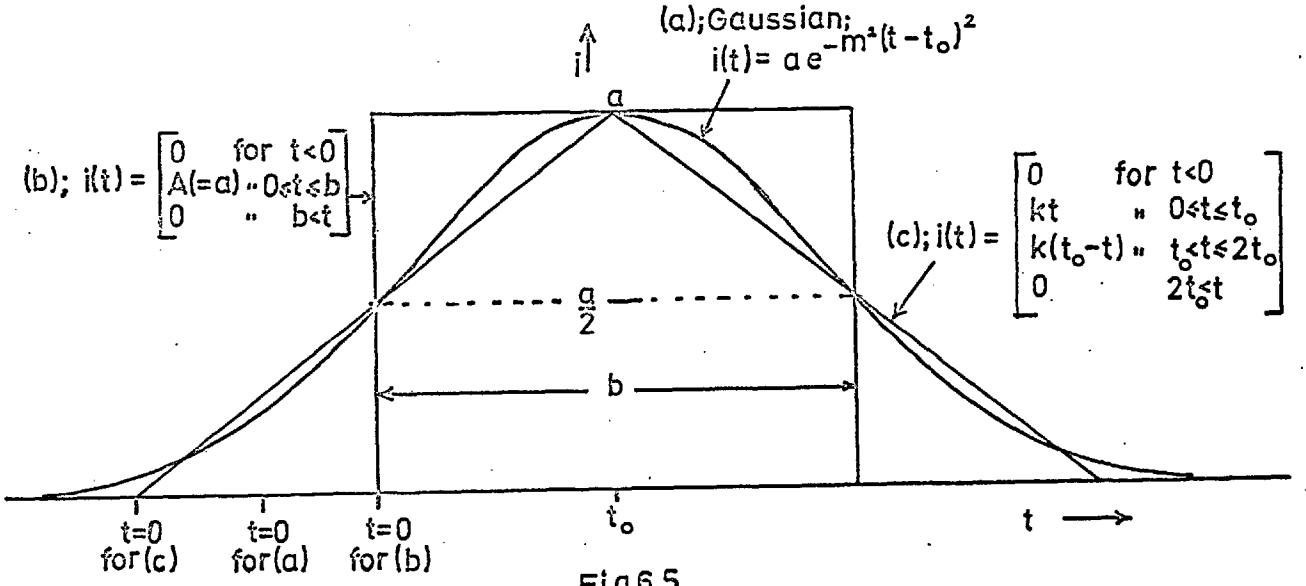
(a);Gaussian;
$i(t) = a e^{-m^2(t-t_o)^2}$
i
a
(b); i(t) = [0 for t<0; A(=a) " 0≤t≤b; 0 " b<t]
(c); i(t) = [0 for t<0; kt " 0≤t≤t_o; k(t_o-t) " t_o≤t≤2t_o; 0 2t_o≤t]
a/2
b
t=0 for (c)
t=0 for (a)
t=0 for (b)
t_o
t

Fig 6.5

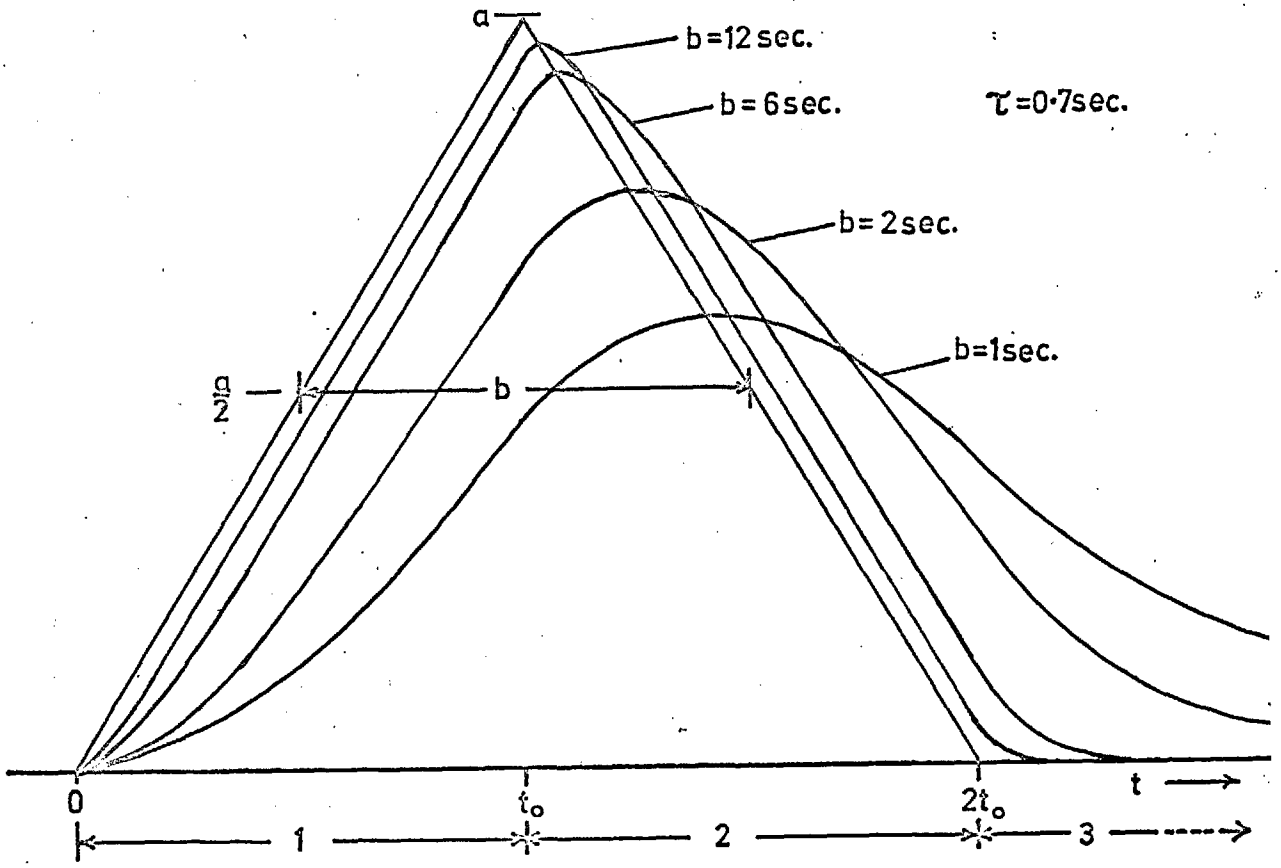
a
b=12 sec.
b=6 sec.
τ=0·7sec.
b=2 sec.
b=1sec.
a/2
b
0
t_o
2t_o
t
1
2
3

Fig 6.6

where t_d represents the delay time between the maximum of the input pulse and that of the output pulse since the origin of t in region 2 is at the input pulse maximum. Equation (6.7) has been plotted on Fig.6.4 to give a comparison with Shepherd's theory using the parabolic input pulse. It can be seen that the limiting shift of the output pulse is here only 0.11 ev compared with 0.18 ev in Shepherd's case and that pulses with half-widths >0.6 ev are all shifted by the same amount. To find the maximum recorded intensity it is necessary to substitute t_d in $V_2(t)$ which gives $V_2(t_d)$.

$$V_2(t_d) = V_{om}(1 - t_d/b) \quad \ldots\ldots\ldots\ldots\ldots\ldots\ldots\ldots\ldots\ldots (6.8)$$

where V_{om} = Ra = the intensity of the output pulse for $\tau = 0$ (perfect response). In Fig.6.7 $V_2(t_d)$ is plotted as a percentage of V_{om} against b, expressed in ev, for $\tau = 0.7$ secs. It can be seen that at a half-width of 1.5 ev the recorded intensity has already reached 92% of the true intensity and at 8 ev has risen to 98%. Also plotted on Fig.6.7 is the corresponding curve obtained from the rectangular input pulse used by Shepherd, which rises to 100% at a half-width of 1.5 ev. In either case the corrections to the intensities recorded are small and in the present experiments, where the intensity of the energy losses are expressed as a fraction of the zero energy loss intensity and the ratios compared for a given loss at 90° scattering and 20° scattering, Sect.7.1, no correction need be applied.

In order to calculate the half-width, b', of the output pulse it is required to calculate the times t_1 and t_2 at which the half maximum intensity points occur. t_1 falls in region 1 (Fig.6.6), but t_2 may fall

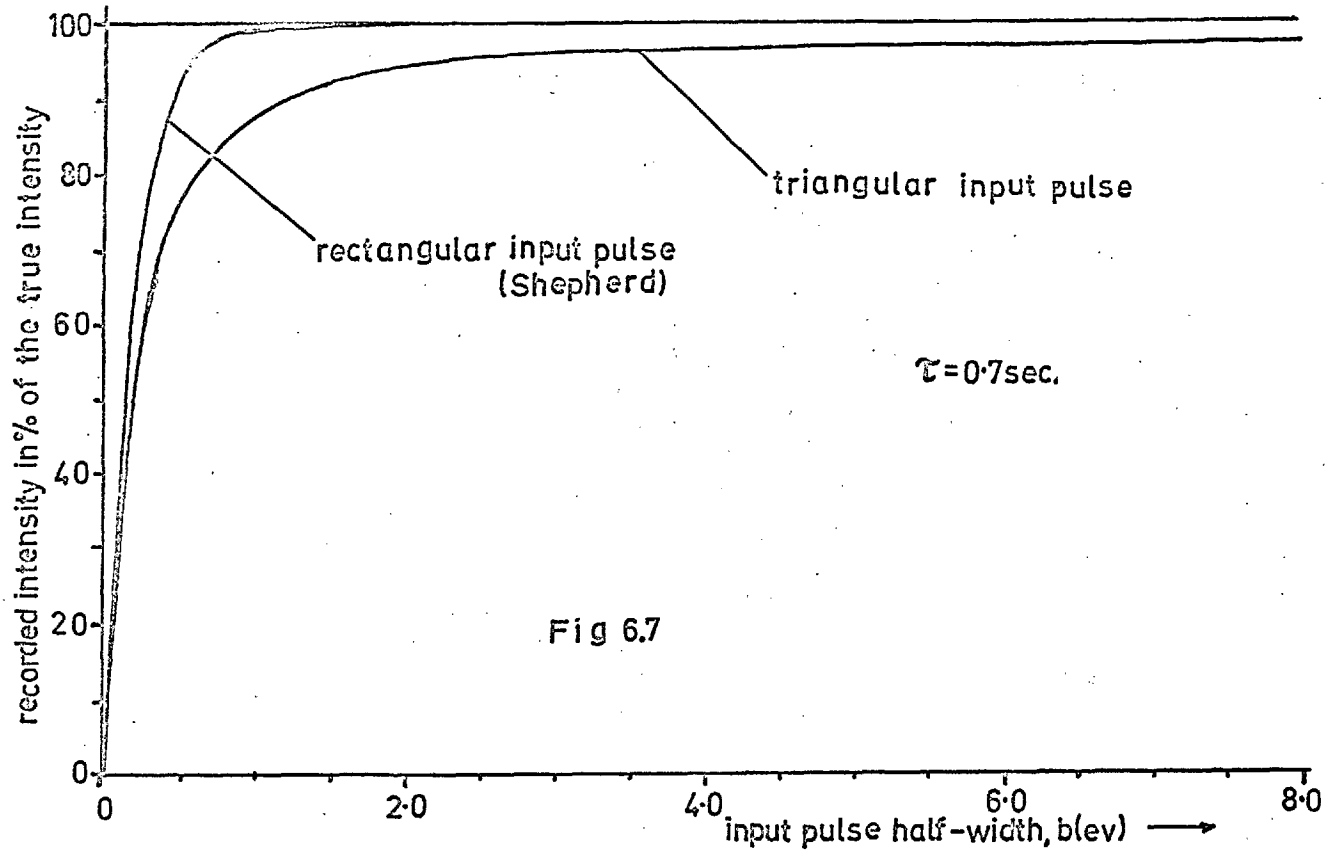
100
80
60
40
20
0
recorded intensity in % of the true intensity
rectangular input pulse
(Shepherd)
triangular input pulse
τ=0·7sec.
0
2·0
4·0
6·0
8·0
input pulse half-width, b(ev)

Fig 6.7

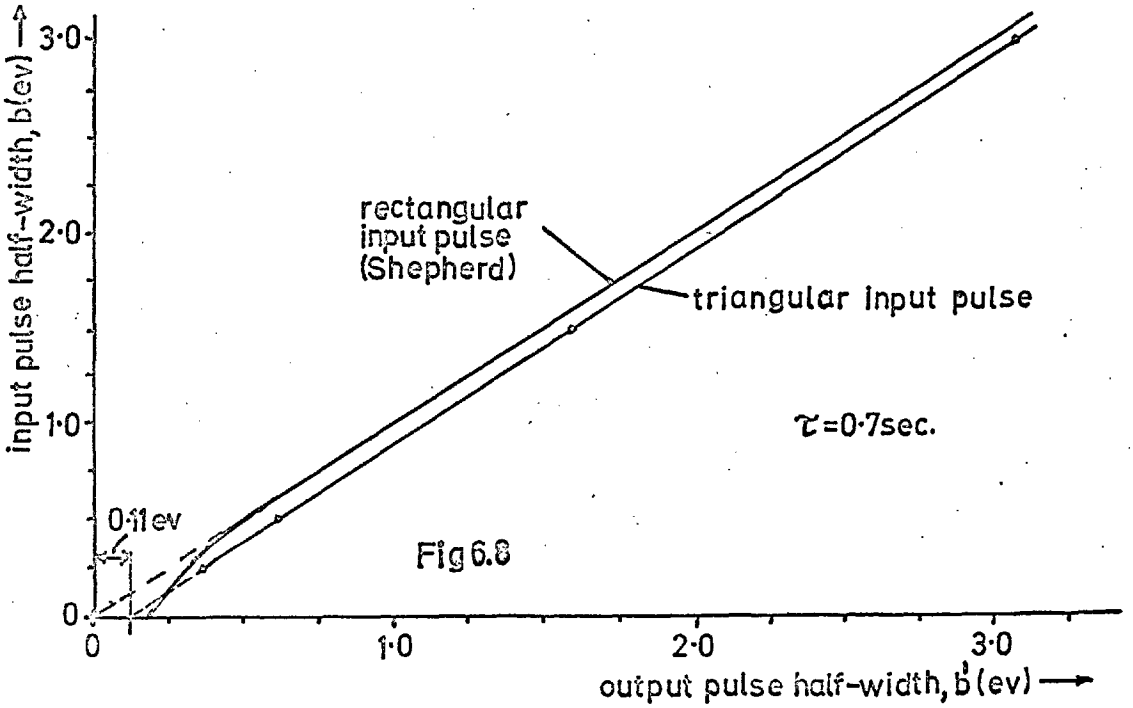
3·0
2·0
1·0
0
input pulse half-width, b(ev)
rectangular
input pulse
(Shepherd)
triangular input pulse
τ=0·7sec.
0·11ev
0
1·0
2·0
3·0
output pulse half-width, b'(ev)

Fig 6.8

in region 2 or region 3. t_2 falls in region 2 if $V_2(t_d)/2 > V_2(t_o)$ since $V_2(t_o)$ is the minimum value of $V_2(t)$. It can be seen from Fig.6.6 that t_2 falls in region 2 if b is $\geq$ 2 secs. Therefore t_1 and t_2 are defined by $V_1(t_1) = V_2(t_d)/2 = V_2(t'_2)$, where $t'_2 = t_2 - t_o$ since the origin of region 2 is at t_o. Therefore, using equns. (6.6), one obtains:-

$$\left[t_1 - \tau(1 - e^{-t_1/\tau})\right] = \tfrac{1}{2}\left[b - \tau\ln(2 - e^{-b/\tau})\right] \quad \ldots\ldots\ldots\ldots\ldots\ldots(6.9)$$

$$\left[b + \tau - t'_2 - \tau(2 - e^{-b/\tau})e^{-t'_2/\tau}\right] = \tfrac{1}{2}\left[b - \tau\ln(2 - e^{-b/\tau})\right] \quad \ldots\ldots(6.10)$$

In order to solve these equations it was assumed that $e^{-t_1/\tau}$ and $e^{-t'_2/\tau}$ were small compared to unity; $e^{-t/\tau} = 0.01$ for $t = 3.7$ sec. and $\tau = 0.7$ sec. In this case only the second decimal of the calculation is affected. Similarly if t_1 and t_2 are of the order of 3.7 sec. then b must be of the order of 7 seconds, therefore $e^{-b/\tau}$ is negligible. In making these approximations the results of equations (6.9) and 6.10) are therefore only valid for b $\geq$7 sec; corresponding to 2 ev in the present case. Equation (6.9) yields $t_1 = b/2 + 0.7\tau$ and (6.10), $t'_2 = b/2 + 1.4\tau$, therefore $t_2 = 3b/2 + 1.4\tau$ (since $t_o = b$). The half-width of the output pulse is therefore

$$b' = t_2 - t_1 = b + 0.7\tau = b + 0.49, \text{ for } \tau = 0.7 \quad \ldots\ldots\ldots\ldots(6.11)$$

For b < 7 sec. the half-widths of the curves shown in Fig.6.6 were measured and plotted against the input pulse half-width. The resulting graph is shown in Fig.6.8. The straight line drawn through the points plotted for b = 1,2 and 6 seconds was found to obey the equation $b' - b = 0.44$, which shows that equation (6.11) can be considered to hold down to b = 1 sec. (0.25 ev) with reasonable accuracy. Therefore, expressed in ev, equn. (6.11) can be written as, $b' - b = 0.13$ ev for all the half-

widths measured in the present experiments. Also plotted in Fig.6.8 is the curve obtained with a rectangular input pulse as used by Shepherd (loc.cit.). There is a significant difference between the two curves, since using the triangular input pulse all measured half-widths require a correction -0.13 ev, whereas with the rectangular pulse only measured half-widths up to about 0.5 ev require correction. With τ= 0.7 sec. and a chart speed of 0.25 ev/sec. there is not a great difference between the rectangular pulse and triangular pulse results, but there is a significant difference for larger values of τ and chart speed; for example, for τ= 3.0 secs. and a chart speed of 0.4v/sec, which are realistic values, the rectangular pulse theory gives zero half-width correction for pulses of measured half-width $\geq$7 ev, whereas the triangular pulse theory would give a correctionof -0.84 ev for these pulses.

In evaluating the spectra obtained, the triangular input pulse theory was used to find the correct half-width of a recorded loss distribution from Fig.6.8, and, using the value obtained, the shift in the output maximum was found from Fig.6.4 using Shepherd's parabolic approximation to the Gaussian input pulse. The smallest half-width measured was 1.3 ev which corresponds to an input pulse half-width of 1.2 ev. Thus the largest correction needed for the spectra recorded was only -0.06 ev and in the majority of cases was smaller than this. The corrections involved therefore were small but were applied to the results, since in some cases the first decimal place of a measured energy loss value could be affected.

6.6 The effect of the Specific Energy Resolution on the Intensities of the Recorded Spectra

Although, as mentioned in Sect.6.5, only ratios of intensities of energy loss distributions were compared with one another and therefore distortion in the recorded intensities is not important, it is as well to note that since the specific energy resolution, $\Delta V_a/V_o$, of the 127° electrostatic analyser is a constant (Equn.4.10), ΔV_a varies throughout the sweep through the spectrum. Therefore as the energy eV_o' , of the electrons focussed by the analyser decreases, ΔV_a also decreases and the recorded intensity of electrons decreases. In order to correct for this it would be necessary to multiply the recorded intensity at each point of the spectrum by V_o/V_o' , where V_o is the voltage of the primary electrons. For 200 ev primary electrons this correction leads, for instance, to an increase of 11% in the recorded intensity for electrons which have lost 20 ev in energy (V_o' = 180V).

CHAPTER 7.

EXPERIMENTAL RESULTS AND THEIR INTERPRETATION *

7.1 The Purpose of the Measurements and the Method Used.

The experiments were performed in an attempt to identify the origin of some of the energy losses of various selected materials, in particular to find out whether these losses were due to plasma oscillations. The variation in intensity of the plasma energy losses with penetration depth of the primary electron beam, described in Chapter 1, was used. For each material investigated the energy loss spectrum was recorded for $\sim 45^{\circ}$ incidence and reflection of the 200 ev primary electron beam and for $\sim 80^{\circ}$ incidence and reflection, the angles being with respect to the normal of the specimen surface. Angles greater than 80° were not used in order to maintain a reasonable intensity of the recorded spectra. In the present experiments the incidence at an angle of $\sim 80^{\circ}$ will be termed "grazing" incidence. In each case the intensities of the recorded energy losses were expressed as fractions of the intensity of the zero energy loss peak. The ratios thus obtained were compared for given energy losses in the two cases. As mentioned in Chapter 1, it is expected that the intensity of surface plasma oscillations should increase with increasing angles of incidence and reflection and that the opposite should be

*(Throughout this chapter the error associated with any set of readings is the standard deviation of that set.)

true for the volume plasma oscillations.

7.2 The Materials Investigated

The materials investigated were aluminium, germanium, gold and copper. Aluminium was chosen to test the present experimental method because it has an experimentally well established characteristic energy loss spectrum of narrow spectral lines and the various energy losses have been successfully identified with the predictions of the plasma oscillation theory as mentioned in Chapter 1. The expected intensity dependence of the energy losses on the angles of incidence and reflection of the primary electron beam should thus show up strongly in aluminium. Germanium, although being a semiconductor, also has an energy loss spectrum which has been interpreted by a simple plasma theory and its energy losses should exhibit the intensity effect. Gold and copper, however, have spectra which do not agree with the predictions of a simple plasma theory and it is not clear which energy losses in their spectra are due to the excitation of plasma oscillations. These two materials were thus included here to see if any conclusions could be drawn regarding the origin of their characteristic energy loss spectra.

7.3 The Characteristic Energy Losses in Aluminium

The aluminium used for the preparation of the evaporated specimens was spectroscopically standardised and was supplied by Johnson, Matthey and Co. Ltd. Typical spectra obtained, recorded at a chart speed of 1"/min. for convenience, are shown in Figs.1(a) and (b) for 200 ev electrons reflected from freshly evaporated layers at 400°C and using

~45° incidence and reflection of the primary beam and grazing incidence and reflection respectively. The multiplication factors shown indicate the relative intensities of those parts of the curves. The peak marked A in Figs. 7.1 is the zero energy loss peak, corresponding to elastically scattered electrons, and the maxima B - F are some of the well-known characteristic energy losses of aluminium, which were measured in these experiments for the 45° case as:-

Table 7.1

Notation	B	C	D	E	F
Energy Loss (ev)	10.1 ± 0.2	15.0 ± 0.2	20.8 ± 0.2	25.3 ± 0.2	30.9 ± 0.4
No. of Recordings	30	30	16	17	22

As mentioned in Chapter 1, the 15 ev and 10 ev energy losses are considered to be due to the excitation of volume and surface plasma oscillations respectively. D, E and F are interpreted as a double surface loss (2 x B), a surface plus a volume loss (B + C) and a double volume loss (2 x C) respectively.

In Fig.7.1(b), for grazing incidence and reflection, it can by seen that the volume plasma loss maximum at C has disappeared together with small maximum at E. A weak loss at F is still visible, which in this case must be interpreted as a triple surface plasma loss (3 x B). Therefore, in going from 45° incidence and reflection to grazing incidence and reflection, energy losses involving the excitation of volume plasma oscillations have all disappeared from the recorded spectrum, leaving only the energy losses involving the excitation of surface plasma

oscillations.

The experiment thus confirms that the 10 ev and 15 ev energy losses in aluminium are due to excitation of surface and volume plasma oscillations respectively.

The energy losses measured in the grazing angle experiments were:-

Table 7.2

Notation	B	C	D	F
Energy Loss(ev)	10.0 ±0.2	?14.8 ±0.2?	20.8 ±0.4	31.1 ±0.4
No. of Recordings	14	7	14	7

It can be seen that the volume plasma loss, C, was present on some of the spectra obtained, but in all cases it was extremely weak in intensity and difficult to locate accurately.

The intensity of the 10 ev energy loss, I_{10}, as a fraction of the zero energy loss intensity, I_o, in the two cases was,

$$(I_{10}/I_o)_{45^o} = 0.138 \pm 0.039 \quad \left(\begin{array}{l} 45^\circ \text{ incidence and reflection.} \\ 11 \text{ recordings} \end{array}\right)$$

and $$(I_{10}/I_o)_{80^o} = 0.320 \pm 0.063 \quad \left(\begin{array}{l} \text{grazing incidence and reflection.} \\ 12 \text{ recordings.} \end{array}\right)$$

which corresponds to an increase of 132% in the intensity of the energy loss. Such a difference is not covered by the errors associated with the readings. A comparison of the two spectra was not feasible for the 20 ev energy loss since its intensity was very small in the first case, see Fig.7.1(a), and its position over the background uncertain. It is however, clear that in Fig.7.1(b) its intensity has increased along with that of the 10 ev energy loss.

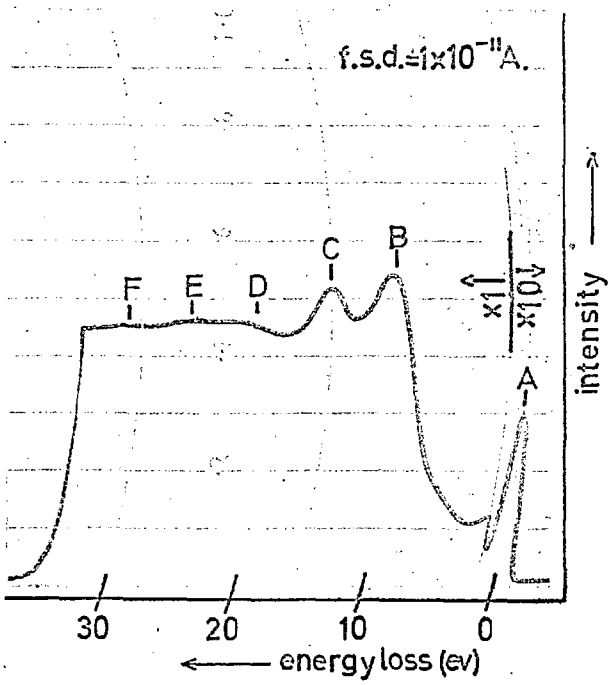

Fig. 7.1(a)

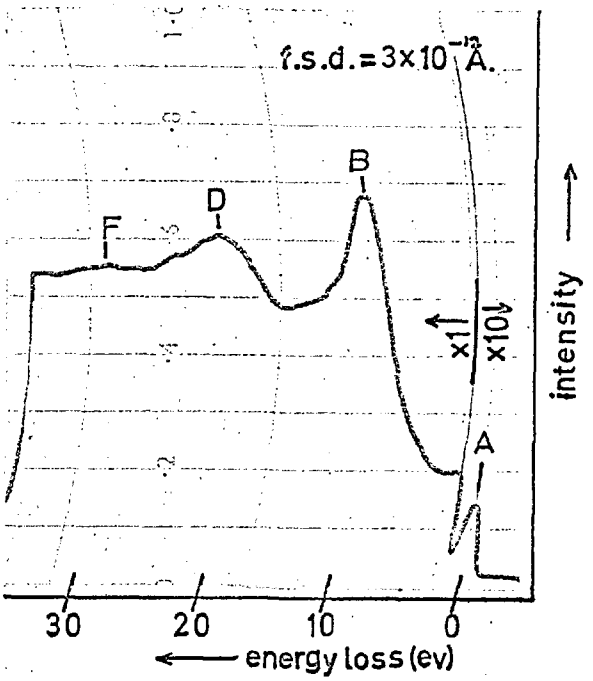

Fig. 7.1(b)

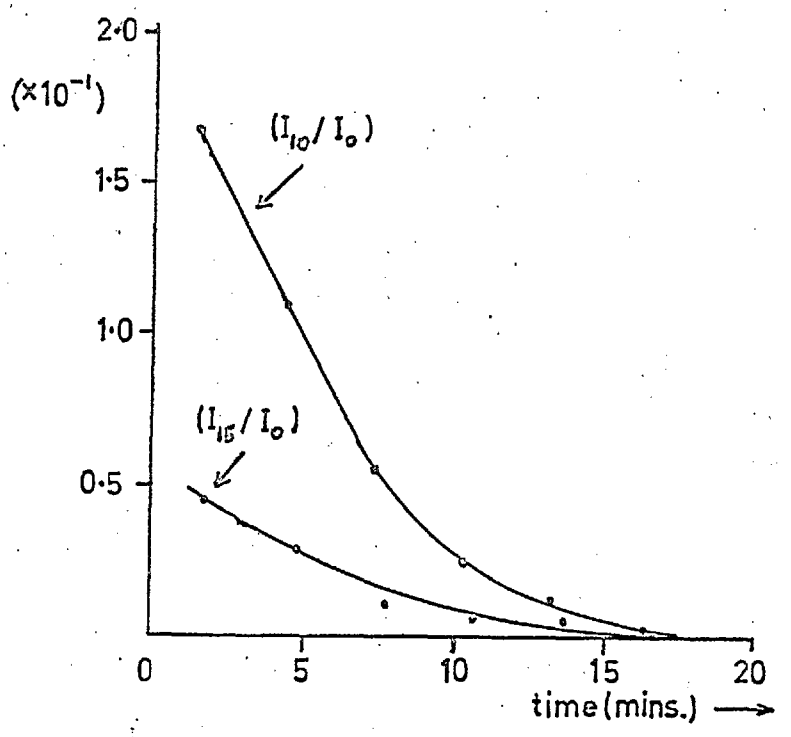

Fig. 7.2

Only freshly evaporated aluminium films were taken into consideration for the intensity measurements since it was found that the spectra were time-dependent; probably due to contamination of the surface of the specimen. The intensities of the losses decreased gradually with time and after 15 - 20 minutes had disappeared completely. The positions of the losses, however, remained unchanged throughout this transition. Over a period of about 10 minutes after the evaporation of the fresh film the energy losses F, E and D shown on Fig.7.1(a) were gradually replaced by a single very broad energy loss of 21 - 22 ev and simultaneously a weak energy loss of 5 - 6 ev appeared in the spectrum. The 15 ev and 10 ev losses then disappeared leaving the spectrum containing only the 5 - 6 ev and 21 - 22 ev energy losses. This time-dependence of the spectra accounts for the relatively large errors in the above intensity ratio measurements, since, as mentioned in Sect.6.2, the "fresh" specimens were approximately 30 seconds old before their spectra began to be recorded and this time delay varied between 20 to 40 seconds for different specimens. The time variation of $(I_{10}/I_o)_{45^o}$ and $(I_{15}/I_o)_{45^o}$ (where I_{15} is the intensity of the 15 ev energy loss) was plotted for one of the series of spectra obtained and is shown in Fig.7.2. There it can be seen that $(I_{10}/I_o)_{45^o}$ and $(I_{15}/I_o)_{45^o}$ decrease most rapidly in the region of t (time) = 0 which, together with slightly different initial conditions for each specimen produced (e.g. variation in the pressure in the vacuum chamber), substantiates the remarks made above concerning the errors in the intensity ratio measurements. It should be noted that I_o increased gradually with time and contributed to the

decay of $(I_{10}/I_o)_{45^o}$ and $(I_{15}/I_o)_{45^o}$ with time.

The residual spectrum remaining after the disappearance of the aluminium characteristic energy losses is discussed in Sect.7.8.

The apparent half-widths of the aluminium energy losses were:-

Table 7.3

Energy Loss	Half-Width (ev)	No. of Recordings
$10ev_{45^o}$	4.5 ± 0.2	11
$10ev_{80^o}$	3.9 ± 0.5	12
$15ev_{45^o}$	2.2 ± 0.2	11
$20ev_{80^o}$	5.8 ± 0.7	10

These half-widths are not the natural half-widths of the spectral lines since part of the energy spread is caused by the finite velocity distribution in the primary beam for which a correction must be applied.

Shepherd (1962) treated the energy loss distributions as error functions and, assuming that they combined as such, obtained the following relationship between the measured and the correct half-widths of a given energy loss:-

$$\Delta_1^2 = \Delta_m^2 - \Delta_o^2 \quad \ldots\ldots\ldots\ldots\ldots\ldots\ldots\ldots\ldots\ldots (7.1)$$

where Δ_1 = the half-width of the energy loss distribution,

Δ_m = the measured half-width,

Δ_o = the half-width of the zero energy loss.

Shepherd also states that in this case the following relationship,

$$\Delta_1 = \Delta_2/2^{\frac{1}{2}} = \Delta_3/3^{\frac{1}{2}} \quad \ldots\ldots\ldots\ldots\ldots\ldots\ldots\ldots\ldots\ldots (7.2),$$

should exist between the half-widths, $\Delta_1, \Delta_2, \Delta_3 \ldots\ldots\ldots$, of energy loss

distributions corresponding to the loss of 1,2,3,.....quanta of energy respectively.

In the present experiments Δ_o was of the order of 1.5 ev. Application of equn.(7.1) to the present results yielded the following corrected half-widths of the energy loss distributions:-

Table 7.4

Energy Loss	Corrected Half-Width (ev)	No. of Recordings
$10ev_{45^o}$	4.2 ± 0.4	11
$10ev_{45^o 80^o}$	3.6 ± 0.5	12
$15ev_{45^o}$	1.6 ± 0.3	11
$20ev_{80^o}$	5.6 ± 0.7	10

The difference in the half-width of the 10ev loss, measured at 45^o and 80^o incidence and reflection of the primary beam respectively, was thought to be due to differences in the background drawn under the loss distribution in the two cases and not due to a genuine change in the half-width. However, since this loss is more intense in the 80^o case and also there the 15ev loss has disappeared, it was considered that the results in this case were to be preferred.

According to equn.(7.2) the ratio of the corrected half-width of the 20ev and 10ev enery losses measured in the grazing angle experiments should be $2^{\frac{1}{2}} (\simeq 1.4)$. This ratio was in fact found to be 1.6 ± 0.2 (10 recordings), which is in reasonable agreement with the predicted value. Errors in estimating the background under the loss distributions, together with the time-dependence of the spectra, probably account for

the relatively large error in the measured value.

In Fig. 7.3 is shown the energy loss spectrum of 200ev electrons scattered through 90° from a freshly evaporated aluminium film with the incident primary beam striking the target at ~80° to the normal of the target surface. It can be seen that all the energy losses, B - F, apparent in Fig. 7.1(a) are also present in this case. This was also found to be so for approximately 10° incidence of the primary beam and 90° scattering. These results imply that for the effect observed at grazing angle incidence, i.e. that for the disappearance of energy losses involving the excitation of volume plasma oscillations, a large angle of incidence is not a necessary condition. However, to avoid excitation of the volume plasma oscillations, the scattering angle must be small enough so that the beam will not penetrate much below the surface of the specimen.

Figure 7.4 shows the spectrum of 200ev electrons reflected from a fresh aluminium film with approximately 60° incidence and reflection angles. It can be seen that this spectrum is intermediate between those shown in Figs. 7.1(a) and (b). The energy losses involving the excitation of volume plasma oscillations, C, E and F, are still present but with a reduced intensity as compared with Fig. 7.1(a).

The overall values of all the energy loss measurements made at all scattering angles were:-

Table 7.5

Energy Loss (ev)	10.1 ± 0.2	15.0 ± 0.2	20.8 ± 0.3	25.3 ± 0.4	30.8 ± 0.4
No. of Recordings	58	38	36	25	30

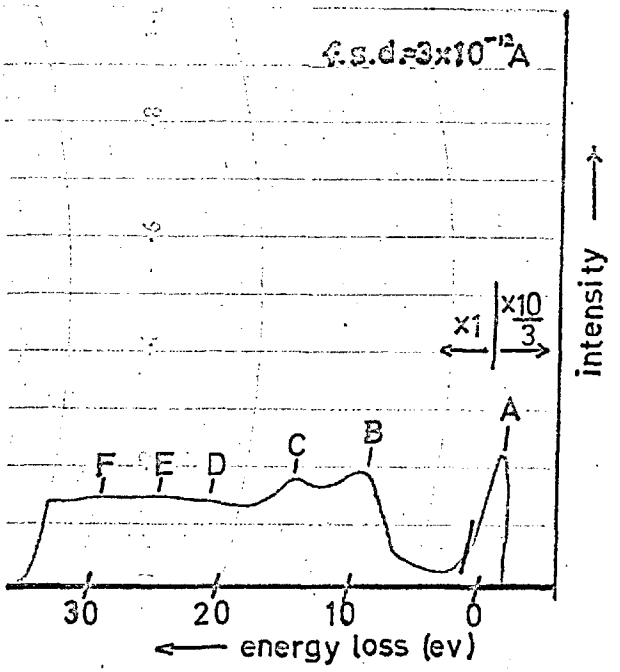
f.s.d.=3x10⁻¹²A
x1
x10/3
intensity
A
B
C
D
E
F
30
20
10
0
energy loss (ev)

Fig. 7.3

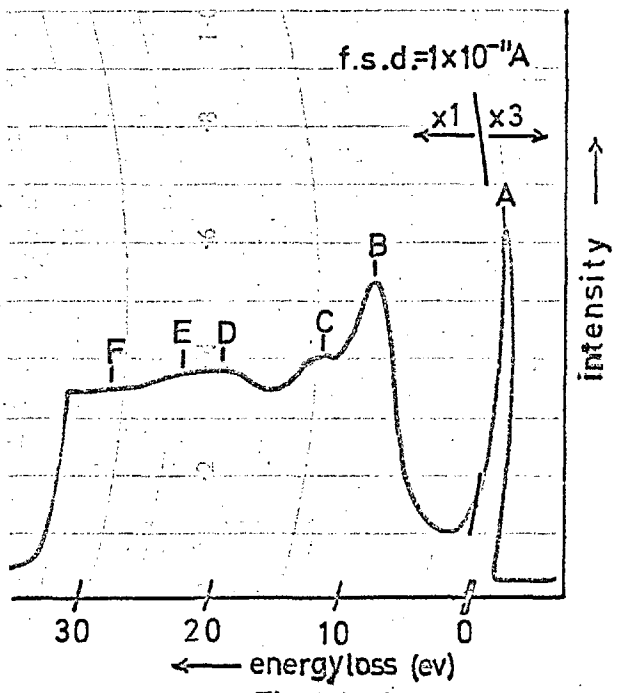
f.s.d.=1x10⁻¹¹A
x1
x3
intensity
A
B
C
D
E
F
30
20
10
0
energy loss (ev)

Fig. 7.4

No significant differences were observed in any of the energy loss values when the scattering angle or the incidence and reflection angles of the primary beam were varied.

7.4 The Characteristic Energy Losses in Germanium

The germanium used for the production of the evaporated specimens was spectroscopically standardised and was supplied by Johnson, Matthey and Co. Ltd. A typical energy loss spectrum for 200 ev electrons scattered from a fresh germanium film at 400°C with ~45° angles of incidence and reflection is shown in Fig.7.5(a). As in the case of aluminium, the peak A represents the elastically reflected electrons and B - F are the recorded energy losses. The energy losses in this case were measured as:-

Table 7.6

Notation	B	C	D	E	F
Energy Loss (ev)	5.2 ± 0.2	11.2 ± 0.2	16.4 ± 0.2	25.8 ± 1.0	31.7 ± 0.3
No. of Recordings	9	25	25	6	24

Spectra up to and including those of films six minutes old were used in compiling the above table. The spectrum of a six minute old film is shown in Fig.7.5(b) where it can be seen that the 5.2ev loss and the 25.8ev loss have disappeared and the 11.2ev loss has decreased in intensity. The 5.2 and 25.8ev energy losses were normally only observed on films up to 3 minutes old. It can be seen from Fig.7.5(a) that they are of very weak intensity even on the fresh films. The decrease in intensity of the 11.2 ev energy loss with time enabled the 16.4 ev loss to be

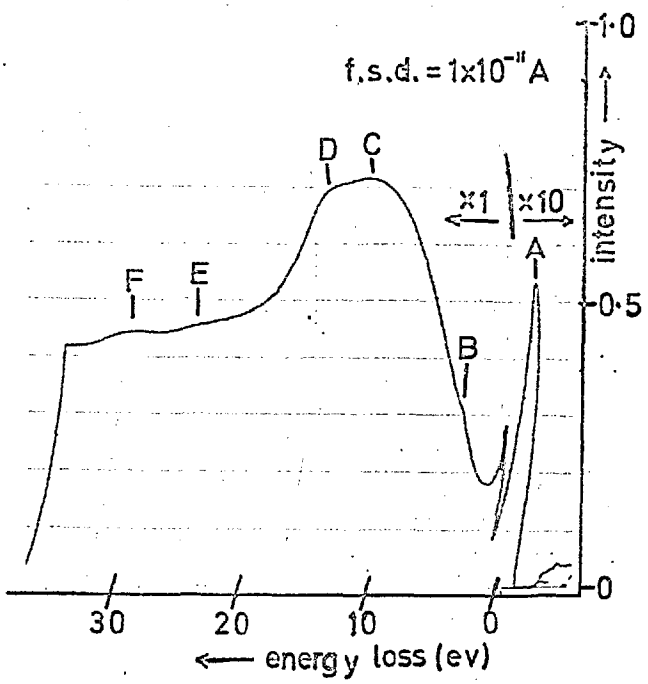

Fig. 7.5(a)

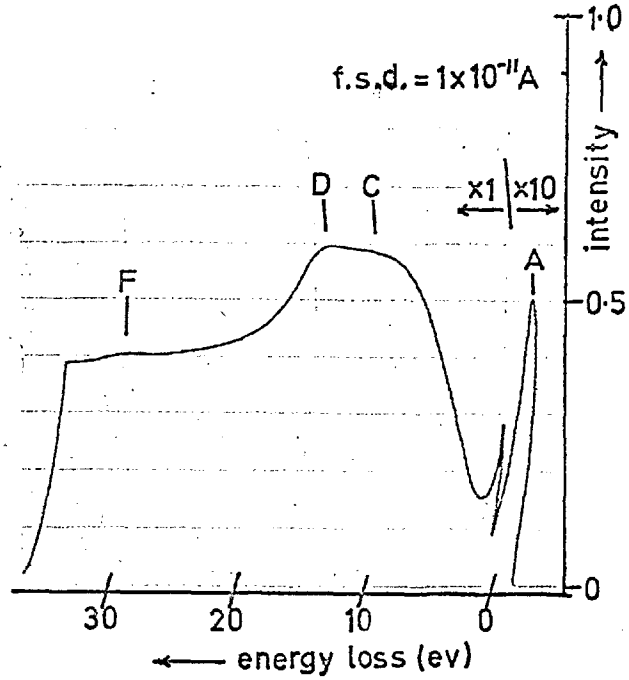

Fig. 7.5(b)

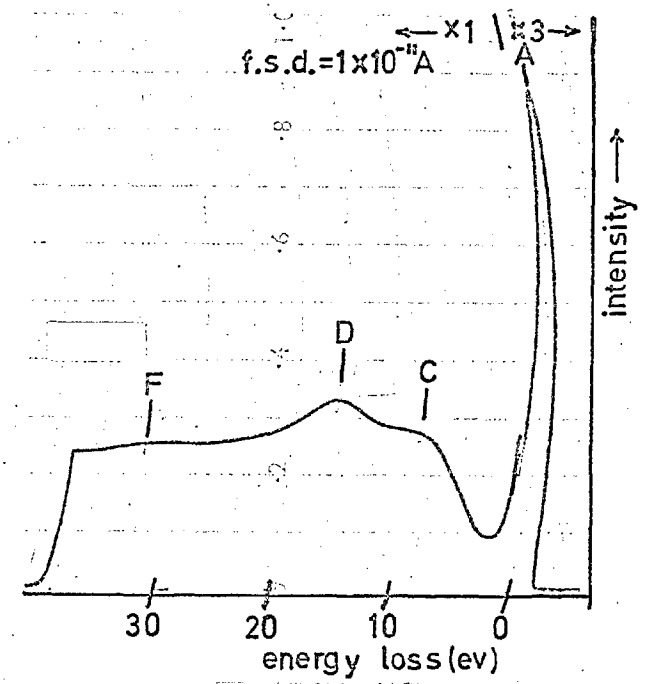

Fig. 7.6(a)

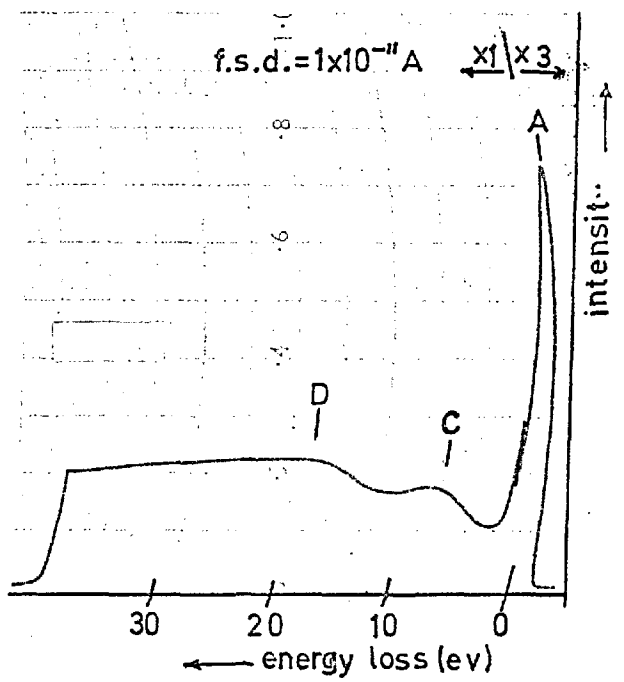

Fig. 7.6(b)

fixed with more accuracy than was possible with the fresh films, where it was more difficult to draw in a realistic background for this loss.

The time dependence of the germanium spectrum for 45° incidence and reflection of the primary beam (see also Sect.7.8) is shown in Figs.7.6 (a) and (b). These Figures show the spectrum of a different film to that used for Figs.7.5(a) and (b), at 27 and 57 minutes after the deposition of the fresh film respectively. It can be seen that the spectrum changed considerably with time. The loss, C, corresponding to the 11.2ev loss in the fresh films, decreased in value, half-width and intensity with time, until it reached a value of about 7 ev after an hour and the loss, D, corresponding to the 16.4 ev loss in the fresh film gradually increased in value to about 18ev in this time. The loss D also seemed to increase in intensity and half-width over the first half-hour or so, but it was thought that this was due to an inability to draw the correct background under this loss in the fresher spectra. There was no definite transition period over which the changes in the spectrum occurred. The changes took place gradually over the period of about an hour. The strong dependence of the 11.2ev loss on time (surface contamination of the specimen) is an indication that it corresponds to surface plasma oscillations.

The grazing angle experiments performed produced spectra of the type shown in Fig.7.7. This spectrum differs considerably to that shown in Fig.7.5(a) for 45° incidence and reflection and it was thought that the spectra obtained were not characteristic of the fresh material, however, no amount of gettering of the work chamber (Sect.6.1) enabled different

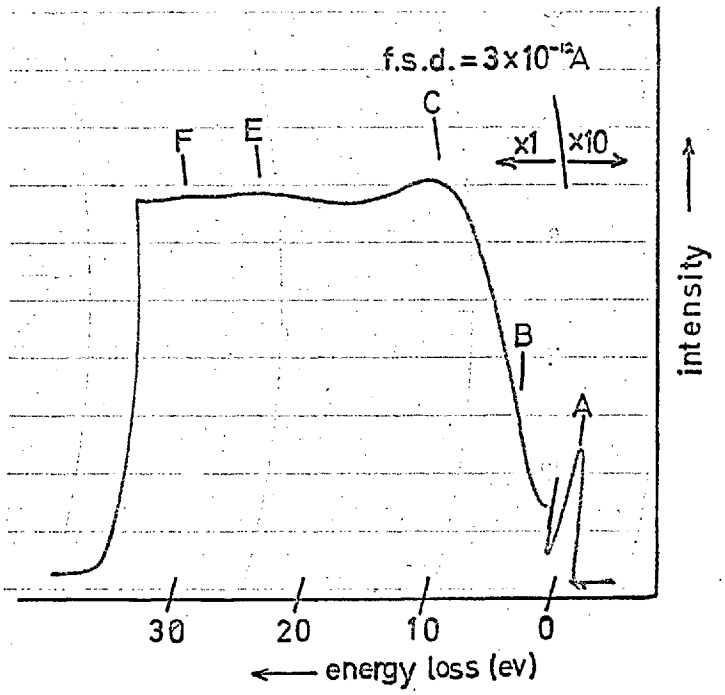

Fig. 7.7

spectra to be obtained. It was then found that the weak 5.2ev energy loss, which was only obtained with the recently evaporated films at 45° incidence and reflection of the primary beam, was also present on several of the spectra taken at grazing angle. It was therefore decided that the spectra in question did in fact represent the loss spectrum characteristic of a clean surface. The energy loss values measured at grazing angle were:-

Table 7.7

Notation	B	C	D	E	F
Energy Loss (ev)	?5.4 ±0.1?	10.3 ±0.3	?16.5 ±0.3?	25.5 ± 1.2	31.2 ± 0.3
No. of Recordings	4	24	3	18	9

where only freshly evaporated films have been considered.

The 16.5 ev loss reported above appeared only very weakly on three of the curves taken and is assumed on this basis to be the volume plasma loss; it does not appear on the spectrum shown in Fig. 7.7. Drawing a realistic background beneath the energy loss C proved to be difficult and it is thought that this is the reason for the loss being measured as 10.3ev in this case as compared with the value of 11.2ev quoted in Table 7.6 for the 45° case. The ratio of the intensity of the 10.3ev loss, I_{10}, compared with the zero energy loss intensity at grazing incidence ($\backsim 80°$) and reflection was,

$$(I_{10}/I_o)_{80°} = 0.125 \pm 0.009 \text{ (24 recordings)}$$

This is to be compared with the ratio of the intensity of the 11.2ev loss, I_{11}, to the zero energy loss intensity in the 45° case, which was,

$$(I_{11}/I_o)_{45^o} = 0.084 \pm 0.003 \text{ (10 recordings)}$$

Assuming that the two losses mentioned are in fact the same loss, this represents an increase of the intensity ratio of 49% in going from 45° to grazing incidence and reflection. However, the background problem mentioned makes this result very dubious, but it seems likely that the 11.2ev loss given in table 7.6 represents an excitation of surface plasma oscillations in germanium.

On the basis of the 11.2ev loss being the surface plasma loss and the 16.4ev loss being the volume plasma loss, all the losses except the 5.2ev loss observed at 45° incidence and reflection of the primary beam, can be accounted for. The 25.8ev loss either corresponds to the excitation of a volume plasmon plus a surface plasmon or to a double surface plasmon excitation (see below) and the 31.7ev loss corresponds to the excitation of two volume plasmons. It is thought that the 5.2ev loss is due to an interband transition and this is discussed in Chapter 8.

The 25.5ev and 31.2ev losses observed at grazing incidence and reflection pose a problem, since if they are of the same origin as the 25.8ev and 31.7ev losses respectively observed in the 45° case, they should not be present at all because they involve the excitation of volume plasma oscillations. The following tentative explanation is put forward for these two energy losses. It was observed that the 25.5ev loss observed at grazing angle was more prominent than than observed at 25.8ev in the 45° case, as can be seen from Figs.7.7 and 7.5(a) respectively. This behaviour is analogous with that of the double

surface plasmon excitation observed in aluminium (see Figs.7.1 a and b). In the present case it is therefore suggested that the 25.5ev loss corresponds to the excitation of two surface plasmons. This loss would be expected to have a half-width of the order of 16ev (see below) whereas its measured half-width was of the order of 9ev. Therefore it is thought that a considerable portion of the energy loss distribution contributing to this loss in fact lies in the background and is not separable from it. This loss would then be expected to be more intense than it actually appears and this may also account for the remarkable difference in the background between the spectra obtained at 45° and at grazing angle. It could also explain the difference in the loss values for the ~llev loss in the two cases and why the double surface loss appears at 25.5ev instead of 22ev. The 31.2ev loss measured at grazing angle is less prominent than the 31.8ev loss measured at 45° and may be due to a weak triple surface loss.

The half-widths of the 11.2 ev and 16.4 ev losses considering only freshly evaporated films and 45° incidence and reflection were:-

Table 7.8

Energy Loss (ev)	11.2	16.4
Half-Width (ev)	11.5± 0.6	3.3± 0.5
No. of Recordings	10	10

where these values have been corrected according to equn.(7.1). Using the relationship expressed in equn.(7.2) the expected half-width of an energy loss involving the creation of two surface plasmons is about 16ev,

which is the value quoted earlier.

The evaporated germanium films used in these experiments were considered to be crystalline and not amorphous. Whether an evaporated germanium film is deposited in the amorphous or crystalline state depends upon the temperature of the substrate and the degree of vacuum in the work chamber, as reported by Kurov (1964). At given pressures there is a transition temperature above which the amorphous germanium is converted to the crystalline form. Kurov states that Semiletov (1956), working in the pressure range of 5×10^{-5} to 1×10^{-4}mm of mercury, found the transition temperature to be 370°C, whereas Kurov, himself, found that at pressures $< 10^{-6}$mm of mercury the evaporated germanium was always deposited in the crystalline form, irrespective of the substrate temperature. Therefore in the present experiments, in which the pressure was $<10^{-5}$mm and the substrate temperature was 400°C, it must be assumed that the evaporated films consisted of crystalline germanium. This is mentioned because Richter and Ruckwied (1960), in a high energy electron transmission experiment, found that the volume plasma loss in amorphous Ge was 15.90 ev, while in crystalline Ge it was 16.49 ev, both measurements being taken at room temperature. Such a change is in agreement with the plasma theory, since the valence electron density is greater in the crystalline state than in the amorphous state. Equn.(1.2) thus predicts different values for the volume plasma loss in the two states.

7.5 The Characteristic Energy Losses in Gold

The specimens used in these experiments were evaporated from gold wire, which was described as fine gold by the suppliers, Johnson,

Matthey and Co. Ltd.

In Figs. 7.8(a) and (b) are shown typical examples of the spectra obtained for 200ev electrons reflected from freshly evaporated gold films with 45° incidence and reflection angles of the primary beam and 80° respectively. The two spectra are very similar; both show the same number of energy losses, denoted by B,C, and D, having about the same intensities in the two cases. The energy loss values measured for 45° incidence and reflection were:-

Table 7.9

Notation	B	C	D
Energy Loss(ev)	3.0±0.1	5.9±0.2	23.7±0.5
No. of Recordings	35	39	39

The corresponding values at grazing angle were:-

Table 7.10

Notation	B	C	D
Energy Loss (ev)	3.1±0.2	6.0 ±0.2	22.6±0.4
No. of Recordings	25	27	18

The difference in the values of the D loss in the two cases was thought to be due to the fact that the voltage sweep cut-off occurred before the whole of this loss had been recorded on the spectrum. An unknown difference in the background in such an event would account for the difference in the measured energy loss values. The values recorded for the D loss are thus not regarded as very accurate. Attention was focussed mainly on the two smaller energy losses.

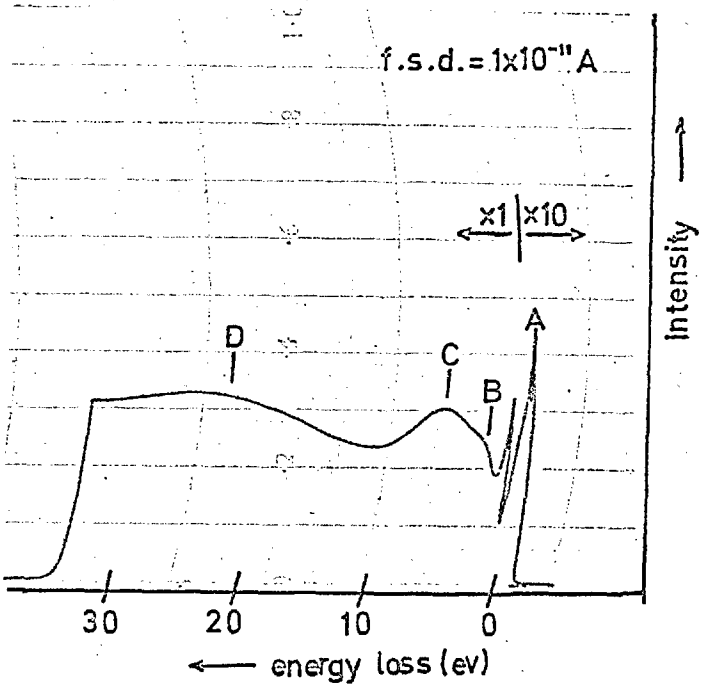

Fig. 7.8(a)

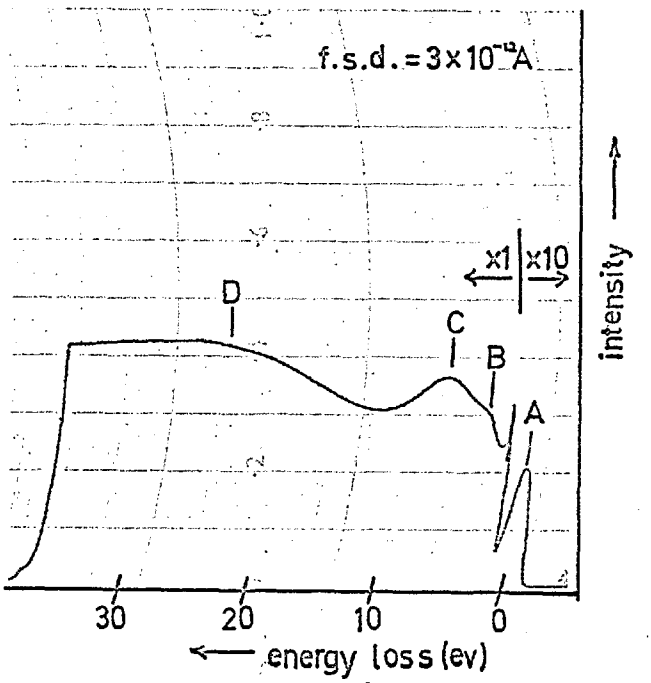

Fig. 7.8(b)

The intensity ratios of the 3 ev and 6 ev energy losses to the zero energy loss in the two cases were:-

Table 7.11

	I_3/I_o	I_6/I_o
45°	0.007 ± 0.002	0.027 ± 0.002
80°	0.008 ± 0.002	0.032 ± 0.006
No. of Recordings = 9 in all cases		

where only freshly evaporated specimens have been considered. The values (I_3/I_o) and (I_6/I_o) have thus increased by 14% and 19% respectively in going from 45° to 80°, however, both of these increases are covered by the errors quoted. Therefore neither of these losses could be definitely associated with plasma oscillations. The 6 ev loss is not a multiple of the 3 ev loss because its intensity is much greater than that of the 3ev loss and also its half-width is much greater (see below).

The half-width of the 3 ev loss (uncorrected for the width of the zero energy loss peak) was 1.4 ±0.1 ev (18 recordings). The average value of the zero loss half-width was also 1.4 ev. Therefore it can be seen that the half-width of the 3 ev loss is due almost entirely to the energy spread in the primary electron beam. The half-width of the 6 ev loss was found to be 4.7 ±0.6 ev, which, corrected according to equn. (7.1), became 4.5 ±0.6 ev (18 recordings). The half-width of the 24 ev loss was of the order of 14 ev, but it may be larger than this for the reason given earlier.

Once again it was found that the spectra obtained were time dependent, but the effect was far less severe than in the cases of aluminium and

germanium mentioned earlier. In fact, this may not have been noticed, had it not been for the disappearance of the weak 3 ev loss after a period of about ten minutes subsequent to the deposition of a fresh specimen and also a change in slope of the background beneath the 6 ev loss over a similar period of about six minutes (see Sect 7.7). The value of (I_6/I_o) remained constant throughout this transition. The dependence of the 3 ev loss on time suggests that it is dependent on surface condition of the specimen, since it is assumed that surface contamination is the cause of its disappearance. Purely on this basis the 3 ev loss was tentatively associated with the excitation of surface plasma oscillations. Neither the 6 ev nor the 24 ev loss could be associated with volume plasma oscillations, but the 24 ev loss requires further investigation applying a greater amplitude of the voltage sweep. The voltage sweep was not extended in the present experiments in order to maintain its linearity (Sect.5.14). The overall values of the energy losses measured in all the experiments were:-

Table 7.12

Energy Loss (ev)	3.0± 0.2	5.9± 0.2	23.4± 0.7
No. of Recordings	60	66	57

7.6 The Characteristic Energy Losses in Copper

The copper used for the preparation of the evaporated specimens was commercial copper wire, which was thought to be more than 99% pure. The work of Shepherd (1962) on alloys showed that the presence of small amounts (several percent) of bulk impurities in copper specimens had little effect on the energy loss spectra obtained.

The characteristic energy losses measured for copper with 45° incidence and reflection of the primary electron beam were:-

Table 7.13

Notation	B	C	D	E	F
Energy Loss(ev)	3.6±0.1	6.6±0.2		21.4±0.7	27.1±0.6
No. of Recordings	35	35	-	35	34

The notation refers to Fig.7.9(a) which shows a typical spectrum. The energy loss D was not apparent on the spectra taken for 45° incidence and reflection but appeared weakly on the spectra taken in the grazing angle experiments for which the recorded energy losses were:-

Table 7.14

Notation	B	C	D	E	F
Energy Loss(ev)	3.6±0.1	6.5±0.2	?13.4±0.1?	22.8±0.9	27.9±0.8
No.of Recordings	36	36	9	36	6

as shown in Fig.7.9(b). Spectra up to and including those six minutes old were used in compiling the above tables. It can be seen that the 27 ev loss appeared less frequently at grazing angle than at 45°, although at grazing angle the 22 ev loss often had a flattish appearance, indicating that the 27 ev loss was in fact present but it was difficult to locate; this is confirmed, to some extent, by the grazing angle 22.8 ev loss lying in between the 21.4 and 27.1 ev losses measured at 45°. As in the case of gold, it is thought that a more extensive voltage sweep would be of use in obtaining more accurate data on the 22 and 27 ev energy losses. Interest was focussed mainly on the smaller energy losses.

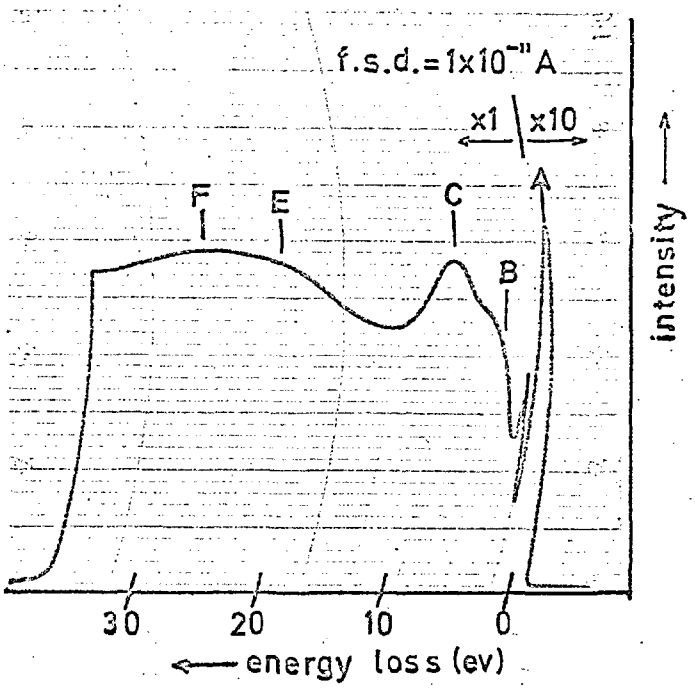

Fig. 7.9(a)

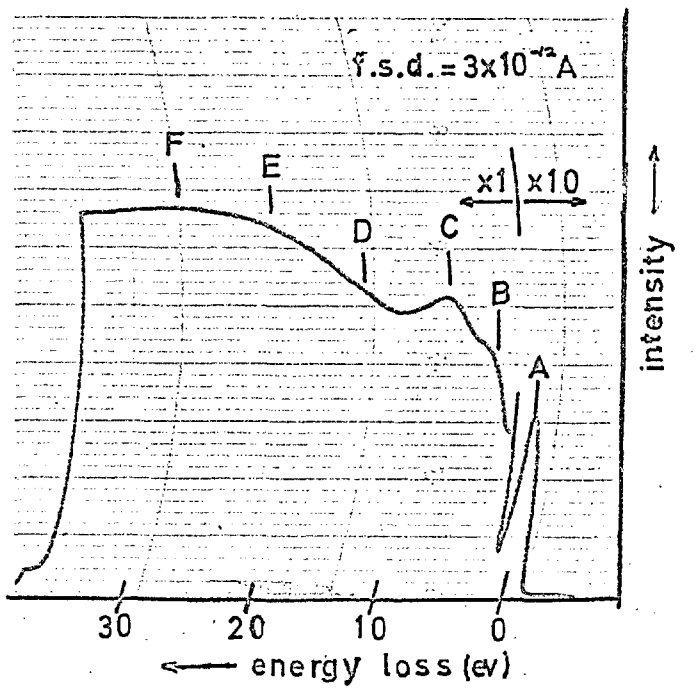

Fig. 7.9(b)

The 6.6 ev loss was not considered to be a multiple of the 3.6 ev loss, for similar reasons given for the corresponding losses in gold (Sect. 7.5).

The relative intensities of the losses, to the intensity of the zero energy loss, in the two cases of 45° and grazing (∿80°) incidence and reflection of the primary beam were:-

Table 7.15

	$I_{3.6}/I_o$	$I_{6.5}/I_o$
45°	0.009 ± 0.001	0.033 ± 0.003
80°	0.014 ± 0.002	0.036 ± 0.005
No. of Recordings = 12 in all cases		

The value of $(I_{3.6}/I_o)$ therefore increased by 56% in going from 45° to 80° and this difference is not covered by the errors associated with the readings. $(I_{6.5}/I_o)$, however, remained almost constant; the difference in the two cases being 9% and this is easily covered by the associated errors. On this basis the 3.6 ev energy loss was interpreted as being due to the excitation of surface plasma oscillations. The 13 ev loss, observed at grazing angle and not in the 45° case, also behaved in the expected manner of a surface loss, but it is very weak indeed and it would be wrong to speculate about this loss before carrying out experiments at different primary energies, in order to see if further information could be obtained about it. No loss could be definitely associated with volume plasma oscillations.

The half-widths of the energy losses were also measured and found to

be:-

Table 7.16

Energy Loss (ev)	3.6	6.6
Half-Width (ev)	1.4 ± 0.3	4.3 ± 0.3
No. of Recordings	24	24

Where readings obtained for freshly evaporated specimens have been included for both 45° and grazing incidence and reflection of the primary beam. The half-widths have been corrected for the zero energy loss distribution according to equn.(7.1).

The spectra were time-dependent in a manner similar to that described for the gold curves. About 12 minutes after the evaporation of a fresh specimen the slope of the background beneath the 6.6 ev loss had changed sign and the 3.6 ev energy loss had disappeared. Also during this time the 6.6 ev loss gradually shifted to 6.0 ev (see Sect. 7.7).

The overall values of the energy losses observed in copper for both cases of incidence and reflection of the primary beam were:-

Table 7.17

Energy Loss(ev)	3.6 ± 0.1	6.6 ± 0.2	?13.4 ± 0.1?	22.1 ± 1.1	27.5 ± 0.7
No. of Recordings	71	71	9	71	40

7.7 The Time Dependence of the Energy Loss Spectra

All the spectra obtained were time dependent, this was not surprising in the cases of aluminium, germanium and copper, all of which oxidise

readily, but the fact that the gold spectrum was also time-dependent, indicated that oxidation was not the only type of contamination present. It was thought that, perhaps, heating the specimen to 400°C did not completely suppress the formation of carbonaceous contamination (Sect. 5.12). The final spectra obtained in each case, when the contamination seemed to be complete, were all somewhat similar, consisting of energy losses of about 6 ev and 20 ev; the 6 ev loss being sharp and distinct and the 20 ev loss being broad and diffuse but much more intense than the 6 ev loss. The spectrum of a contaminated germanium film is shown in Fig.7.6(b) and that of an aluminium film thought to be completely contaminated, in Fig.7.10. The low energy loss part of the corresponding spectra for copper and gold (both recorded at a chart speed of 6" per min.) are shown in Figs.7.11 and 7.12 respectively. The similarity between the curves is clear. The germanium curve is the only curve which differs in the shape of the background beneath the energy losses.

To test the theory that the contamination may be carbonaceous, the target was left at room temperature and bombarded by 200 ev electrons for half an hour. At the end of this time a black stain, assumed to be carbonaceous contamination (Sect.5.10), had formed on the target. The low energy loss part of the spectrum of this contamination, taken with 45° incidence and reflection of the 200 ev primary beam, is shown in Fig.7.13. The spectrum is different to those mentioned above, in that there are two small energy losses, of 4.1 ev (weak) and 6.1 ev, in place of the single small energy loss, and the background below these losses slopes in the opposite direction to that in the other curves (except

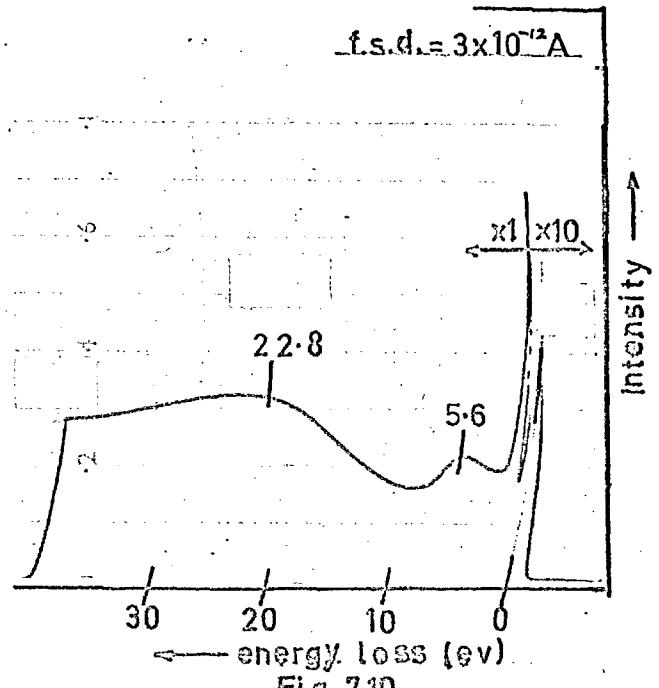

Fig. 7.10

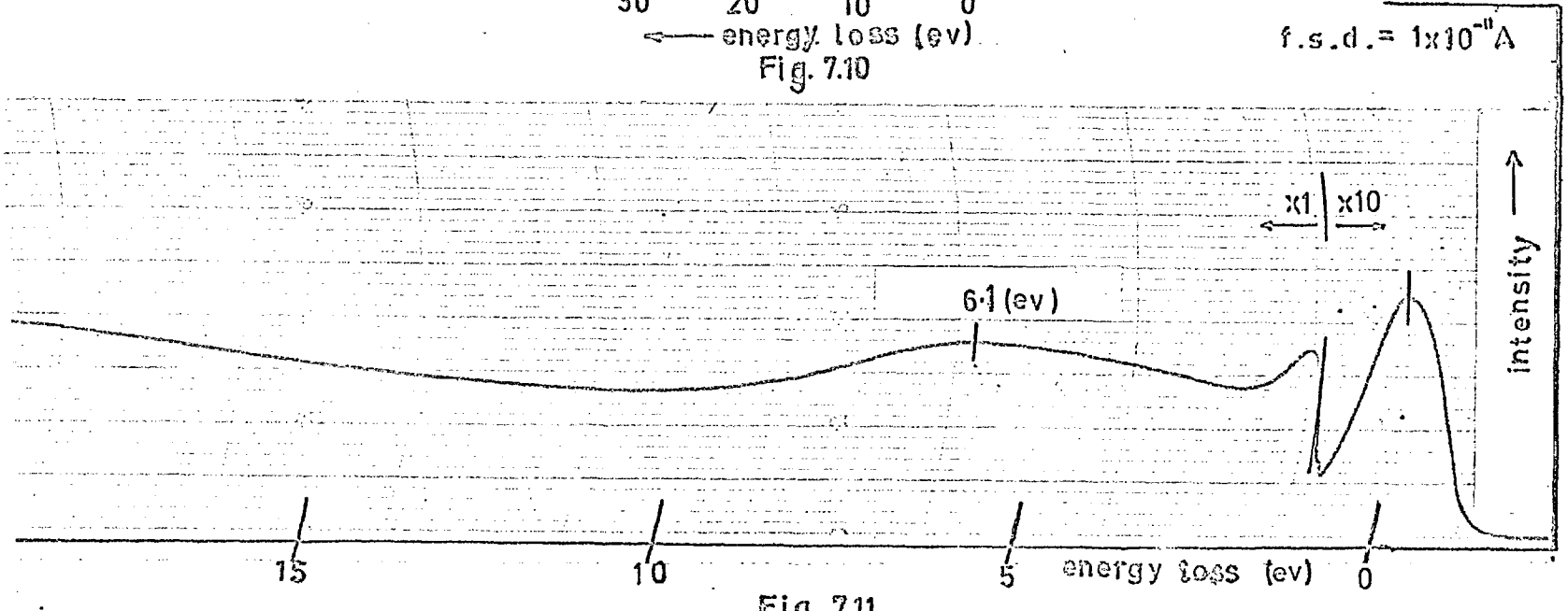

Fig. 7.11

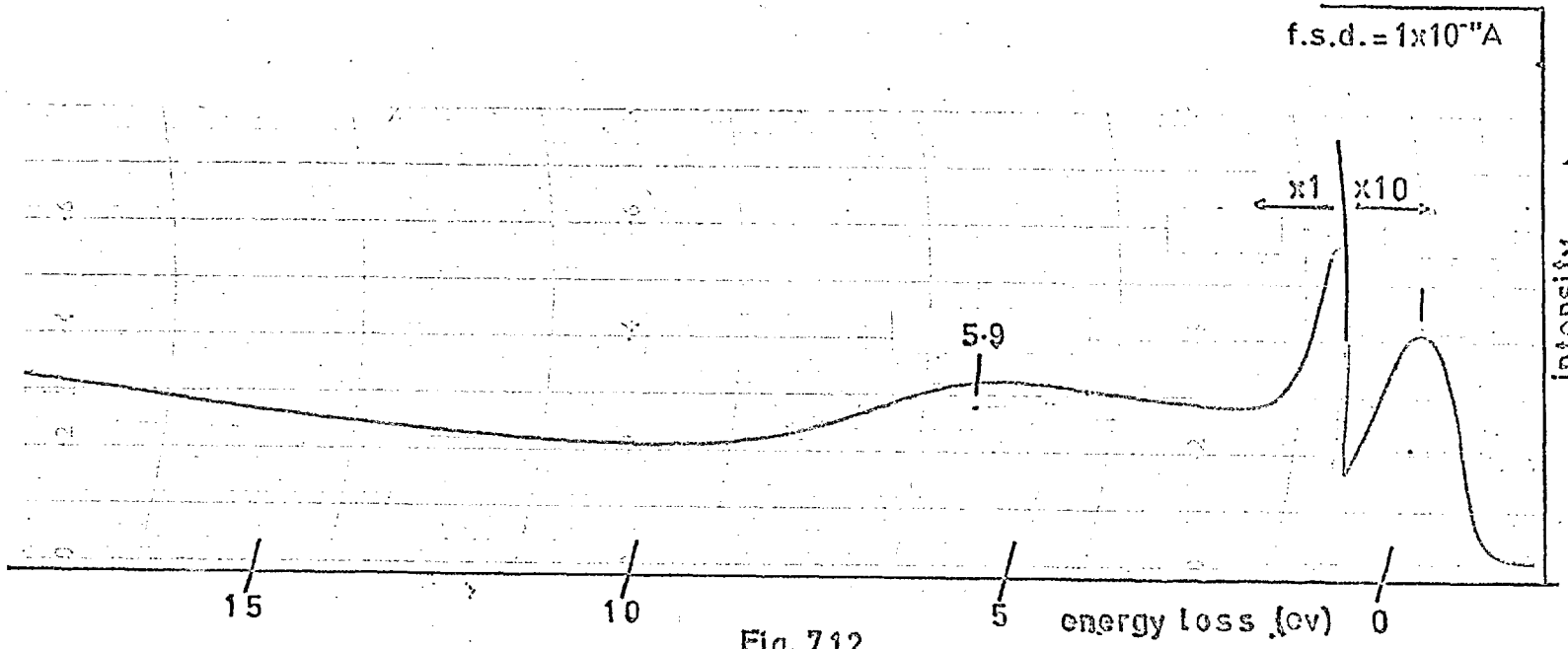

Fig. 7.12

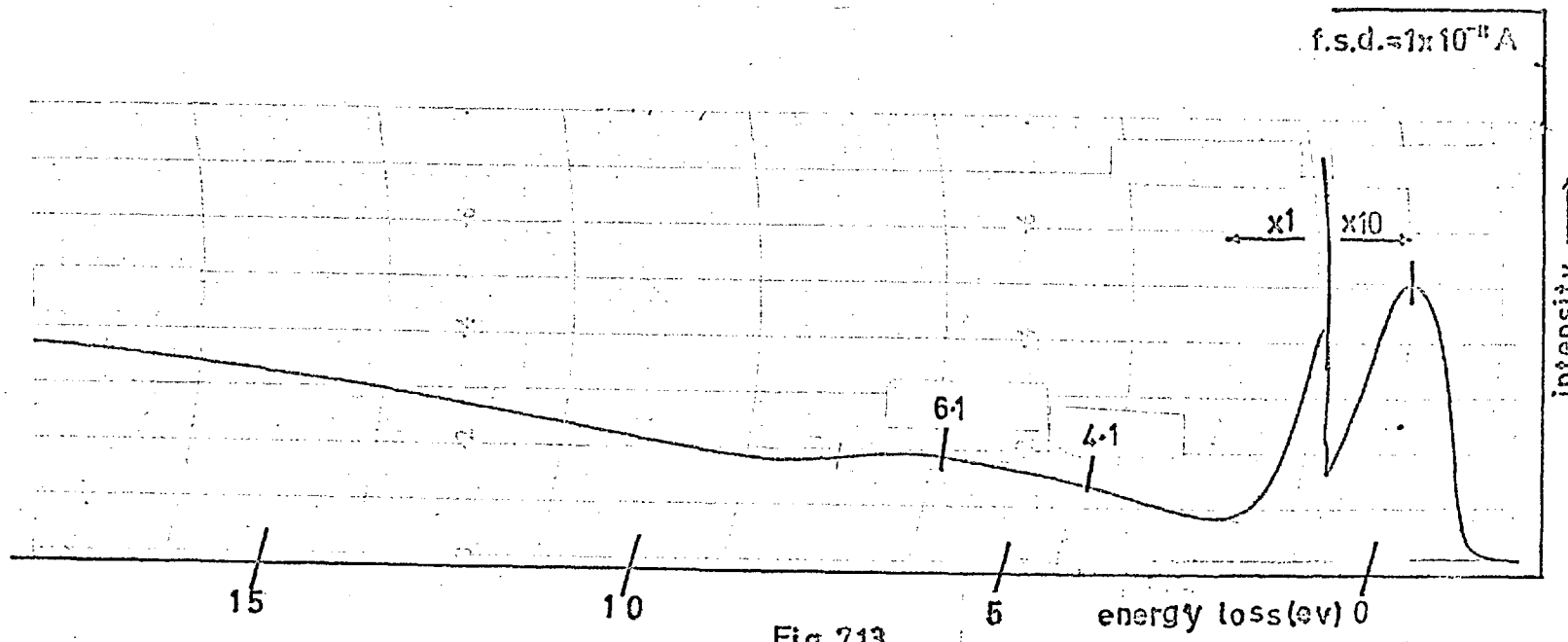

Fig. 7.13

germanium). Also the main broad loss seems to lie at a lower value, but the voltage sweep would have to be extended to confirm this fully. The germanium curve differs from the contamination spectrum in that the 7.2 ev loss in the germanium case, is greater than the 6.1 ev contamination loss and the half-width of this loss is ~5.0 ev compared with ~3.5 ev for the contamination loss. It can therefore be said that the time-dependence of the spectra of the elements investigated was not due to carbonaceous contamination. Oxidation is an important factor in each case, except for gold. The time-dependence of the gold spectra shows that there is a further, unknown, source of contamination. Adsorption of gas by the specimens is a possible, but unlikely, explanation (Sect. 5.10), but contamination by deposits from the primary electron beam could not yet be fully ruled out.

The spectrum of aluminium oxide has been measured by a number of investigators in high energy electron transmission experiments and by Powell and Swan (1960) in a low energy reflection experiment. None of the investigators reported an energy loss of 6 ev, but all observed a broad loss of 22 - 23 ev. It is unlikely therefore that the 6 ev loss observed in the case of aluminium is due to oxidation, which substantiates the remarks made previously concerning a further source of contamination.

7.8 Energy Loss Measurements on Magnesium

Magnesium like aluminium behaves in accordance with the plasma oscillation theory, see for example Powell and Swan (1959b and 1960).

Several attempts were made to observe the characteristic energy loss spectrum of magnesium but were unsuccessful. Only on two of the spectra

obtained did the energy losses appear and then they were very weak in intensity. There are two possible explanations for this failure, either the magnesium contaminated so rapidly that the losses were quenched, or little, if any, magnesium was deposited onto the target during evaporation. Magnesium sublimates at a low temperature (443°C, Holland, 1960) from the evaporation filament and normally the target was at 400°C. It is unlikely, under these conditions, that any magnesium would stick to the target and no losses were observed under these conditions. It was attempted to observe the losses by evaporating magnesium onto the target at temperatures between room temperature and 200°C and then heating it rapidly to 300°C to prevent contamination by the electron beam. In this way one spectrum was obtained which differed from that of the substrate; this showed a weak loss at ~8 ev, which was thought to be a combination of the plasma and surface plasma losses. By very rapidly evaporating the magnesium onto the target at 300°C one spectrum was obtained which showed weak energy losses of 6.7, 10.7, 16.9 ev and an intense broad loss of 24.2 ev, but this could not be repeated. The first three losses correspond to a surface plasma loss, a volume plasma loss, and a surface plus a volume plasma loss (after Powell and Swan 1959b). The fourth loss almost certainly belonged to the substrate.

A method by which magnesium might be investigated, is to evaporate gold or silver onto the substrate at 200 - 300°C and then to evaporate magnesium onto this immediately afterwards. The first evaporation would provide a substrate for the magnesium which would be relatively free from adsorbed gases and contamination to which the magnesium would

stick (see Holland 1960).

7.9 The Background in the Spectrum of the Characteristic Energy Losses

The general background which is always present beneath the energy loss peaks is due to small inelastic collisions of the primary electrons with the atomic and conduction electrons of the specimen, producing energy losses of the Bohr-Bethe type (see for example Birkhoff 1958) and secondary electrons. There, the energy of the primary electrons must be high enough to consider the atomic or conduction electrons respectively, to be quasi-free of binding forces. Energy losses of these types differ from the characteristic energy losses in that the primary electron does not lose a well-defined quantum of energy in such a collision; instead, a broad spectrum of energy losses is produced and it is this spectrum upon which the characteristic energy losses are superimposed. The most probable energy loss in such a broad spectrum (i.e. the maximum of the energy spectrum) arising from multiple collisions, is a function of the thickness of material traversed by the primary electron beam.

In the present experiments the primary electron beam penetrates deeper into the specimen when its incidence and reflection angles are 45° than when they are ~80°. It is therefore expected that the background beneath the characteristic energy losses should be different in the two cases. For all the materials investigated the background intensity, compared with the zero energy loss intensity, was greater in the grazing angle condition than in the 45° incidence and reflection case. This may be explained qualitatively on the basis that at grazing angle an incident

primary electron may experience many acts of multiple scattering and still escape from the specimen surface, while at 45° incidence if the electron is to leave the surface again it must be scattered essentially by a single scattering act which is an elastic collision with a nucleus.

CHAPTER 8.

DISCUSSION OF RESULTS AND TECHNIQUE

8.1 Aluminium

The characteristic energy loss spectrum of this element has been investigated by many authors (see Ch.1) and there is much agreement about its interpretation. The present experiments confirmed that the 10.1 and 15.0 ev energy losses are due to excitation of surface and volume plasma oscillations respectively.

The ratio of the volume plasma energy loss to the surface plasma energy loss was (15.0/10.1) = 1.49, which is identical with the value found by Powell and Swan (1959a), but is slightly different to the value of $2^{\frac{1}{2}}$ ($\simeq$1.41) predicted by Ritchie (1957) for a specimen with a plane surface (see Ch.1). However, agglomeration of the aluminium specimen would be expected to raise the predicted value, since Ritchie points out that for a specimen film consisting of an agglomeration of spheres the expected ratio would be $3^{\frac{1}{2}}$ ($\simeq$1.73). Therefore, if the specimen surface were not perfectly flat and smooth, one would anticipate an increase in the ratio, to a value between 1.41 and 1.73. The value of 1.49 obtained is therefore considered to be in reasonable agreement with Ritchie's prediction.

Although aluminium has been studied by many authors (see Klemperer and Shepherd 1963) almost all of the experiments have been of the high

energy transmission type, in which the surface plasma loss either does not appear, or appears as a weak modified surface loss due to oxidation of the surface of the specimen, as mentioned in Ch.1. The only work with which the present results can be directly compared is that of Powell and Swan (1959a), who used a similar system to the present author's and investigated freshly evaporated aluminium specimens with 760 - 2020 ev primary electrons reflected through 90° by the specimen. The following table gives a comparison of the results:-

Table 8.1

Powell and Swan (1959a)	10.3	15.3	20.5	25.6	30.5
Present Work *	10.1	15.0	20.8	25.3	30.8

*Overall results from Table 7.5

The agreement between the two sets of results is quite good. It is to be expected that the present loss values should be slightly less than Powell and Swan's values since the present experiments were carried out at 400°C while Powell and Swan's were carried out at 200°C. Meyer (1957) has measured the temperature dependence of the 15 ev energy loss, in a high energy electron transmission experiment, over the range 20°C - 400°C and found that the loss decreased at the rate of $5.8 \pm 0.7 \times 10^{-4}$ ev/°C as the temperature increased. This is due to the thermal expansion of the aluminium and the accompanying drop in the electron density. This would account for a difference of approximately 0.1 ev in the 15 ev loss values given above and a slightly smaller difference of about $(0.1/2^{\frac{1}{2}})$ ev in the 10 ev loss values.

Powell and Swan quote a value of 1.4 ± 0.1 ev for the half-width of the 15 ev energy loss, but this was obtained by subtracting the zero energy loss half-width from the measured value of the energy loss half-width. Shepherd (1962) pointed out that if the correction given in equn.(7.1) is applied to these results a half-width of 2.6 ± 0.2 ev is obtained. Shepherd in a transmission experiment obtained a value of 2.07 ± 0.46 ev, which is in reasonable agreement with the value found in the present experiments of 1.6 ± 0.3 ev (Table 7.4). Recent work by Hartl(1964, 1966), using highly monochromatic primary electron beams (half-width 0.03 - 0.12 ev) in transmission experiments, gives a half-width for the 15 ev loss of only 0.9 ± 0.1 ev, which agrees with the value of approximately 1.0 ev predicted by the dielectric model of electron energy losses from the optical data of Ehrenreich et al.(1963).

The modified surface plasma energy loss predicted by Stern and Ferrell (1960) and found by Powell and Swan (1960) at 7.1 ev (see Ch.1) for oxidised Al specimens, was not observed on any of the spectra obtained for the Al specimens which were allowed to age in the vacuum chamber. It is not thought that the loss found at about 6 ev on old Al specimens (Sec.7.7) is the modified surface loss. Powell and Swan (loc.cit.) showed that the modified surface loss reached its maximum intensity when the 10 ev surface loss was almost quenched by specimen surface oxidation. Further oxidation resulted in the gradual disappearance of the modified surface loss. This behaviour is not characteristic of the 6 ev loss found in the present experiments. The 6 ev loss mentioned here was discussed in Sect.7.7. However, it is surprising

that no modified surface loss appeared, for irrespective of the nature of the surface contamination such a loss would be expected at some period in the ageing of a specimen. Perhaps the answer lies in the low primary energy used. Powell and Swan used 750 ev primaries compared with 200 ev in the present experiments.

As far as the present author is aware, energy loss measurements on Al have not previously been performed for primary energies as low as 200 ev. The previous lowest energy was that of 750 ev used by Powell and Swan (1960). The intensities of the volume and surface losses follow the trend of Powell and Swan's (1959a) results. At 2020 ev they found that the volume loss was much more intense than the surface loss and at 760 ev the losses were of approximately equal intensity, while in the present 200 ev experiments, the surface loss is much more intense than the volume loss.

8.2 Germanium

The interpretation of the 11.2 ev loss as the surface plasma loss and the 16.4 ev loss as the volume plasma loss is in agreement with the simple plasma theory and with the interpretation of Powell (1960) using the method of variation of the energy loss intensities with primary electron energy described in Ch.1. Gornyi (1961) has also carried out low energy reflection measurements on Ge using primary energies of 30 - 140 ev. The following table gives a summary of the present results, for 45° incidence and reflection of the primary beam (Table 7.6) compared with Powell's (primary energy 1500 ev, specimen at room temperature) and Gornyi's results for a primary energy of 140 ev (specimen at 400°C).

All values are in ev.

Table 8.2

Present Work		5.2		11.2		16.4		25.8	31.7
Powell (1960)				11.1		16.4		27.1	32.5
Gornyi (1961)	2.0	5.0*	9.4		13.4	16	19.2		33

* Observed using a primary energy of 40 ev.

As in the case of Al one would expect the present results to be slightly smaller in value than Powell's, since Meyer (1957) has shown that there is a temperature dependence of the 16 ev volume plasma loss, which he states is $<5 \times 10^{-4}$ ev/°C. This is not apparent in the results quoted here. There is reasonable agreement between the present results and Powell's, but Gornyi's results differ considerably from these. Gornyi interprets his 16 ev loss as a volume plasma loss, but he accounts for all the other losses using the interband theory of Viatskin(1958). He used a spherical retarding field energy analyser which analysed the energies of all the scattered electrons and not just one scattered ray as in Powell's and the present case.

The 5.2 ev loss found in the present work is attributed to an interband transition. It corresponds to a maximum in the optical absorption coefficient of Ge at 4.4 ev observed by Philipp and Taft (1959). They in fact observe three peaks of 2.5, 4.4 and ~5.9 ev situated on a background which has a maximum at about 5 ev. The 4.4 ev maximum is the most intense of the three peaks. All the peaks are associated with valence band to conduction band transitions according to Ehrenreich et al.(1962). This loss is not associated with the 5 ev loss observed when 15 - 50 kev

electrons are transmitted through Ge films of the order of 100Å thick, since Creuzburg (1963) identified this as a modified surface loss (see Ch.1). Also if high energy electrons are reflected from a Ge crystal surface, the surface loss, which is not present in the transmission experiments, appears at 10.7 ev (see e.g. Creuzburg and Raether, 1963) in reasonable agreement with Powell's and the present results. The 5.2 ev loss was only present for newly evaporated specimens; as the specimen aged the loss quickly disappeared while the surface loss was still strong in intensity and this behaviour is not characteristic of a modified surface loss.

The optical constants of Ge have been measured by Philipp and Ehrenreich (1963a) in the photon energy range of 1.5 - 25 ev. They found that the energy loss function, given in equn.(1.9), has an intense peak at 16.0 ev, of half-width ~7 ev, corresponding to volume plasma oscillations and a weak structure at about 5 ev corresponding to the interband transitions mentioned above. The corrected half-width of the 16.4 ev loss in the present experiments was 3.3 ± 0.5 ev, which is less than half the value predicted above. Raether (1965) points out that Zeppenfeld (unpublished work) has measured the half-width of the 16 ev loss in mono- and polycrystalline Ge as 3.2 and 3.5 ev respectively, and suggests that the difference between the measured values and the value predicted by the dielectric theory, is that the measurements of the optical constants are performed on crystal surfaces which have been polished and etched. The optical properties of such surfaces may be different from the bulk material and evaporated films.

It is interesting that Powell (loc.cit.) observed the 27.1 ev loss given in Table 8.2 using a primary energy of 1500 ev but not when he used a primary energy of 750 ev. This is in favour of the 25.8 ev loss observed in the present experiments being a double surface loss and not a volume plus a surface loss (see Sect.7.4). The 25.8 ev loss is of very small intensity and appears on a sloping background and its position is very uncertain. This strengthens the suggestion made in Sect.7.4 that the 25.5 ev loss observed in the grazing angle condition (see Table 7.7) is a double surface loss.

As in the case of Al no modified surface loss was observed as the specimens aged in the vacuum system. Powell (1960) does not report a modified surface loss for Ge. The loss at about 7 ev observed for old Ge films in the present work (see Sects. 7.4 and 7.7) is not thought to be a modified surface loss because the change in loss value with time (increasing surface contamination) was gradual and not abrupt. This is not characteristic of the modified surface loss, as mentioned in Ch.1.

Apart from the 5 ev loss reported by Gornyi (Table 8.2), which disappeared for primary energies greater than 40 ev, no previous report of an energy loss at about 5 ev in Ge has been found.

8.3 Gold

The present results are compared in Table 8.3 with the low energy reflection experiment results of Rudberg (1930a, 1936) and Robins (1961). Also included are the high energy transmission results of Sueoka and Fujimoto (1965); these are the only authors to report, in a transmission experiment, an energy loss of about 3 ev.

Table 8.3

	Primary Energy (ev)					
Present Work*	200	3.0	5.9			23.4
Robins (1961)	1500 & 800		6.3		16.0	25.8
Rudberg (1930a)	40 - 900		7.3	10.1		25.9
Rudberg (1936)	50 - 400	3.05	5.8			24
Sueoka and Fujimoto (1965)	30,000	2.65	5.8	11.1	16.2	24.1

*Overall values from Table 7.12

Due to the overlapping of the s and d energy bands in Au there is coupling between the bands, and the simple plasma theory does not apply. If the single 6s electron is assumed to be free to take part in plasma oscillations, then equn.(1.2) predicts a volume plasma loss of 8.9 ev, whereas if the eleven 5d and 6s electrons are considered as free this is calculated to be 29.6 ev. There is no prominent loss in the reflection or transmission experiments at either of these values. The energy loss which has most often been associated with volume plasma oscillations is the intense broad loss observed at 24 - 25 ev, which is the most prominent loss in the Au spectrum (see e.g. Ferrell, 1956).

Of the results given in Table 8.3 those of the present author, and those of Rudberg (1936) and of Sueoka and Fujimoto (1965) are in reasonable agreement. Rudberg's (1930a) earlier results are not considered representative of a well-defined surface according to Rudberg (1936).

Robins (1961) interprets the 6.3 ev loss which he find as the surface plasma loss on the basis of its intensity variation with primary energy. In the present experiments it was not definitely possible to

identify the surface loss (Sect.7.5) but this was tentatively suggested to be the 3.0 ev loss, not because of any angular dependence but because of its time dependence. Sueoka and Fujimoto (loc.cit.) have interpreted their 2.65 ev loss as the surface plasma loss on the basis of measurements on the optical constants of evaporated Au films by Fukutani and Sueoka (1965). These authors showed that the condition for surface plasma oscillations, given in equn.(1.11), is satisfied for a photon energy of 2.53 ev. These optical measurements, however, extend to only 4.5 ev and the volume plasma loss was not identified.

Canfield et al. (1964) have measured the optical properties of evaporated Au films in the region 6 - 60 ev. They found that the energy loss function, $-\mathrm{Im}(\frac{1}{\varepsilon})$, shows maxima at 6.7, 16.3, 25.8 and 32.6 ev. The most intense of these peaks is at 25.8 ev. These values agree quite well with the experimental results given in Table 8.3.

The 5.9 ev loss found in the present case is thought to be due to an interband transition corresponding to the 6.7 ev loss mentioned above. Canfield et al. (loc.cit.), however, did not identify the maxima they found with the energy transitions responsible for them. Simons (1943) has observed optical absorption maxima at 3.7 ev and 9.1 ev in Au and associates them with 6s - 6p and 5d - 6p interband transitions respectively with a possibility of a 5d - 6s contribution to the 3.7 ev loss. He states that the 5d - 6s transition would be about 5 ev, such a transition may account for the present observed energy loss of 5.9 ev. This corresponds to an original suggestion by Gauthé (1958) according to which this loss is produced by transitions from the d-band to the Fermi level.

The half-widths (assumed to be uncorrected for the zero loss distribution) of the 2.65 and 5.8 ev losses observed by Sueoka and Fujimoto (1965) are 0.95 ± 0.1 nd 3.3 ± 0.5 ev respectively, which are in reasonable agreement with the present (uncorrected) values of 1.4 ± 0.1 and 4.7 ± 0.6 ev. There is however, a large discrepancy for the half-width of the loss at about 24 ev which Sueoka and Fujimoto have measured as 6.3 ± 0.8 ev compared to the present value of about 14 ev, but it must be remembered the experiments were carried out under widely differing conditions and that the overall shape of the spectra obtained is different.

The losses at about 10 and 16 ev reported by various authors seem to require a primary electron energy of the order of 1 kev before they are excited with sufficient intensity to be observed, since neither the present author nor Rudberg (1936) observe them. The 16 ev loss is almost invariably present in high energy transmission experiments (see the summary by Robins, 1961).

Sueoka and Fujimoto (1965) explain the value of the surface plasma loss in terms of Wilson's (1960) dielectric theory. For the free electron model (assuming one electron per atom) the surface loss in Au should be 6.3 ev, according to Wilson's theory this value can be shifted to a higher or lower value by the presence of a narrow optical absorption band in its vicinity, such that the surface loss lies either above or below the absorption band. They assume that the loss is depressed in this case by 5d - 6s and 6s - 6p interband transitions of the type assumed to account for the 5.9 ev loss in the present experiments. However,

more optical data are required for a better understanding of the gold energy loss spectrum and in particular for the identification of the volume plasma loss.

It should be mentioned that neither Viatskin's (1958) interband theory nor correlation with x-ray absorption energy spectra (Gauthé, 1958) can account for the 5.9 ev energy loss found in Au.

Some remarks relevant to Au are also made in the following section.

8.4 Copper

The present results are compared in Table 8.4 below with the results of other authors from low energy reflection measurements of the characteristic energy losses. The high energy measurements at grazing angle reflection by Kleinn (1954) are also included.

Table 8.4

	Primary Energy(ev)						
Present Work *	200	3.6		6.6	?13.4?	22.1	27.5
Powell (1960)	(750 & (1500		4.4	7.2		19.9	27.1
Robins & Swan(1960)	1200		4.5	7.6		19.1	27.3
Rudberg (1930a)	40-900	3.4		6.9	12.3		25.5
Rudberg (1936)	50-400		4.2	7.3			
Reichertz and Farnsworth (1949)	(59.5 & (114.5	3.0		6.0	12.3	20.0	
Kleinn (1954)	35,000	3.1	4.3	6.4		21.0	

*Overall values from Table 7.17

Copper, like gold, terminates a series of transition elements, both

have a completed outermost d-shell and one s-electron. The binding energy of the d-electrons is however not high enough to prevent overlapping of the s- and d-energy bands in the solid state and coupling occurs between the two bands. One might therefore expect some similarity between the energy loss spectra of Cu and Au. This is in fact the case, as can be seen from Figs. 7.9(a) and 7.8(a) respectively. The general shape of the two curves is very similar but there is a larger number of energy losses for Cu than for Au (see Tables 8.4 and 8.3).

The volume plasma loss of Cu, calculated using equn.(1.2), is 10.8 ev if the 4s electron is considered to be free, but if the ten 3d electrons are also able to take part in collective oscillations, the loss is calculated to be 35.9 ev. Neither of these values correspond to prominent, sharp, energy losses. The present experiments were not capable of detecting an energy loss as high as 35.9 ev, but the results of Gauthé (1958) and of Robins and Swan (1960) for high energy transmission and low energy reflection measurements respectively verify the above statement. Pines (1956) is of the opinion that the energy loss at about 20 ev is the volume plasma loss which has been depressed from 35.9 ev by high energy interband transitions. Beaglehole (1966), using his own measured values of the optical constants of Cu, has shown that interband transitions from the s and d bands don't saturate until energies substantially higher than 50 ev are reached. Pines (loc.cit.) based his decision on the fact that the 20 ev loss was the most intense loss in the spectrum and in some transmission experiments (see e.g. Shepherd, 1962) it is the only loss observed.

Powell (1960), by varying the energy of his primary beam and observing the change in intensity of the energy losses (see Ch.1), identified the surface and volume plasma losses as the 7.2 and 19.9 ev losses which he observed, as shown in Table 8.4. He also found that slight oxidation of the specimen caused the 7.2 ev loss to disappear and be replaced by a 3.7 ev modified lowered loss. Robins and Swan (1960) adopt Powell's interpretation of the losses and attribute their 4.5 ev loss to ionisation of the M_{45} atomic energy level. However, in the present investigation the 3.6 ev loss was identified as the surface plasma loss. This is almost identical in value with Powell's modified surface loss mentioned above, but the present author is not of the opinion that the freshly evaporated specimens used in the present investigation were oxidised. Apart from the shift in the two losses below 10 ev the general shape of Powell's unoxidised spectrum and the present spectrum is similar.

The 6.6 ev loss in the present experiments is thought to be due to 3d - 4p interband transitions analogous to those causing the 5.9 ev loss in Au, since the intensity of this loss was independent of the scattering angle of the primary beam. Beaglehole (1966) has proposed that such transitions may account for low energy optical absorption peaks at about 2.5ev and 5 ev which he measured (Beaglehole, 1965) for electropolished Cu specimens. A similar explanation for both the losses observed by Rudberg (1936) below 10 ev was put forward by Rudberg and Slater (1936).

The two remaining energy losses to be identified are the very weak

loss at 13.4 ev, which was only observed in the grazing angle condition, and the 27.5 ev loss. Gauthé (1958) and Robins and Swan (1960) have associated the 27.5 ev loss with the fine structure on the high energy side of the x-ray K-absorption edge of Cu (see Ch.1). Robins and Swan (loc.cit.), using the x-ray data of Beeman and Friedmann (1939), show that energy losses of 18.1 ev and 27.5 ev might be expected. The second of these losses would correspond to the 27.5 ev observed here, but the 18.1 ev loss was not observed in the present experiments. No alternative to this explanation of the 27.5 ev loss can be offered here. The present author suggests that the 13.4 ev loss may be explained by a similar process using the x-ray data for the L-absorption edge as given by Cauchois (1953). Cauchois shows that the energy difference between the L α emission line and the L_{III} absorption limit is 3.0 ev ($=\delta E$). The absorption maxima (ΔE) on the high energy side of the L_{III} limit are at 1.0, 5.0 and 9.0 ev. According to the discussion in Ch.1, the energy losses predicted using these data are, $\delta E + \Delta E$ = 4.0, 8.0 and 12.0 ev respectively. The 12.0 ev loss may correspond to the 13.4 ev observed here. These data also offer an alternative interpretation of the 3.6 ev loss observed as due to an interband transition, but the earlier explanation, given here in terms of surface plasma oscillations, must be accepted because of the observed intensity variation with scattering angle.

Ehrenreich and Philipp (1962) have measured the optical constants of electrolytically polished bulk Cu in the ultraviolet and from their data have plotted the energy loss function, $-\mathrm{Im}(1/\varepsilon)$, up to 25 ev. Maxima are found in this function at 4.1, 7.5 and 20 ev, which agree reasonably well

with some of the losses given in Table 8.4. The condition for plasma oscillations, $\varepsilon = 0$, was not found to occur, but the maximum at 7.5 ev is a free-electron-like resonance in that both ε_1 and ε_2 are small in this region and ε_1 is increasing while ε_2 is decreasing with increasing energy, as in a free electron gas. The present experiments did not indicate a volume plasma loss behaviour for the 6.6 ev energy loss found, which in this case was associated with the 7.5 ev loss of Ehrenreich and Philipp (loc.cit.).

Ehrenreich and Philipp admit that their specimen was conceivably subject to atmospheric contamination. Beaglehole (1965) stresses this and criticises their method of determining ε_1 and ε_2, his results differ somewhat from Ehrenreich and Philipp's but the general agreement is reasonable. The free-electron-like resonance would occur at about 9ev on the basis of Beaglehole's results. This indicates that, as yet, the optical measurements should be treated with some caution. This is not to say that the electron beam studies can be trusted explicitly, since a glance at Table 8.4 reveals large discrepancies between the results of different workers. Such variation in results has been discussed in previous literature (Marton, 1956; Klemperer and Shepherd, 1963). The results given in Table 8.4 are all for reflection type experiments and the surface condition of the specimens used has a significant effect on the results. It may be relevant that the present measurements were made at 400°C, Rudberg's (1930a) with the specimen heated to incandescence and Kleinn's (1954) at 200°C. Also Reichertz and Farnsworth (1949) heated their single crystal specimen to dull red heat to degas it before taking

measurements. In all these cases the first loss is in the region 3.0 to 3.6 ev. The results of Powell (1960), Robins and Swan (1960) and Rudberg (1936) were all taken using freshly evaporated specimens, as in the present experiments, but at room temperature, and the first loss appears at 4.2 to 4.5 ev. It might be possible that the heat treatment of the different specimens is responsible for the variation in the energy losses recorded. Pradal and Saporte (1958) have reflected 40 kev electrons at grazing angle from polycrystalline Cu and single crystal Cu surfaces but they give little information concerning the energy losses observed. Their published curves show that the reflected electron energy spectrum depends strongly on the orientation of the crystal, and the polycrystalline sample gave a spectrum similar to those observed in normal high energy transmission experiments using evaporated films. All these factors may contribute to the variation in the losses as observed by different authors. It should be mentioned that for Cu, as in the case of Au, Rudberg (1936) gives preference to his later results (see Table 8.4).

It can be seen from the results that Ritchie's (1957) theory of the surface plasma loss does not seem to predict the correct values for the losses in Au and Cu. Of course the volume plasma loss may be incorrectly assigned. The present author has had to accept the evidence of other authors to identify this loss in both cases. Even allowing that the loss of 7.5 ev predicted by Ehrenreich and Phillip's (1962) optical measurements on Cu is the volume plasma loss, there is no loss corresponding to Ritchie's (loc.cit.) predicted surface loss value. If

the present losses in Cu are correctly assigned the ratio of the volume loss to the surface loss is about 6.1 compared with Ritchie's value of about 1.4. The behaviour of Au and Cu thus indicate the enormous influence which interband transitions can have upon the simple free-electron plasma theory of characteristic energy losses.

8.5 Summary of Results

Table 8.5

Giving the energy losses observed in the present investigation and their proposed interpretation.

Al	10.1,L.	15.0,P.	20.8,2xL.	25.3,P+L	30.8,2xP
Ge	5.2,B.	11.2,L.	16.4,P.	25.8,(2xL or P+L	31.7,2xP
Au	3.0,L.	5.9,B.	23.4,P.		
Cu	3.6,L.	6.6,B.	13.4,X	22.1,P.	27.5,X.

Here P = Volume plasma loss

L = Lowered, or surface, plasma loss

B = Interband transition

X = Transition involving an excitation to a maximum in an x-ray absorption spectrum.

8.6 Discussion of Technique and Further Work

The grazing angle technique described in Ch.1 was found to work well for Al but was not quite as effective for Ge, probably because of the large half-width of the surface loss in this case. In the cases of Au and Cu which, unlike the above mentioned metals, do not obey a simple

plasma theory, a positive result was obtained for Cu in that one of the low lying losses showed an intensity variation with scattering angle of the primary beam, but no such effect was observed for any of the losses in Au. The assignment of the surface plasma loss for Cu differs from that determined using the method of Powell and Swan (1959a,b) which is described here in Ch.1. The present author feels that the method used here should certainly be worth pursuing and combining with the method of Powell and Swan (loc.cit.), so that grazing angle experiments can be carried out at various primary energies. In this way the two techniques can be compared directly using identical specimens, and the identification of the plasma losses should be made more easy.

It is obvious, from the results for Au and Cu, that only small changes occur in the intensity of plasma losses with scattering angle of the primary beam for metals whose free-electron behaviour is influenced strongly by interband effects. It is thus important to have a consistent method for preparation of the specimens so that variations in intensity of the losses from specimen to specimen is rendered unimportant. This was not the case in all of the present experiments, as can be seen from the intensity ratio values quoted in Ch.7. Continuous evaporation of the specimen onto the target during the energy loss measurements would be the ideal method to be employed. In this way oxidation of the specimen and contamination from other sources could be reduced to a minimum and, at the moment, these seem to be the greatest drawbacks of the technique used.

The great advantage of the present technique over other methods of

identifying the plasma losses, as mentioned in Ch.1, is its simplicity.

It is perhaps, a little surprising that the present interpretation of the surface plasma loss in Cu differs from that given by Powell (1960). It would be interesting to investigate the energy loss spectra of all the metals in the first transition series and to see if the identification of the lowered plasma loss in these metals agrees with that given by Robins and Swan (1960). These authors attribute the lowest energy loss in all these metals (except Mn) to ionisation of the M_{45} atomic energy level, whereas, in analogy to the results for Cu in the present experiments, these losses may be due to surface plasma oscillations. Also, the fact that optical measurements sometimes predict plasma losses different to the losses identified in electron reflection experiments as plasma losses, requires investigation. For example, Robins (1961) identified the surface and volume plasma losses in Ag as the 7.3 and 25 ev losses which he observed, while the optical measurements of Ehrenreich and Philipp (1962) predict these losses at 3.6 and 3.75 ev. The latter values are supported by recent transmission and radiation emission experiments (see Ch.1 and Raether 1965). Thus further work must be carried out before the true origins of all the energy losses can be accounted for.

CAPTIONS -

Fig.

2.1 The Liquid nitrogen trap.

2.2 A vacuum lead-in for nine leads.

2.3 The degaussing coils.

3.1 The post-acceleration target.

3.2 The tetrode gun.

3.3 The beam characteristics of the tetrode gun.

3.4 The seven electrode gun:-
a) general diagram,
b) detail of an anode A_3.

3.5 Beam current characteristic (0 - 70ev) of the seven electrode gun, using a 0.1 mm tungsten hairpin cathode.

3.6 The tantalum strip cathode.

3.7 Beam current characteristic (200 - 800ev) of the seven electrode gun, using the tantalum strip cathode.

4.1 The principle of the retarding field analyser:-
a) schematic diagram,
b) energy analysis and the beam divergance effect on the resolution.

4.2 The aperture effect on the resolution of a retarding field analyser.

4.3 A schematic electron filter lens.

4.4 The filter lens analyser.

4.5 An analysis of 800ev electrons using the filter lens analyser.

4.6 The principle of the inverse retarding field analyser:-
a) schematic diagram,
b) an ideal energy analysis curve for electrons of energy eV_o.

4.7 Illustrating the presence of an energy loss of $e\Delta V$ in an inverse retarding field energy analysis curve.

4.8 The inverse retarding field analyser.

Fig.

4.9 Analysis of a 400ev electron beam with the inverse retarding field analyser.

4.10 The principle of the 127° electrostatic deflection analyser :-
a) schematic diagram,
b) illustrating the imperfect refocussing.

4.11 The 127° deflection analyser:-
a) plan,
b) front view,
c) vertical section.

4.12 a) The calibration circuit for the deflection analyser,
b) deflection voltage, V_d, versus beam voltage, V_o.

5.1 The layout of the retarding field spectrometers:-
a) elevation,
b) plan.

5.2 Schematic circuit diagram for the retarding field spectrometers.

5.3 The energy spectrum of 400ev electrons reflected from a contaminated layer of Al, using the inverse retarding field spectrometer.

5.4 As for Fig. 5.3, using the filter lens spectrometer.

5.5 The final spectrometer:-
a) elevation,
b) plan.

5.6 The energy spectrum of 800ev electrons reflected from a contaminated layer of Al, using the final spectrometer.

5.7 The heated target:-
a) the heating element,
b) the tantalum box,
c) the complete assembly,
d) the replaceable front surface.

5.8 The energy spectrum of 800ev electrons reflected from Al at 400°C.

5.9 As for Fig. 5.8, using 267ev electrons.

5.10 The sweep voltage circuit:-
a) the circuit,
b) the waveforms produced.

5.11 The electron gun circuit.

Fig.

Fig.

REFERENCES

Arakawa, E.T., Davis, N.O., Emerson, L.C. and Birkhoff, R.D., 1964, J. Phys. Radium, 25, 129.

Banner, A.E., 1966, J. Scient. Instrum., 43, No.3, 138.

Beaglehole, D., 1965, Proc. Phys. Soc., 85, 1007.

Beaglehole, D., 1966, Proc. Phys. Soc., 87, Part 2, No.556, 461.

Beeman, W.W., and Friedmann, H., 1939, Phys. Rev., 56, 392.

Best, P.E., 1962, Proc. Phys. Soc., 80, 1308.

Birkhoff, R.D., 1958, "Handbuch der Physik", 34, 53.

Bland, C.J., 1961, Ph.D. Thesis, University of London.

Boersch, H. and Schweda, S., 1962, Z. Phys., 167, 1.

Boersch, H., Geiger, J., Hellwig, H. and Michel, H., 1962, Z. Phys., 169, 252.

Boersch, H., Dobberstein, P., Fritzsche, D. and Sauerbrey, G., 1965 Z. Phys., 187, 97.

Bohm, D. and Pines, D., 1951, Phys. Rev., 82, 625.

Bohm, D. and Pines, D., 1952, Phys. Rev., 85, 338.

Bohm, D. and Pines, D., 1953, Phys. Rev., 92, 609.

Brown, R.W., Wessel, P. and Trounson, E.P., 1960, Phys. Rev. Lett., 5, 472.

Bull, C.S. and Klemperer, O., 1943, J. Scient. Instrum., 20, 179.

Butterworth, G.J., 1964, Ph.D. Thesis, University of London.

Canfield, L.R., Hass, G. and Hunter, W.R., 1964, J. Phys. Radium, 25, 124.

Cauchois, Y., 1953, Phil. Mag., 44, 173.

Craig, H., 1947, Proc. Phys. Soc., 59, 804.

Creuzburg, M., 1963, Z. Phys., 174, 511.

Creuzburg, M. and Raether, H., 1963, Z. Phys., 171, 436.

Creuzburg, M. and Raether, H., 1964a, Sol. State Comm., 2, 175.

Creuzburg, M. and Raether, H., 1964b, Sol. State Comm., 2, 345.

Ehrenreich, H. and Philipp, H.R., 1962, Phys. Rev., 128, 1622.

Ehrenreich, H., Philipp, H.R. and Phillips, J.C., 1962, Phys. Rev. Lett., 8, 59.

Ehrenreich, H., Philipp, H.R. and Segal, B., 1963, Phys. Rev., 132, 1918.

Ennos, A.E., 1953, Br. J. Appl. Phys., 4, 101.

Ennos, A.E., 1954, Br. J. Appl. Phys., 5, 27.

Ferrell, R.A., 1956, Phys. Rev., 101, 554.

Ferrell, R.A., 1957, Phys. Rev., 107, 450.

Ferrell, R.A., 1958, Phys. Rev., 111, 1214.

Fröhlich, H. and Pelzer, H., 1955, Proc. Phys. Soc., A68, 525.

Fukutani, H. and Sueoka, O., 1965, J. Phys. Soc. Japan, 20, 620.

Gauthé, B., 1958, Annls. Phys. (Paris), 3, 915.

Geiger, J., 1961, Z. Phys., 161, 243.

Gornyi, N.B., 1957, Soviet Phys. JETP., 4, 131.

Gornyi, N.B., 1961, Soviet Phys. Sol. State, 3, 507.

Haberstroh, G., 1956, Z. Phys., 145, 20.

Harrower, G.A., 1956a, Phys. Rev., 102, 340.

Harrower, G.A., 1956b, Phys. Rev., 102, 1288.

Hart, P.A.H. and Weber, C., 1961, Philips Res. Rep., 16, 376.

Hartl, W.A.M., 1964, Phys. Letters, 13, 133.

Hartl, W.A.M., 1966, Z. Phys., 191, No.5, 487.

Haworth, L.J., 1931, Phys. Rev., 37, 93.

Holland, L., 1960, "Vacuum Deposition of Thin Films", Chapman and Hall, Ltd., London.

Hubbard, J., 1955a, Proc. Phys. Soc., A68, 441.

Hubbard, J., 1955b, Proc. Phys. Soc., A68, 976.

Hughes, A.L.L. and McMillen, J.H., 1929, Phys. Rev., 34, 291.

Hughes, A.L.L. and Rojansky, V., 1929, Phys. Rev., 34, 284.

Jones, G.E., Cram, L.S. and Arakawa, E.T., Phys. Rev. (to be published.)

Kleinn, W., 1954, Optik, 11, 226.

Klemperer, O., 1943, Brit. Pat., 555, 134.

Klemperer, O., 1965, Rep. Prog. Phys., 28, 77.

Klemperer, O. and Shepherd, J.P.G., 1963, Adv. Phys., 12, 355.

Klemperer, O. and Thirlwell, J., 1966, Sol. State Comm., 4, 15.

Kunz, C., 1962, Z. Phys., 167, 53.

Kunz, C., 1964, Z. Phys., 180, 127.

Kunz, C. and Raether, H., 1963, Sol. State Comm., 1, 214.

Kurov, G.A., 1964, Soviet Phys. Sol. State, 6, 1507.

Leder, L.B., 1957, Phys. Rev., 107, 1569.

Leder, L.B., Mendlowitz, H. and Marton, L., 1956, Phys. Rev., 101, 1460.

Leder, L.B. and Simpson, J.A., 1958, Rev. Scient. Instrum., 29, 571.

Marton, L., 1956, Rev. Mod. Phys., 28, 172.

Marton, L., Leder, L.B. and Mendlowitz, H., 1955a, Adv. Electronics and Electron Phys., 7, 183.

Marton, L., Simpson, J.A. and McGraw, T.F., 1955b, Phys. Rev., 99, 495.

Mendlowitz, H., 1959, Bull. Am. Phys. Soc. Series II, 4, 44.

Meyer, G., 1957, Z. Phys., 148, 61.

Mott, N.F. and Jones, H., 1958, "The Theory of the Properties of Metals and Alloys", Dover Publications Inc. New York.

Philipp, H.R. and Ehrenreich, H., 1963a, Phys. Rev., 129, 1550.

Philipp, H.R. and Ehrenreich, H., 1963b, Phys. Rev., 131, 2016.

Philipp, H.R. and Taft, E.A., 1959, Phys. Rev., 113, 1002.

Pines, D., 1955, Solid State Physics, 1, 473, Academic Press, New York.

Pines, D., 1956, Rev. Mod. Phys., 28, 184.

Powell, C.J., 1960, Proc. Phys. Soc., 76, 593.

Powell, C.J., 1965a, Bull. Am. Phys. Soc. Series II, 10, 433.

Powell, C.J., 1965b, Phys. Rev. Lett., 15, 852.

Powell, C.J., Robins, J.L. and Swan, J.B., 1958, Phys. Rev., 110, 657.

Powell, C.J. and Swan, J.B., 1959a, Phys. Rev., 115, 869.

Powell, C.J. and Swan, J.B., 1959b, Phys. Rev., 116, 81.

Powell, C.J. and Swan J.B., 1960, Phys. Rev., 118, 640.

Pradal, F. and Saporte, R., 1958, C.R. Acad. Sci., 246, 2880.

Pradal, F., Gout, G. and Fabre, D., 1965, J. Phys. Radium, 26, 372.

Raether, H., 1965, Ergebn. Exakt. Naturw., 38, 84.

Reichertz, P.P. and Farnsworth, H.E., 1949, Phys. Rev., 75, 1902.

Richter, H. and Ruckwied, A., 1960, Z. Phys., 160, 473.

Ritchie, R.H., 1957, Phys. Rev., 106, 874.

Ritchie, R.H. and Eldrige, H.B., 1962, Phys. Rev., 126, 1935.

Robins, J.L., 1961, Proc. Phys. Soc., 78, 1177.

Robins, J.L. and Swan, J.B., 1960, Proc. Phys. Soc., 76, 857.

Rudberg, E., 1930a, Proc. Roy. Soc., A127, 111.

Rudberg, E., 1930b, Proc. Roy. Soc., A129, 628.

Rudberg, E., 1936, Phys. Rev., 50, 138.

Rudberg, E. and Slater, J.C., 1936, Phys. Rev., 50, 150.

Ruthemann, G., 1941, Naturwiss., 29, 648.

Ruthemann, G., 1942, Naturwiss., 30, 145.

Schmüser, P., 1964, Z. Phys., 180, 105.

Seitz. F., 1940, "The Modern Theory of Solids", McGraw-Hill Book Co. Inc., New York.

Semiletov, S.A., 1956, Kristallographia, 1, 542.

Shepherd, J.P.G., 1962, Ph.D. Thesis, University of London.

Simons, C.F.E., 1943, Physica, 10, 141.

Simpson, J.A., 1961, Rev. Scient. Instrum., 32, 1283.

Simpson, J.A. and Kuyatt, C.E., 1963, Rev. Scient. Instrum., 34, 265.

Steinmann, W., 1960, Phys. Rev. Lett., 5, 470.

Stern, E.A., 1962, Phys. Rev. Lett., 8, 7.

Stern, E.A. and Ferrell, R.A., 1960, Phys. Rev., 120, 130.

Sternglass, E.J., 1956, Nature, 178, 1387.

Sueoka, O. and Fujimoto, F., 1965, J. Phys. Soc. Japan, 20, 569.

Turnbull, J.C. and Farnsworth, H.E., 1938, Phys. Rev., 54, 509.

Viatskin, A.Ia., 1958, Soviet Phys. Tech. Phys., 3, 2038 and 2252.

Wagner, M.D., Marton, L. and Simpson, J.A., 1960, Bull. Am. Phys. Soc., Series II, 5, 68.

Watanabe, H., 1956, J. Phys. Soc. Japan, 11, 112.

Watanabe, H., 1961, J. Phys. Soc. Japan, 16, 912.

Wilson, C.B., 1960, Proc. Phys. Soc., 76, 481.

Wolff, P.A., 1953, Phys. Rev., 92, 18.

Young, J.R., 1956, J. Appl. Phys. 27, 1.